TEKNILLINEN KORKEAKOULU

INSINÖÖRITIETEIDEN JA ARKKITEHTUURIN TIEDEKUNTA

ANTTI LARKELA

MODELING OF A PILE GROUP UNDER STATIC LATERAL LOADING

Pohjarakennuksen ja maamekaniikan syventymiskohteen diplomityö, joka on jätetty opinnäytetyönä diplomi-insinöörin tutkintoa varten.

Espoossa, 24.1.2008.

Valvoja: Professori Olli Ravaska, TKK

Ohjaaja: Professori Corneliu Athanasiu, NTNU

TEKNILLINEN KORKEKOULU DIPLOMITYÖN TIIVISTELMÄ

Tekijä:	Antti Larkela		
Työn nimi:	Staattisesti sivukuormitetun paaluryhmän mallintaminen		
Päivämäärä:	24.1.2008	Sivumäärä:	131 s. + liitteet 3 s.
Osasto:	Yhdyskunta- ja ympäristötekniikka	Professuuri:	Pohjarakennus ja maamekaniikka
Työn valvoja:	Professori Olli Ravaska, TKK		
Työn ohjaaja:	Professori Corneliu Athanasiu, NTNU		
Avainsanat:	Paaluryhmä, p-y kuvaaja, siirtymäelementtimenetelmä, paaluryhmän mallintaminen		

Tässä diplomityössä käsitellään staattisesti sivukuormitetun paaluryhmän mallintamista siirtymäelementtimenetelmään pohjautuvilla laskentaohjelmilla. Esitys käsittelee kolmen erityyppisen paaluryhmänmallinnusohjelman laskentaprosessia sekä analysoi laskentatulosten luotettavuutta vertailukohteena käytettävän paaluryhmän kuormituskokeen mittaustuloksiin.

Tutkimuksen perustaksi on kerätty aikaisempien sivukuormitettujen paaluryhmien kenttäkokeiden tuloksia sekä niiden perusteella annettuja suosituksia. Lisäksi esitykseen on koottu paalun sivuvastuksen huomioimiseksi johdettuja matemaattisia laskentamalleja, jotka perustuvat vahvasti edeltäviin kenttäkokeisiin sekä soveltuvat siirtymäelementtimenetelmää käyttäviin laskentaohjelmiin.

Työssä käydään läpi yksittäisen sivukuormitetun paalun mallintaminen sekä sen eroavaisuudet paaluryhmässä olevan paalun mallintamiseen. Alustavassa laskentatekniikassa käydään läpi yksittäisen paalun lineaarisesti elastinen mallinnustapa, josta edetään epälineaarisen elasto-plastisen paaluryhmän laskentaprosessiin. Esiteltyjä menetelmiä sovelletaan kenttäkokeen paaluryhmän mallintamiseen.

Käytettyjen elasto-plastista laskentamenetelmää noudattavien paaluryhmäohjelmien suurimpana eroina on niiden tapa mallintaa yksittäisen paalun siirtymien aiheuttamien jännityksien vaikutuksia ympäröivissä paaluissa. Yleisimmin käytetty ryhmävaikutuksen huomioiva tapa on vähentää paalun sivuvastusta erikseen määritettävällä kertoimella. Vaihtoehtoinen metodi analysoi paaluja ympäröivän maan elastisena massana, jossa paalun sivusiirtymät johtuvat jännityskenttänä ympäröiviin paaluihin.

Tässä diplomityössä keskitytään paalun sivuttaisliikkeiden sekä taipumien, eikä niinkään aksiaalisten jännitysten tai geoteknisen kantavuuden selvittämiseen. Tarkoituksena ei ole vertailla mitoitusohjeisiin perustuvia laskentatapoja, vaan esittää menetelmiä paaluryhmän matemaattiseen mallintamiseen. Tarkoituksena ei myöskään ole esitellä miten mallinnusohjelma tulisi ohjelmoida, vaan lähinnä esitellä millaisia asioita mallinnusohjelman kokoamisessa pitäisi ottaa huomioon ja miten kyseisten asioiden huomioiminen siirtymäelementtimenetelmällä on mahdollista toteuttaa.

HELSINKI UNIVERSITY OF TECHNOLOGY

ABSTRACT OF THE MASTER'S THESIS

Author:	Antti Larkela		
Name of the thesis:	Modeling of a Pile Group under Static Lateral Loading		
Date:	24.1.2008	Number of pages:	131 p. + appendices 3 p.
Department:	Department of Civil and Environmental Engineering	Chair:	Soil Mechanics and Foundation Engineering
Supervisor:	Olli Ravaska, Professor, HUT		
Supervisor:	Corneliu Athanasiu, Professor, NTNU		
Keywords:	Pile group, p-y curve, finite element method, modeling of a pile group		

This thesis explores the modeling of a pile group under static lateral loading with computer programs based on finite element method. This investigation discusses three various types of a pile group computation program and analyses the reliability of computation results with measurement results from a field test.

Various results from previous field tests of laterally loaded pile groups are collected and also recommendations based on these tests are presented. In addition, mathematical calculation models for modeling the side resistance of a pile group are collected which are strongly based on previous results. The presented mathematical formulas are especially suitable for finite element modeling programs.

This investigation introduces mathematical modeling of a laterally loaded single pile, the modeling of a laterally loaded pile group and presents the differences. In the basic mathematical modeling method of a single pile, the pile is modeled as a linearly elastic beam. From this simple model the research advances to elasto-plastic modeling of a pile group. The presented modeling methods are applied to calculate a field load test of a pile group.

The leading difference between the used elasto-plastic pile group computation programs is in the process of modeling the stress fields within a pile group formed by the lateral movement of a single pile. A more common method is to reduce the lateral soil resistance with a multiplier whereas an alternative method analyses the surrounding soil of a single pile as an elastic mass.

This thesis focuses on lateral movement and bending of a pile and ignores the discussion of axial stresses within the pile and the geotechnical bearing capacity of surrounding soil. The intention of this thesis is to present methods to calculate an accurate mathematical model of a pile group under static lateral loading and does not incorporate the assessment of the different pile group designing methods. In addition the aim of this thesis is not to provide guidance or recommendation to programming techniques, but to present different features to take into consideration in a reliable modeling application.

Preface

This thesis is submitted in partial fulfillment of Master of Science in Civil Engineering degree for Soil Mechanics and Foundation Engineering laboratory in Helsinki University of Technology. This work has been supervised by professor Olli Ravaska (HUT) and the secondary supervision has been conducted by professor Corneliu Athanasiu (NTNU) and by assistant professor Arnfinn Emdal (NTNU).

This thesis has been funded by Rambøll Finland and Maa- ja Vesitekniikan Tuki ry.

I express my gratitude to everybody and everyone for the advice, material and comments that I have received during the working process. I specially want to thank Algis Vilkénas and Anders Westin, who have inspired in finding the topic for my thesis.

The Norwegian University of Science and Technology's personal and Rambøll concern I would like to thank for the support, advice and the provision of the working space.

In Espoo, 24st of January 2008.

Antti Larkela

Table of Contents

Symbols and Notations

1'-2'-3'	Orthogonal coordinate system attached to a pile head, axes parallel to the global pile group coordinate system I-II-III
1-2-3	Orthogonal coordinate system attached to a pile head, axis 3 pointing to the pile tip
A	Total area, cross-sectional area of a pile material, cross-sectional area of a pile [m^2]
A'_s	Coefficient for forming p-y curve in submerged soil when static load is applied [-]
A_q	Single pile head's placement modification matrix
A_s	Coefficient for forming p-y curve in unsubmerged soil [-]
A_{ss}	Coefficient for p-y curve for sand with API recommendations [-]
b	Width of a pile [m]
C'	Parameter for describing p-y curves in submerged soil
c_a	Average undrained shear strength over some specific depth [kN/m^2]
$C_{1,2,3}$	Coefficient for forming p-y curve [-]
C_q	Single pile head's stiffness modification matrix
c_u	Undrained shear strength [kN/m^2]
D	Pile diameter [m]
D_r	Relative density [%]
E	Modulus of elasticity, Young's modulus [kN/m^2]
E_0	Elastic modulus at the ground surface [kN/m^2]
EI	Bending stiffness [kNm^2]
EI_i	Beam element's bending stiffness [kNm^2]
E_{py}	Modulus of a parameter that relates p and y [kN/m^2]
E_{py_max}	Initial slope of a p-y curve [kN/m^2]
F	Force [kN]
F'_q	Single pile head's force vector in coordinate system 1'-2'-3' [kN]
f_{comp}	Compression force [kN]
F_f	Force due to the skin friction [kN]
f_i	Force vector's element [kN]

f'_i	Force vector's element in coordinate system 1'-2'-3'[kN]
f_M	Bending moment within a single pile [kNm]
f_m	Pile group efficient multiplier, p-multiplier [-]
f_{mi}	Reduction factor for a single pile i in a pile group [-]
F_q	Single pile's force vector [kN]
f_V	Shear force within a single pile [kN]
f_{tot}	Loading vector of a single pile [kN]
G	Shear modulus [kPa]
H	Height [m]
i	Object number [-]
I-II-III	Orthogonal coordinate system fixed to the pile cap, global coordinate system
J	Torsional bending stiffness [m^4]
J_e	Experimentally determined parameter, API-J parameter [-]
K_0	Coefficient of soil at rest [-]
K_A	Coefficient of active soil [-]
K_i	Stiffness matrix of a pile element i [kN/m]
$k_{i,j}$	Single pile head's stiffness matrix's element i,j [kN/m]
K_{py}	Initial slope of p-y curve [kN/m^3]
K_q	Single pile head's stiffness matrix [kN/m]
k_s	Lateral spring constant [kN/m]
L	Length [m]
L_a	L_{df} if the pile is in a frictional soil and L_{dc} if the pile is in a cohesive soil [m]
L_d	Deflecting length of a pile in soil [m]
L_{dc}	Single pile's deflection length, when the pile is in cohesive soil [m]
L_{df}	Single pile's deflection length, when the pile is in frictional soil [m]
L_r	Free length L_f divided by deflecting pile length in soil L_d [-]
L_f	Pile length above ground surface, free pile length [m]
LVDT	Linear Variable Differential Transformer
M	Moment [kNm]
m	Pile head fixity parameter [-]
$M_{1,2,3}$	Mindlin's elastic space coefficient. [kN/m]

$M_{i,j}$	Inertial bending moment within a pile element [kNm]
M_s	Moment force due to skin friction [kNm]
n	Object numbering [-]
ø	Inertial friction angle of soil [°]
O	Origin
O.D.	Outer diameter of a pile
p	Reaction from the soil due to lateral deflection of the pile, soil resistance [kN/m]
p_c	Soil resistance in clay [kN/m]
p_{cd}	Soil resistance in clay, wedge method [kN/m]
p_{ct}	Soil resistance in clay, compression method [kN/m]
p_{gp}	Group pile resistance [kN/m]
p_m	Soil resistance at which 50 percent of the shear strength has mobilized [kN/m]
P_q	Global loading vector of a single pile [kN]
p_{red}	Reduced soil resistance [kN/m]
p_s	Soil resistance in sand [kN/m]
p_{sp}	Single pile resistance [kN/m]
p_u	Ultimate soil resistance [kN/m]
p_x, p_y	Lateral soil resistances at directions x and y [kN/m]
Q	Perpendicular force to a pile axis [kN]
q	Pile number [-]
q_{tip}	Ultimate pile tip loading to soil [kPa]
R	Pile group's system loading vector [kN]
R_1, R_2	Distances between two points [m]
R_i	Lateral point force to a single pile's element's node point [kN]
r_i	Pile group loading vector element i [kN]
s	Pile spacing [m]
S	System stiffness matrix [kN/m]
s_u	Operational undrained shear strength of a geomaterial [kN/m^2]
t	Axial skin friction [kPa]
t_{comp}	Axial skin friction in compression [kPa]
t_{max}	Ultimate axial skin friction [kPa]

t_{res}	Residual axial skin friction [kPa]
t_{tens}	Axial skin friction in tension [kPa]
tz_{res}	Axial deflection of a pile where the residual skin friction is achieved [m]
T	Transpose of a matrix
U	Pile group deflection vector [m]
u_i	Pile group deflection vector element i [m]
$V_{i,j}$	Inertial shear force within a pile element i,j [kN]
W	Weight [kN]
x	Coordinate along the pile measured from the pile head [m]
x_i	Single pile head's displacement vector's element i [m]
X_q	Single pile head's displacement vector [m]
y	Lateral displacement [m]
y_0	Gap's width [m]
y_{50}	Lateral displacement at which 50 percent of the shear strength has mobilized [m]
y_m	A half of the value of lateral displacement from the point where the ultimate soil resistance occurs [m]
y_u	Lateral deflection at which the maximum soil resistance takes place [m]
z	Depth [m]
z_1, z_2, z_3	Single pile head's coordinates in global coordinate system I – II – III [m]
z_e	Equivalent depth
z_r	Relative depth [m]
z_{tip}/D	Factor relating deflection at max tip bearing with diameter [-]
α	Angle between coordinate axes 1-2 and 1'-2' [°]
β	Angle between coordinate axes 3 and 3' [°]
β_a	Group efficiency factor for piles in a row [-]
β_{bl}	Group efficiency factor for leading pile in a pile line [-]
β_{bt}	Group efficiency factor for trailing piles in a pile line [-]
β_{ni}	Group effect reduction factor [-]
β_s	Group efficiency factor for skewing piles [-]
γ'	Effective unit weight [kN/m^3]

γ	Unit weight [kN/m^3]
δ_i	Displacement vector of a single pile element [m]
δ_{tot}	Displacement vector of a single pile [m]
ε	Strain corresponding to compressive stress [-]
ε_{50}	Strain at which 50 percent mobilization in triaxial test [-]
θ	Batter angle of a pile [°]
λ	Time effect multiplier [-]
ν	Poisson's ratio [-]
ν_i	Lateral displacement of a single pile element's node point [m]
ν_x, ν_y, ν_z	Pile element's node point's displacements to directions x, y and z [m]
$\rho_{x,y,z}$	Displacements to directions x, y and z [m]
σ_y	Yield stress [kPa]
φ	Angular displacement [°]
$\varphi_{i,j}$	Angular displacement of a pile element i,j [°]

1 Background

1.1 Introduction

Many buildings and structures require the use of deep foundations to utilize the bearing capacity of stronger soil layers. Pile groups are one particular type of deep foundation commonly used for large structures. In addition to vertical loads that must be sustained by the piles, significant lateral loads may be present and must be accounted for in design. These lateral loads can come from variety of sources such as wind forces, collisions, wave or ice impact, earthquake shaking, liquefaction and slope failure.

1.2 Response of Soil from a Pile under Lateral Loading

Soil response to a given lateral load is modeled by developing a relationship between the pile's lateral deflection and the resistance of the soil. This relationship is represented graphically in a p-y curve, where y represents the lateral displacement of the pile and p represents the soil resistance per unit length of the pile. Each layer of soil that the pile passes through will have a different amount of resistance depending on the strength of the soil, and therefore a different p-y curve. These various p-y curves are modeled as non-linear springs representing the various soil layers along the length of the pile as illustrated in Figure 1.1.

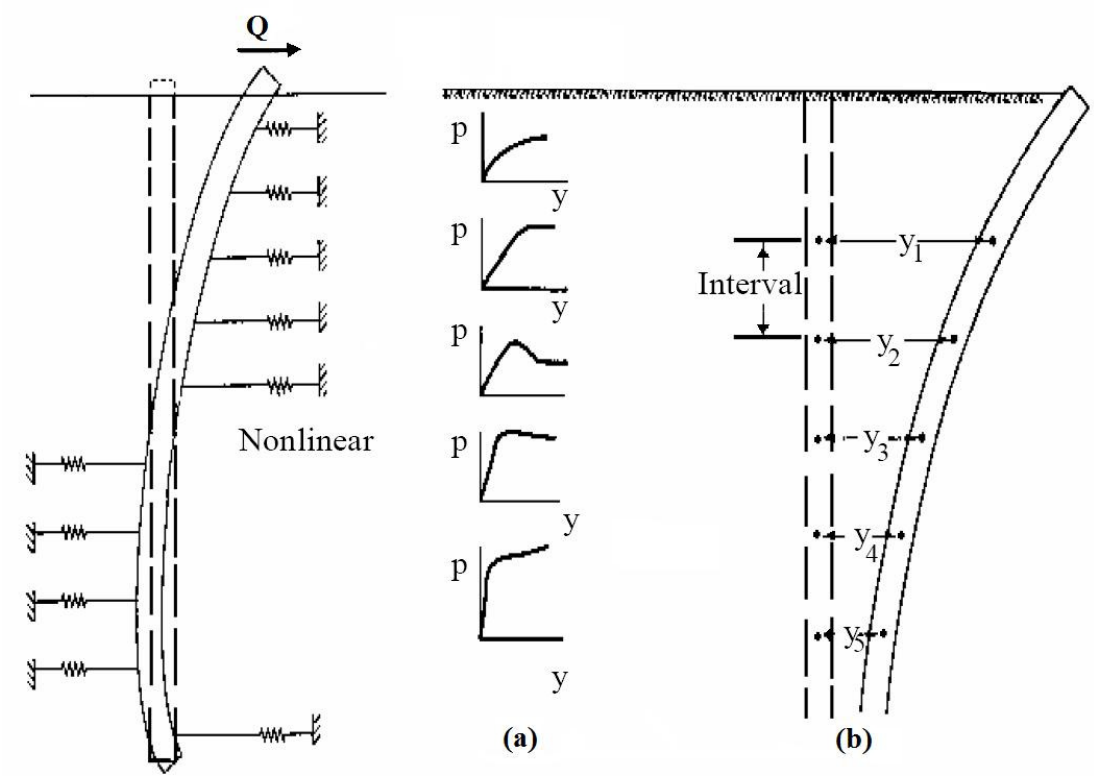

Figure 1.1: Illustration of the p-y curve approach for evaluating lateral pile behavior. (Christensen, 2006)

In addition, the surrounding soil causes skin friction to the bending pile, which effects to the pile's angular transition. This phenomenon may be modeled with non-linear M_s- φ springs attached at the centerline of the pile axis (Figure 1.2), where M_s represents the moment force due to the skin friction at the pile axis and φ stands for angular transition.

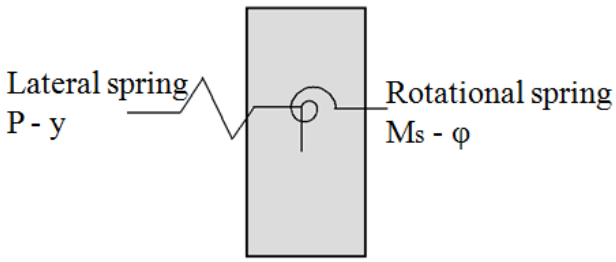

Figure 1.2: Spring elements attached to a single pile element's axis (Niraula, 2004)

From a modeling point of view, an approximately similar phenomenon occurs as the pile deflects laterally. It is assumed that until some specific depth H, from the ground

surface, the soil moves up and out at the ground surface as a wedge. An up-moving soil wedge, with external forces is shown in Figure 1.3.

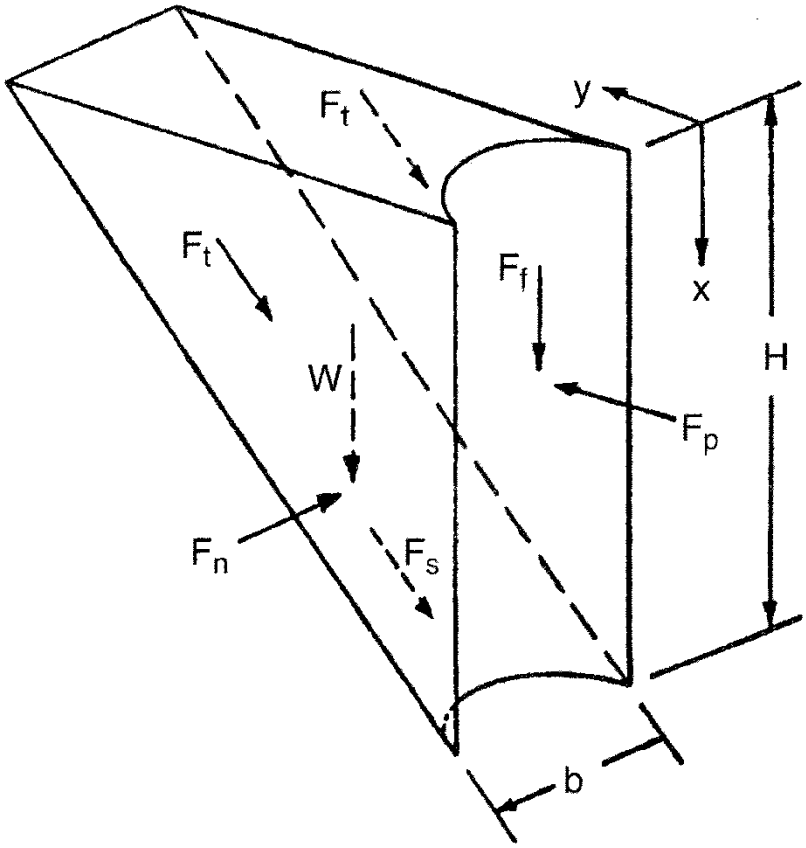

Figure 1.3: Moving soil wedge with external forces. (Reese Lymon, 2006)

As the wedge moves upward, it creates a skin friction F_f to passive side of the pile surface, which then causes momentous forces to the pile axis. This phenomenon may as well be modeled with non-linear M_s spring element attached to the pile axis as shown in Figure 1.2.

These last two mentioned phenomena are usually negligible, especially with slender piles and loose soil, but the details are discussed in Chapter 4.

1.3 Single Pile's Efficiency in a Laterally Loaded Pile Group

Today, piles are sometimes used as single-piles but are usually put into pile-groups in order to strengthen load resistance. Although a pile-group strengthens overall

lateral load resistance it can weaken the individual pile response of the piles in the group. The overall lateral load is divided among each of the piles in the group. Each pile pushes against the soil behind it creating a shear zone in the soil. These shear zones begin to enlarge and overlap as the lateral load increases. More overlapping occurs if the piles are spaced very closely together. When overlapping occurs between two piles in the same row it is called "edge effects" and when overlapping occurs between piles in different rows it is known as "shadowing effects." All of these "group interaction effects" result in less lateral resistance per pile. Figure 1.4 displays the shear zones and the various group effects that occur within a laterally loaded pile-group. The leading row of piles has the highest resistance of any of the rows in the group since it only experiences edge effects. The piles in the leading row are therefore only slightly less resistant than a single isolated pile under the same loading. The piles in the other rows, 2 and 3, have even lower resistance because they experience edge effects and shadowing effects. The gaps that form behind the piles also assist in decreasing the resistance of the piles behind them.

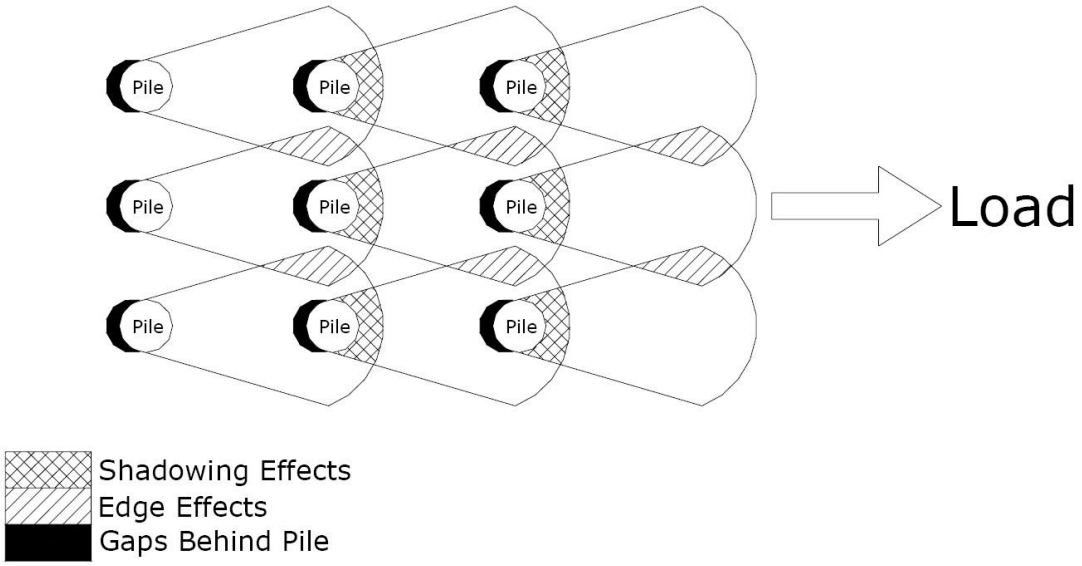

Figure 1.4: Illustration of shadow and edge effects on a laterally loaded pile group. (Walsh, 2005)

Bogard and Matloc (1983) present a method in which the p-y curves for a single pile can be modified with a p-multiplier (f_m), to take the group effect into account. P-multiplier is simply a reduction factor used to decrease the p-value (soil resistance) in the p-y curve. The p-values for the group piles are therefore found by multiplying the

p-value of the single pile by a p-multiplier (f_m). This concept of p-multipliers is displayed in Figure 1.5. P-multipliers are dependent on soil conditions and pile spacing. As piles are spaced farther and farther apart the pile interaction decreases and therefore the p-multipliers should increase to a maximum value of 1.0. This method is presented with more details in Chapter 7.2.

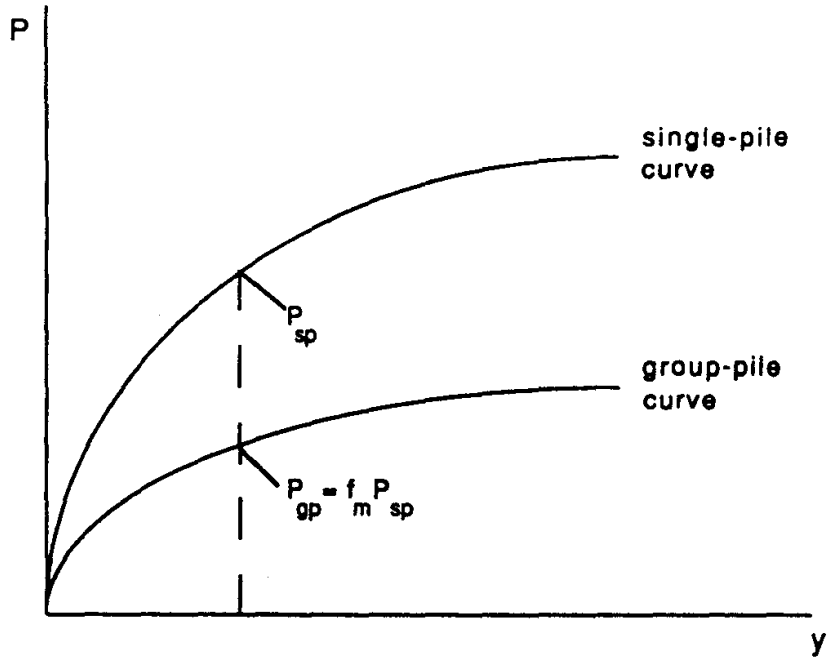

Figure 1.5: Comparison of p-y curves for a single pile (p_{sp}) to a group pile (p_{gp}). (Bogard and Matloc, 1983)

There is an alternative modeling technique for analyzing pile-soil-pile interaction. This method models the soil as an elastic mass, where displacement of a single pile element's node point, causes stresses to the surrounding soil and thereby affects the node points of the surrounding piles. This method is based on Mindlin-solutions and will be discussed deeper in Chapter 7.3.

2 Previous Research on Full-Scale Tests

2.1 Introduction

Full-scale tests are generally believed to provide the most accurate results but are rare because of the large costs required to successfully perform a test. The next section will discuss the results of previous research by full scale tests.

2.2 Lateral Pile-Loading Tests (Feagin, 1937)

Tests were conducted in Alton, Illinois at Lock and Dam No. 26 with the results as well as discussions published by Feagin (1937). The tests were conducted in Mississippi River sand on concrete and timber single piles and pile groups of four, twelve, and twenty piles with a pile head fixity provided by a pile cap. The main purpose of the tests was simply to "secure data on the movement of timber and concrete pile groups of various sizes when subjected to lateral loads." All pile groups were arranged in a 2 x n configuration and spaced about 3 pile diameters. Feagin (1937) concluded that for all lateral movements less than 6 mm, average resistance per pile is similar for all pile groups. For larger movements, the average pile resistance decreases as the number of piles in the group increases.

2.3 Full-Scale Lateral Load Tests of Pile Groups (Kim and Brungraber, 1976)

Kim and Brungraber (1976) performed full-scale lateral load tests in cohesive soil in Pennsylvania. The soil profile consisted of relatively uniform clay underlain by fractured limestone. Three 2 x 3 pile groups spaced at 3.6D and 4.8D and two isolated single piles were formed with 10BP42 steel piles in a fixed head condition. One of the pile groups had some of the piles battered and one single isolated pile was battered. Pile groups with some battered piles provided more resistance with less bending stresses. Increased spacing increased the resistance of the pile group but the average load per pile for the group test was lower than that for a single isolated pile at the same deflection.

2.4 Pile Cap Interaction from Full-Scale Lateral Load Tests (Kim et al., 1979)

Kim et al. (1979) conducted another test on the same pile groups and single piles used by Kim and Brungraber (1976). In these tests, 100 mm of the soil from under the cap was removed and the load-deflection curves were compared the results with the previous test. Analysis confirmed the result from the previous tests that increasing the spacing or battering the piles can improve of efficiency of the pile group. The absence of contact of the soil underneath cap became significant at relatively high lateral loads (greater than 74 kN/pile) but only when less than half of the piles were battered. The removal of the soil resulted in deflection and maximum bending moments that were nearly twice what was observed with the soil contact. Group efficiencies were determined by comparing the lateral resistance of a single isolated pile to the resistance of fixed head pile within the group. The group efficiency decreased and approached unity at the pile top. Group efficiency greater than 1.0 is attributed to the restraint of pile cap causing double curvature bending for the piles in the group.

2.5 Pile Group Behavior under Long-Term Lateral Monotonic and Cyclic Loading (Meimon et at., 1986)

Full-scale lateral load tests were conducted by Meimon et al. (1986) with 3 x 2 pinned head pile groups spaced at three pile widths (I-beam cross section) in the loading direction and two pile widths normal to the load direction. The piles used were box-shaped I beams with a height of 0.270 m and a width of 0.284 m and were driven to a depth of 7.5 m. The subsurface profile contained 1 m of high plastic clay underlain by 4 m of low plasticity clay and 4 m of silty sand.

Results showed there were increased group interaction effects leading to reduced stiffness as the load was increased. Higher shear force and bending moment are measured in the lead row piles compared to the trailing row piles, although, the shear force and bending moments were similar for individual piles within a given row. Meimon et al. (1986) concluded that the group interaction factors for each row approached unity with large number of load cycles.

2.6 Cyclic Lateral Loading of a Large-Scale Pile Group (Brown et al., 1987)

Tests were performed on nine closed-ended steel pipe piles (273 mm O.D., 9.27 mm wall thickness) in Houston, Texas. The subsurface profile consisted of stiff, overconsolidated clay of depth of 13.1 m with water above the ground surface. The piles were arranged in a 3 x 3 pattern spaced at 3D in both directions.

Brown et al. (1987) concluded that the depth of the maximum bending moment increased from front row to back row. The bending moments were greater for the piles in the group than the single pile and occurred at greater depths. The front and middle row experienced similar maximum bending moments whereas the back row was lower in magnitude. P-y curves were generated based on the Winkler-type soil model with polynomial curve fitting to the bending moment data.

The maximum soil resistance for piles within the group was significantly reduced compared to the single pile for both static and cyclic loadings. The pile group deflection was significantly greater than the single pile under the same average load per pile. Brown et al. (1987) concluded that the elasticity-based methods did not accurately predict the distribution of load within a pile group and that empirical modification factors were necessary.

2.7 Lateral Load Behavior of Pile Group in Sand (Brown et al., 1988)

A full-scale test was conducted by Brown et al. (1988) on a 3 x 3 pile group in medium dense sand placed and compacted to the depth of 2.9 m underlain by very stiff clay. The sand had relative density (D_r) of 50%. The same type and size of steel pipe pile was used for this test as was used the full-scale test conducted by Brown et al. (1987). The pile group was spaced at 3D on centers. In addition, a single isolated pile was tested for comparison. The piles were subjected to two-way cyclic lateral loading.

Brown et al. (1988) concluded that the pile group “was observed to deflect significantly more than the isolated single pile when loaded to a similar average load

per pile." In addition, the row position had an effect on the efficiency of the particular piles. The front row piles exhibited stiffer responses than the trailing row. The "shadowing" effect was more significant in the sand compared to the clay as was reported in Brown et al. (1987). However, when the piles were subjected to two-way cyclic loading, group effects were still significant in the sand. This is contrary to the reduced significance of "shadowing" with cyclic loading that was observed in clay.

The concept of p-multipliers (f_m) was introduced to modify the single pile p-y curve to generate the group pile p-y curve. This was performed at various depths by methods of visual curve fitting of p-y curves. The results of the p-multiplier determination are presented in Figure 2.1. Brown et al. (1988) suggested using p-multipliers of 0.8, 0.4 and 0.3 for the front, middle, and back rows, respectively.

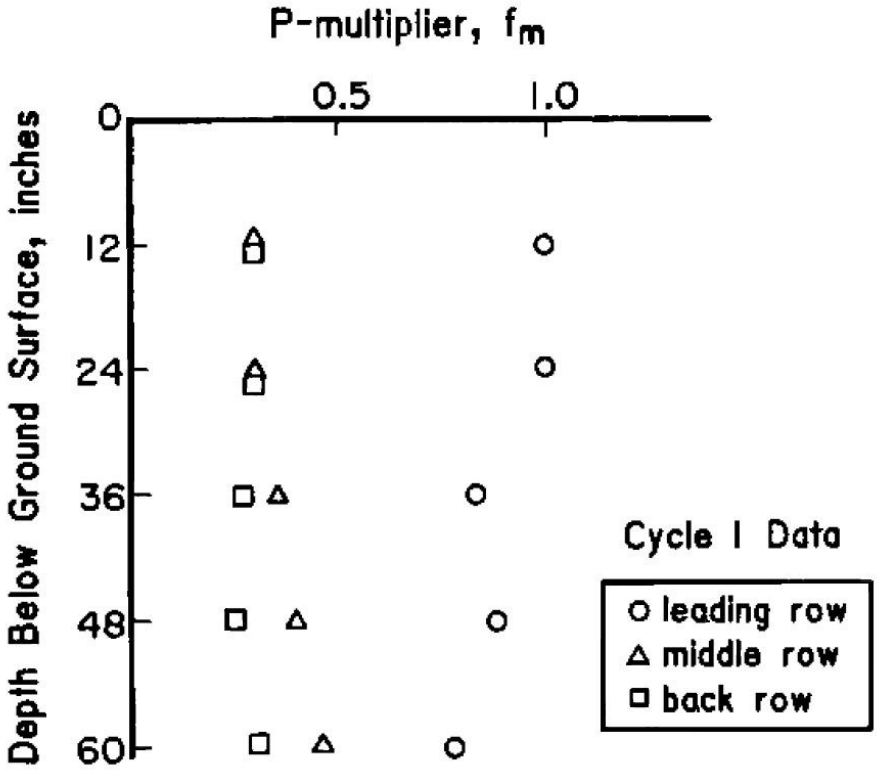

Figure 2.1: Experimental p-multipliers (f_m) vs. depth. (Brown et al., 1987)

2.8 Evaluation of Laterally Loaded Pile Group at Roosevelt Bridge (Ruesta and Townsend et al., 1997)

Full-scale lateral load test was conducted by Ruesta and Townsend (1997) on pre-stressed concrete piles with an 87 mm square cross section. Two pile groups in a free-head condition and one in a fixed-head condition, were arranged in 4 x 4 pattern spaced at 3D on centers in each direction. A single pile was also tested for comparison. The soil profile consisted of loose sand to depth of 4 m overlaying cemented sand. The group load-deflection efficiency was 80%.

The back-calculated p-multipliers for the free-head group were determined to be 0.8, 0.7, 0.3, and 0.3 from leading to trailing rows respectively with an overall group p-multiplier of 0.55. Similar results were obtained for the fixity-head group. Ruesta and Townsend et al. (1997) also concluded that the outer piles within a row took more loads that the inner piles attributed to shadowing as well as pile driving sequence. For given load, the maximum bending moments for all rows were within 15 % of each other with lower bending moments in the trailing rows.

2.9 Lateral Load Behavior of Full-Scale Pile Group in Clay (Rollins et al., 1998)

Rollins et al. (1998) concluded tests on a 3 x 3 pile group spaced at 2.8D with a pinned-head connection. The soil consisted of soft to medium-stiff clays overlaying dense sand. A single pile test was conducted to provide a comparison. Closed-end steel pile piles with an inner diameter of 0.305 and 9.5 mm wall thickness were used. The pile group deflection turned out to be more than two times the single pile for the same average load applied. The p-multiplier approach was used to provide a match between computed and measured results. The p-multipliers were determined to be 0.6, 0.38, and 0.43 for the front, middle and back rows respectively.

2.10 Static and Dynamic Lateral Load Behavior of Pile Group Based Full-Scale Testing (Rolls et al., 2003a)

Rolls et al. (2003a) conducted a full-scale test on a 3 x 3 pile group spaced 5.65D. The subsurface profile consisted of low-plasticity silts and clays. The tests were conducted on 324 mm O.D. closed-end steel pipe piles. To account for the reduced resistance of the pile group compared to a single isolated pile, p-multipliers were backcalculated using pile group program GROUP (Reese and Wang, 1996). Table 2.1 outlines the p-multipliers obtained from Rollins et al. (1998) and Rollins et al. (2003a).

Table 2.1: Summary of back-calculated p-multipliers (Rolls et al., 1998, 2003a)

Pile Spacing / Pile Diameter	Front-Row p-multiplier (f_m)	Middle-Row p-multiplier (f_m)	Back-Row p-multiplier (f_m)
2.8	0.6	0.38	0.43
5.65	0.98	0.95	0.88

Rollins et al. (2003a) concluded that the lateral resistance of a pile within a closely spaced pile group is a function of row location within the group and not within the row. The "group effects" were less noticeable as spacing increased from 2.8D to 5.65D.

2.11 Response, Analysis, and Design of Pile Groups, Subjected to Static and Dynamic Lateral Loads (Rollins et al., 2003b)

Full-scale tests were performed in Salt Lake City, Utah several miles south of the test site for Rolls et al. (1998, 2003a). The soil profile at this site consists mainly of medium stiff clays with some sand layers close to the surface. The medium stiff clay is underlain by soft clay with some layers of silty clay and sand. The full-scale tests were performed on three single piles and four pile groups spaced at 3.0, 3.3, 4.4 and 5.6 pile diameters. The free-headed pile groups ranged from a 3 x 3 to a 3 x 5 configuration.

Several conclusions were drawn from the full-scale tests. First, the lateral resistance of the piles within the group was a function of row location. All the piles within a

row carried the same amount of load. Additionally, the front row piles carried more load than the trailing row piles with the second row carrying the next highest load followed by third row. However, the fourth and fifth rows carried approximately the same load as the third with the back row carrying a slightly higher load than the preceding row. Spacing also affected the lateral resistance of the pile groups. The group spaced at 5.6D showed very little reduction on lateral resistance. However, lateral resistance consistently decreased with closer spacing.

The maximum bending moments in the trailing rows tended to be higher for a given load and occurred at a lower depth due to group effects causing reduced soil resistance close to the surface. However, for a given deflection maximum bending moments in the lead row were higher than the trailing row, which can be attributed to the lower loads carried by the trailing rows for a given deflection level.

Piles of different diameters were tested. One pile group had piles with 610 mm O.D. at 3D spacing and the other remaining groups had piles with 324 mm O.D. One pile group with the lateral outer diameter was spaced at 3.3D. Comparisons of these two pile groups resulted in similar p-multipliers suggesting that pile stiffness has little effect on p-multipliers. The p-multipliers were back calculated using LPILE plus 4.0 (Reese et al., 2000) to match the single pile and GROUP (Reese and Wang, 1996) to determine p-multipliers. Analyses were performed with the test results being compared with GROUP (Reese and Wang, 1996) and LPILE plus 4.0. The default p-multipliers were needed. The summary of back calculated p-multipliers is included on Table 2.2.

Table 2.2: Summary of back-calculated p-multipliers. (Rollins et al., 2003b)

Row Spacing Center to Center	Pile Diameter (mm)	p-multipliers				
		Row 1	Row 2	Row 3	Row 4	Row 5
5.6	324	0.94	0.88	0.77	---	---
4.4	324	0.90	0.80	0.69	0.73	---
3.3	324	0.90	0.61	0.45	0.45	0.46 to 0.51
3.0	610	0.82	0.61	0.45	---	---

Table 2.3: Summary of reported full-scale test p-multipliers

Researchers	Soil Type	Comments	Spacing (Diameters)	p-multipliers				
				Row 1	Row 2	Row 3	Row 4	Row 5
Meimon et al. (1986)*	stiff silty clay	---	3	0.90	0.50	---	---	---
Brown et al. (1987)*	stiff clay	30 mm deflection	3	0.70	0.60	0.50	---	---
Brown et al. (1987)*	stiff clay	50 mm deflection	3	0.70	0.50	0.40	---	---
Brown et al. (1988)	medium dense sand over clay	---	3	0.80	0.40	0.30	---	---
Ruesta and Townsend (1997)	sand over cemented sand	---	3	0.80	0.70	0.30	0.30	---
Rollins et al. (1998)	silts and soft clays	---	2.82	0.60	0.38	0.43	---	---
Rollins et al. (2003a)	silts and soft clays	50 mm deflection	5.65	0.98	0.95	0.88	---	---
Rollins et al. (2003a)	silts and soft clays	99 mm deflection	5.65	0.90	0.80	0.63	---	---
Rollins et al. (2003b)	medium stiff clays with sand	---	3	0.82	0.61	0.45	---	---
Rollins et al. (2003b)	medium stiff clays with sand	---	3.3	0.82	0.61	0.45	0.45	0.46
Rollins et al. (2003b)	medium stiff clays with sand	---	4.4	0.90	0.80	0.69	0.73	---
Rollins et al. (2003b)	medium stiff clays with sand	---	5.6	0.94	0.88	0.77	---	---
* Reported by Brown and Shie (1991)								

2.12 Conclusions from Previous Research

The main conclusions that can be drawn from the review of the literature on the subject of laterally loaded piles are as follows:

1. Group or "shadow effect" in closely spaced piles decrease the total lateral resistance of a pile group.
2. The pile group deflects significantly more than the isolated single pile when subject to the same average load per pile
3. Group effect are relatively insignificant at small deflections but become more pronounced at higher loads or deflection levels. This effect eventually stabilizes at a constant level.
4. Group effects are significant for piles in a group spaced at about three diameters. These effects lessen with increased spacing.
5. The lead row in the direction of load tends to perform similar to a single isolated pile with the decrease in lateral resistance becoming more pronounced in subsequent rows. Group effects relative to location within a row are negligible as most of the research show.
6. Group effects become more negligible for row spacing greater than six to eight pile diameters. The group effects of pile spacing within a row are negligible at about three pile diameters.
7. Bending moments in closely spaced pile groups tend to be greater than in a single isolated pile for the same load per pile.
8. The peak bending moment per pile load is greater on the trailing rows than the lead row. Also, the peak bending moments peak at greater depths in the lead row. In cyclic loading, the bending moment increases and occurs at a greater depth.
9. The p-multiplier concept introduced by Brown et al. (1988) is a valid method to match the total group load as well as row distribution up to large deflections. Some researchers show that p-multipliers are independent of cyclic effects, pile-head fixity, and soil density.
10. Computer programs such as GROUP (Reese and Wang, 1996) do not provide accurate prediction of field response suggesting the need for modification for various soil and type conditions.

11. GROUP with user-defined p-multipliers that are determined from design curves (p-multipliers vs. pile spacing) based on full-scale tests can effectively predict pile performance.

3 Characteristics of p-y Curves

3.1 Introduction

A typical p-y curve is shown in Figure 3.1 (a), it is meant to represent the soil resistance-soil transition case where a short-term monotonic loading or static lateral loading is applied to a pile. The three curves in Figure 3.1 show a straight-line relationship between p and y from the origin to the point a, assuming that the strain of soil is linearly related to stress for small strains. The assumption follows that p is linearly related to y in small deflections. This assumption is used in Chapter 5, with linearly elastic modeling of a single pile.

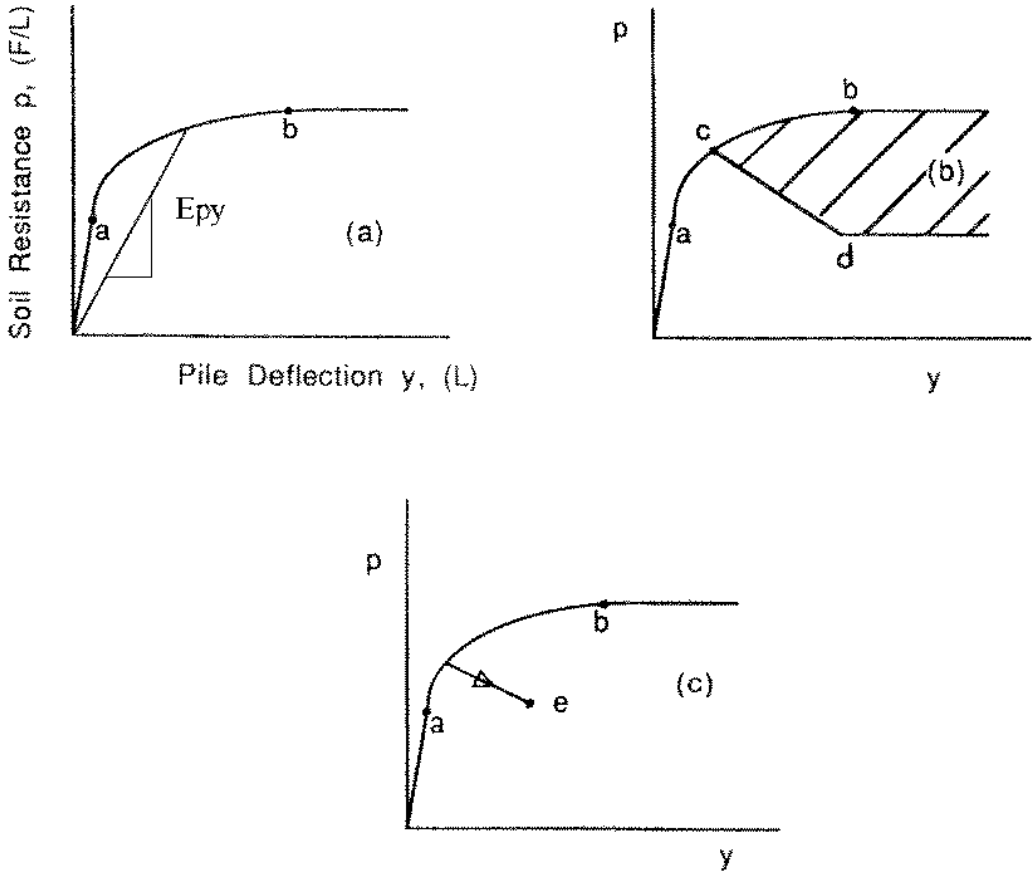

Figure 3.1: Conceptual p-y curves (a), (b), and (c). (Reese et al., 2006)

The portion of the curve in Figure 3.1 (a) from point a to point b shows that the values of p is increasing at a decreasing rate with respect to y. This behavior reflects

the nonlinear portion of the stress-strain curve for natural soil. The horizontal portion of the p-y curve in Figure 3.1 (a) indicates that the soil is behaving as viscous material, with no increase of shear strength with increasing strain. The shaded portion of the p-y curve shown in Figure 3.1 (b), shows decreasing values of p from point c to d. The decrease reflects the effect of cyclic loading, or strain softening behavior of overconsolidated clay. The curves in Figure 3.1 (a) and Figure 3.1 (b) are identical up to point c, which implies that cyclic loading has little or no effect on a p-y curve for small deflections. The loss of resistance represented by the shaded area is related to the number of loading cycles.

The possible effect of lateral loading of a pile in normally consolidated clay is shown in Figure 3.1 (c), where there is an increase in y with a loss of p. For a pile in normally consolidated clay, lateral loading will cause an increase in porewater pressure and deflection will increase as the porewater pressure is dissipated. The decrease in the value of p, suggests that resistance is shifted to other elements along the pile as deflection occurs at a particular point. A prediction of the effect of sustainable loading for piles in soft or normally consolidated clays must be developed from field testing or estimated using the theory of consolidation.

3.2 Recommendations for Creating p-y Curves

3.2.1 Introduction

Some recommendations by Reese et al. (2006), for non-linear p-y curves will be presented in this chapter on soils under static loading conditions. The recommendations are based on mathematics as much as possible but, more importantly, are based strongly on full-scale experiments for granular soil and overconsolidated clay. Field tests are recommended for piles in normally consolidated clay under sustained loading.

Prediction of the p-y curves for a particular solution must be given careful and detailed attention, starting with the acquisition of data on soils at the site, with particular reference to the role of water, use of soil mechanics to the extent possible, consideration of the nature of the loading at the site.

3.2.2 Soft Clay Short-Term Static Load in the Presence of Free Water

The following step-by-step procedure is recommended for computing values for p-y curves for soft clay in presence of free water. The procedure below is for short-term static loading and is illustrated in Figure 3.2 (a).

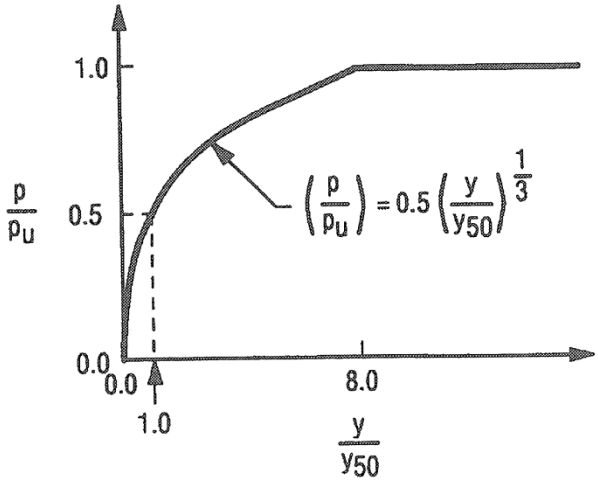

Figure 3.2: Characteristic shape of p-y curve for soft clay in the presence of free water and under static loading. (Matlock, 1970)

1. Obtain the best possible estimate of variation of undrained shear strength c_u and submerged unit weight with depth. Also, obtain the value of the strain correspondence to one-half of the maximum principal stress difference. If no stress-strain curves are available, typical values of ε_{50} are given in Table 3.1.
2. Compute the ultimate soil resistance per unit length of pile, using the smaller of the values given by the following equations (3.1) and (3.2).

$$p_u = \left(3 + \frac{\gamma'}{c_u} + \frac{J_e}{b} \cdot z \right) \cdot c_u \cdot b \tag{3.1}$$

$$p_u = 9 c_u \cdot b \tag{3.2}$$

where

γ' is average effective unit weight from ground surface to p-y curve

z is depth from ground surface to p-y curve

b is width of pile

J_e is experimentally determined parameter, normally from 0.25 to 0.8

Table 3.1: Representative Values of ε_{50}. (Reese et al., 2006)

Consistency of Clay	Undrained Shear Strength [kPa]	ε_{50}
Very soft	< 12	0.02
Soft	12-24	0.02
Medium	24-48	0.01
Stiff	48-96	0.006
Very stiff	96-192	0.005
Hard	> 192	0.004

Matlock (1970) stated that the value of J_e was determined to be 0.5 for soft clay and about 0.25 for medium clay. The value of 0.5 is frequently used for J_e. The value of p_u is computed at each depth where a p-y curve is desired based in shear strength at that depth.

3. Compute the deflection y_{50} at one-half of the ultimate soil resistance from the following equation (3.3):

$$y_{50} = 2.5 \cdot \varepsilon_{50} \cdot b \tag{3.3}$$

4. Compute points describing the p-y curve from the following relationship (3.4):

$$\frac{p}{p_u} = 0.5 \left(\frac{y}{y_{50}} \right)^{\frac{1}{3}} \tag{3.4}$$

The value of p remains constant beyond $y = 8y_{50}$. Equation (3.4) shows the slope of the p-y curve to be infinite at the origin, an anomalous result. The reasonable suggestion is made that the initial slope of the p-y curve be established by using K_{py} from Table 3.2.

Table 3.2: Representative Values of K_{py} for Clays. (Reese et al., 2006)

Undrained Shear Strength	50-100	200-300	300-400	kPa
K_{py}	135	270	540	MN/m^3

3.2.3 Stiff Clay Short-term Static Loads in the Presence of Free Water

The following procedure is for forming a p-y curve of stiff clay in the presence of free water. Characteristic shape of a curve is illustrated in Figure 3.3.

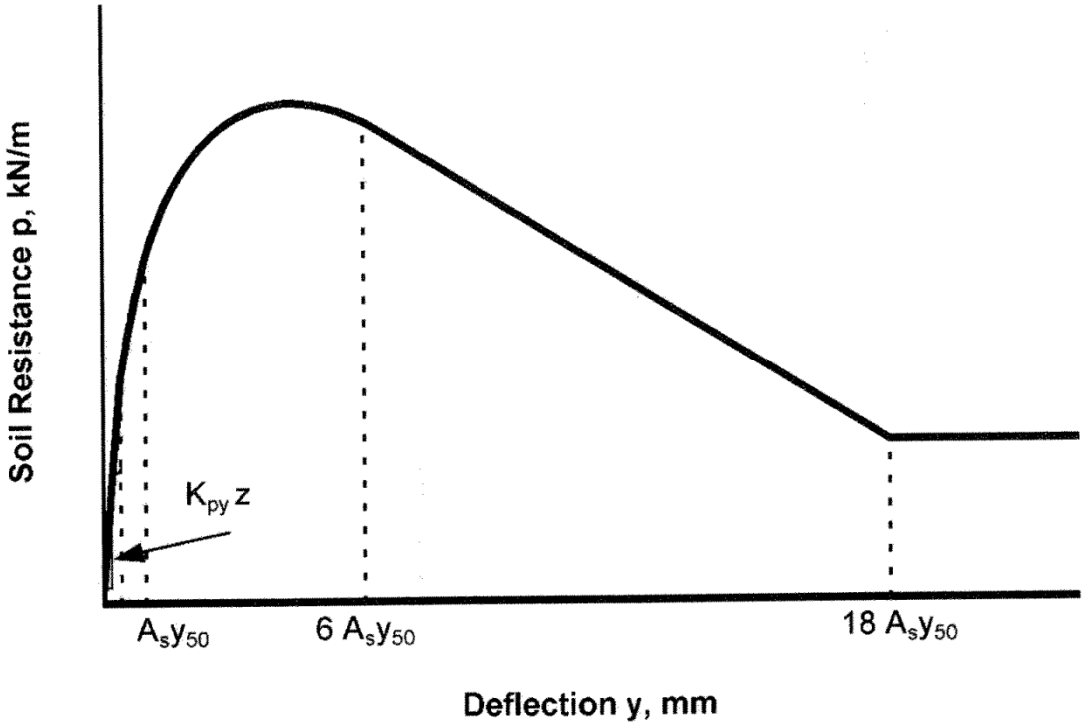

Figure 3.3: Characteristic shape of p-y curves for static loading in stiff clay in the presence of free water. (Reese et al., 2006)

1. Obtain values of undrained shear strength c_u, submerged unit weight of soil γ', and pile diameter b.
2. Compute the average undrained shear strength c_{ua} over the depth z.
3. Compute the ultimate soil resistance per unit length of pile using the smaller of the values given by following equations (3.5) and (3.6):

$$p_{ct} = 2c_{ua} \cdot b + \gamma' bz + 2.83 c_{ua} \cdot z \tag{3.5}$$

$$p_{cd} = 11 \cdot c_u \cdot b \tag{3.6}$$

4. Choose the appropriate value of A_s from Figure 3.4 for shaping the p-y curves, where x is coordinate axis along the pile measured from the pile head.

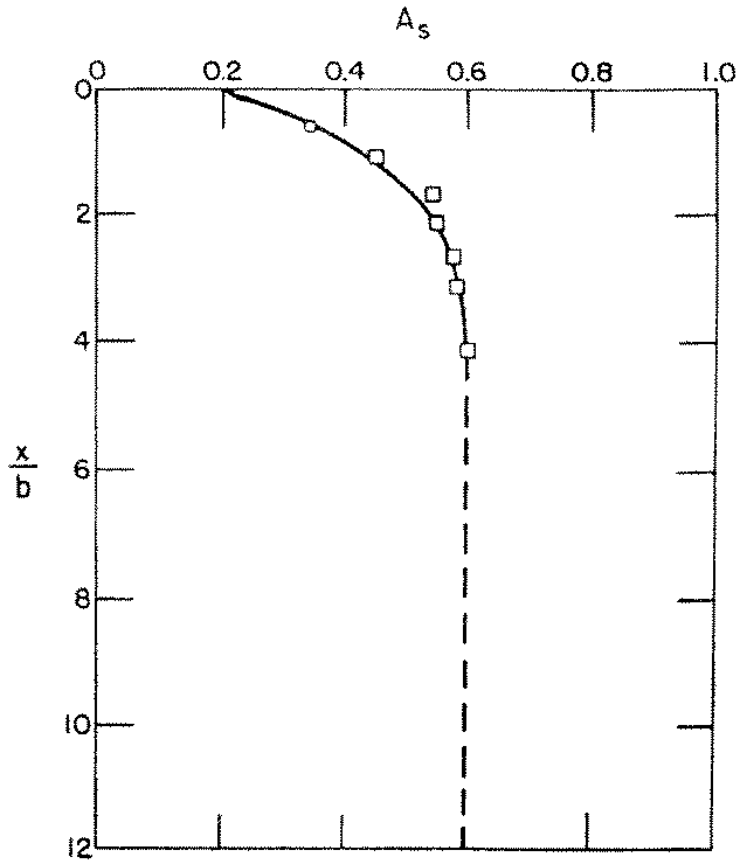

Figure 3.4: Values of constants A_s. (Reese et al., 2006)

5. Establish the initial straight-line portion of the p-y curve with equation (3.7):

$$p = \left(K_{py} \cdot z\right) \cdot y \tag{3.7}$$

6. Use the appropriate value K_{py} from Table 3.2.
7. Compute the following formula (3.8):

$$y_{50} = \varepsilon_{50} \cdot b \tag{3.8}$$

8. Use the appropriate value of ε_{50} from results of laboratory tests, or in the absence of laboratory tests, from Table 3.1.
9. Establish the first parabolic portion of the p-y curve, using the following equation (3.9) and obtaining p_c either from Equation (3.5) or from (3.6):

$$p = 0.5 \cdot p_c \left(\frac{y}{y_{50}}\right)^{0.5} \tag{3.9}$$

Equation (3.9) should define the portion of the p-y curve from the point of the intersection with Equation (3.7) to a point where y is equal to $A_s y_{50}$.

10. Establish the second parabolic portion of the p-y curve with Equation (3.10):

$$p = 0.5 \cdot p_c \left(\frac{y}{y_{50}} \right)^{0.5} - 0.0055\, p_c \left(\frac{y - A_s \cdot y_{50}}{y_{50}} \right)^{1.25} \quad (3.10)$$

Equation (3.10) should define the portion of the p-y curve from the point where y is equal to $A_s y_{50}$ to a point where y is equal to 6 $A_s y_{50}$.

11. Establish the next straight-line portion of the p-y curve with Equation (3.11):

$$p = 0.5\, p_c \left(6A_s\right)^{0.5} - 0.411 p_c - \frac{0.0625}{y_{50}} \cdot p_c \cdot \left(y - 6 \cdot A_s \cdot y_{50}\right) \quad (3.11)$$

Equation (3.11) should define the portion of the p-y curve from the point where y is equal to $6A_s y_{50}$ to a point where y is equal to $18A_s y_{50}$.

12. Establish the final straight-line portion of the p-y curve with Equation (3.12):

$$p = p_c \left(1.225 A_s^{\,0.5} - 0.75 \cdot A_s - 0.411 \right) \quad (3.12)$$

Equation (3.12) should define the portion of the p-y curve from the point where y is equal to $18A_s y_{50}$. For all larger values of y, see the following note.

Note: The step-by-step procedure is outlined, and Figure 3.3 is drawn, as if there is an intersection between Equations (3.7) and (3.9). However, there may be no intersection of Equation (3.7) with any of the other equations defining the p-y curve. Equation (3.7) defines the p-y curve until it intersects with one of the other equations; if no intersection occurs, Equation (3.7) defines the complete p-y curve.

3.2.4 Response of Stiff Clay with No Free Water

The correlations developed by Reese and Welch (1972) provide the basis of the method for forming p-y curve for static loading in stiff clay with no free water. The procedure is illustrated in Figure 3.5.

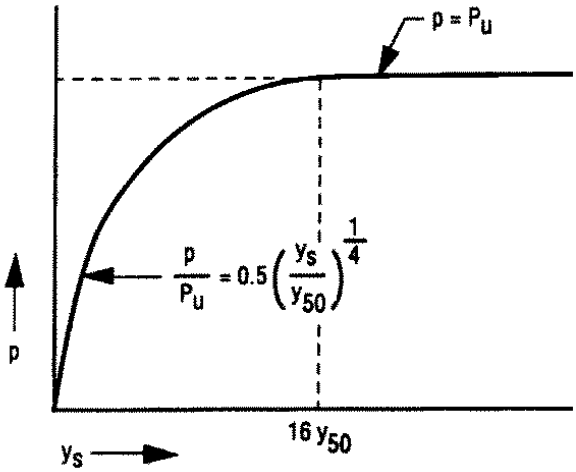

Figure 3.5: Characteristic shape of the p-y curve for static loading in stiff clay with no free water. (Reese et al., 2006)

1. Obtain values for undrained shear strength c_u, soil unit weight γ, and pile diameter b. Also obtain the values for ε_{50} from stress-strain curves. If no stress-strain curves are available, use a value of ε_{50} as given in Table 3.1.
2. Compute the ultimate soil resistance p_u per unit length of pile using the smaller of the values given by Equations (3.1) and (3.2) (In using Equation (3.1), the shear strength is taken as the average from the ground surface to the depth being considered and J_e is taken as 0.5. The unit weight of the soil should reflect the position of the water table.)
3. Compute the deflection y_{50} at one-half of the ultimate soil resistance from Equation (3.3)

   Compute points describing the p-y curve from the following relationship (3.13):

$$\frac{p}{p_u} = 0.5 \cdot \left(\frac{y}{y_{50}}\right)^{0.25} \tag{3.13}$$

   Beyond $y = 18y_{50}$, p is equal to p_u for all values of y.

3.2.5 Response of Sand Above and Below the Water Table

The following procedure is for forming a p-y curve of sand above or below the water table under short-term static loading. The procedure is illustrated in Figure 3.6.

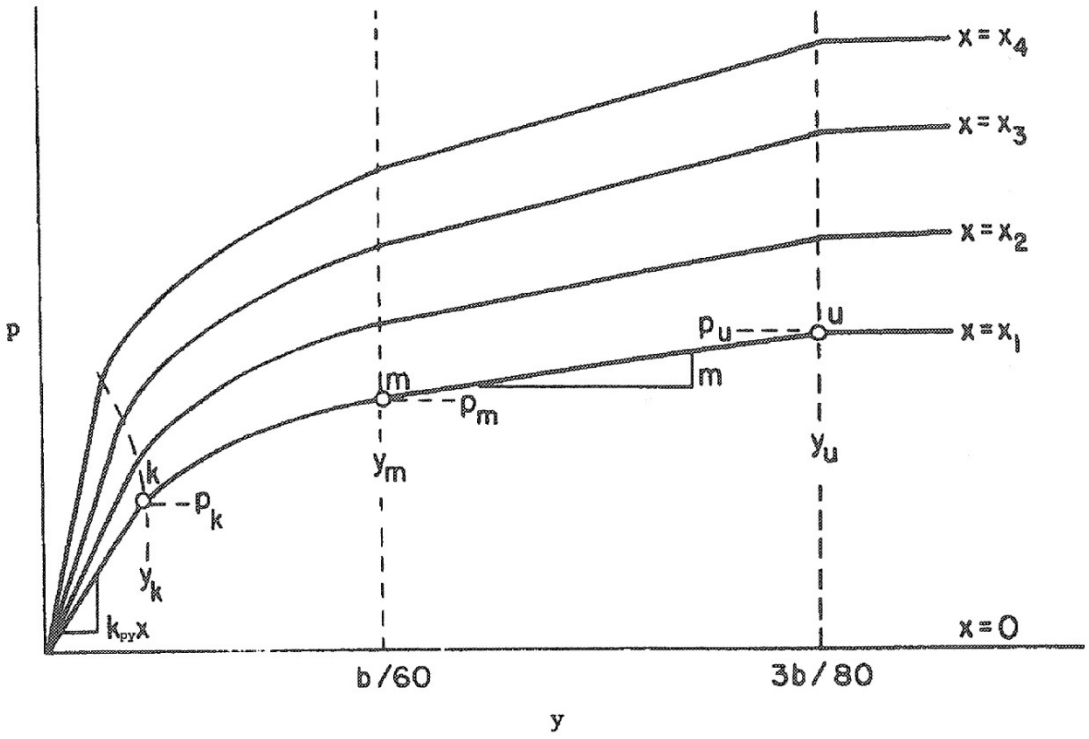

Figure 3.6: Characteristic shape of a family of p-y curves for static loading in sand. (Reese et al., 1974)

1. Obtain values for the inertial friction angle ø, the soil unit weight γ, and the pile width b (note: use buoyant unit weight for sand below the water table and total unit weight for sand above the water table). K_A is the coefficient of moving soil and K_0 is the coefficient of soil at rest.
2. Compute the ultimate soil resistance per unit length of pile using the smaller of the values given by the following equations (3.14) and (3.15):

$$p_{st} = \gamma \cdot z \cdot \left[\frac{K_0 \cdot \tan(\phi) \cdot \tan(\beta)}{\tan(\beta - \phi) \cdot \cos\left(\frac{\phi}{2}\right)} + \frac{\tan(\beta)}{\tan(\beta - \phi)} \cdot \left(b + z \cdot \tan(\beta) \cdot \tan\left(\frac{\phi}{2}\right) \right) \ldots \right.$$
$$\left. + K_0 \cdot z \cdot \tan(\beta) \cdot \left(\tan(\phi) \cdot \sin(\beta) - \tan\left(\frac{\phi}{2}\right) \right) - K_A \cdot b \right] \quad (3.14)$$

$$p_{st} = K_A \cdot b \cdot \gamma \cdot z \left(\tan(\beta)^8 - 1 \right) + K_0 \cdot b \cdot \gamma \cdot z \cdot \tan(\phi) \cdot \tan(\beta)^4 \quad (3.15)$$

In making the computation in Step 2, find the depth z_t at which there is an intersection at Equation (3.14) and (3.15). Above z_t use Equation (3.14). Below z_t use Equation (3.15).

3. Select a depth at which a p-y curve is desired.

Establish y_u as 3b/80. Compute p_u by the following equation (3.16):

$$p_u = A'_s \cdot p_s \tag{3.16}$$

Use the appropriate value of A'_s from Figure 3.7 for the particular nondimensional depth. Use the appropriate equation for p_s, Equation (3.14) or Equation (3.15), by referring to the computation in Step 3.

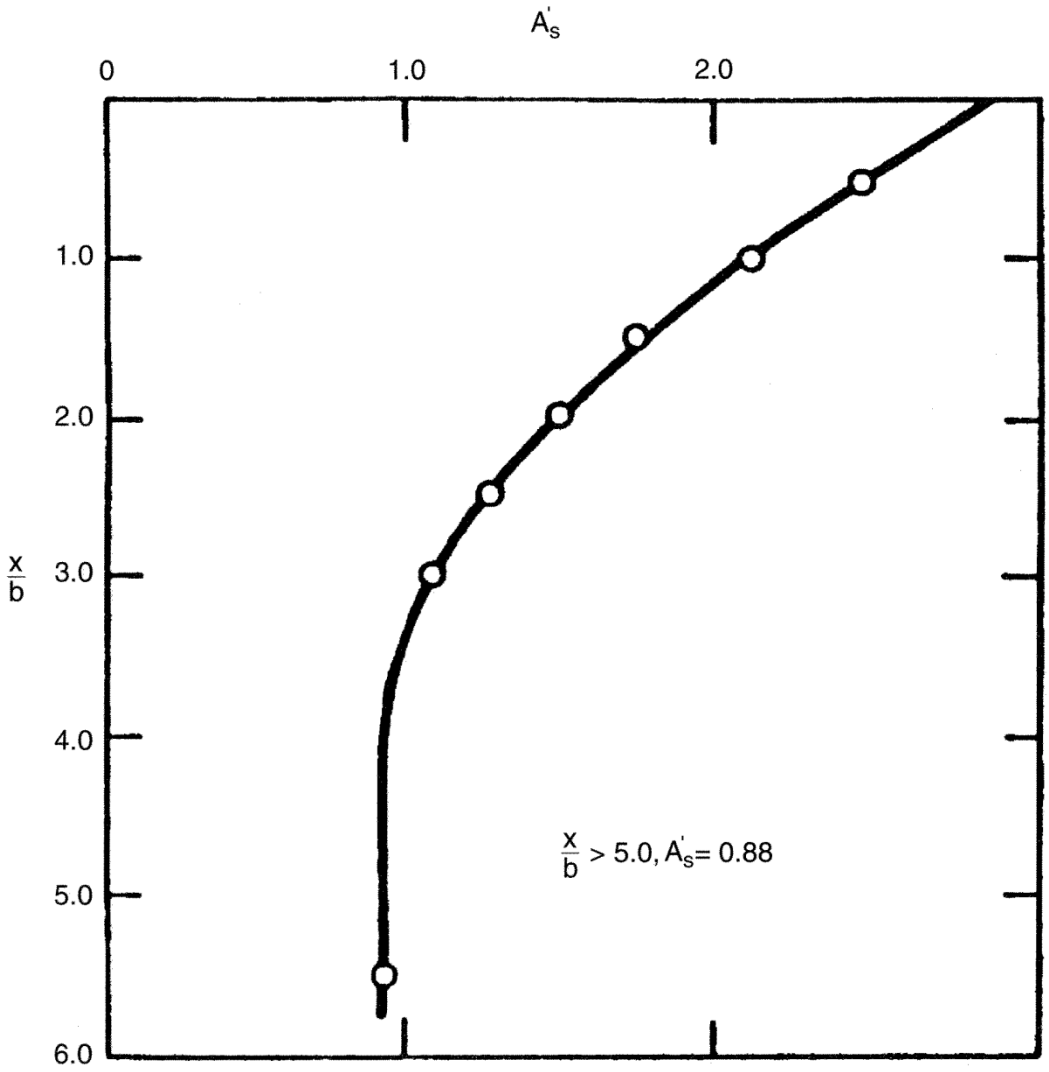

Figure 3.7: Values of coefficient A'$_s$. (Reese et al., 2006)

Establish y_m as b/60. Compute p_m by the following equation (3.17).

$$p_m = B_s \cdot p_s \tag{3.17}$$

4. Use the appropriate value of B_s from Figure 3.8 for the particular non-dimensional depth. Use the appropriate equation for p_s. The two straight-line portions of the p-y curve, beyond the point where y is equal to b/60, can now be established.

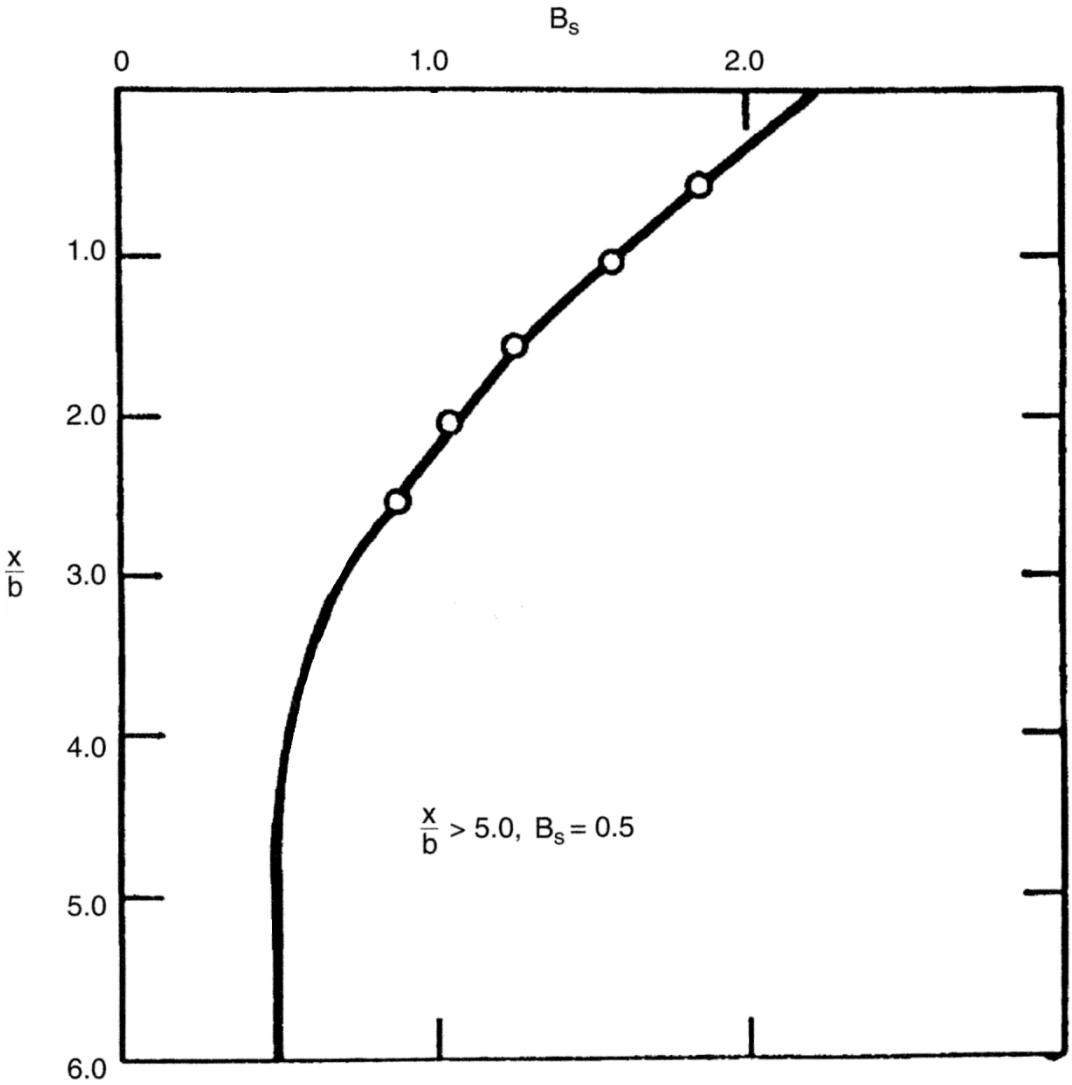

Figure 3.8: Values of coefficients B_s. (Reese et al., 2006)

Establish the initial straight-line portion of the p-y curve with Equation (3.18):

$$p = K_{py} \cdot z \cdot y \tag{3.18}$$

Use the appropriate value of K_{py} from Table 3.3.

Table 3.3: Representative Value of K_{py} for sand. (Reese et al., 2006)

Relative density (D_r)	Loose	Normal	Dense	
Unsubmerged	6.8	24.4	61	MN/m^3
Submerged	5.4	16.3	34	MN/m^3

Establish the parabolic section of the p-y curve with Equation (3.19):

$$p = C' y^{\frac{1}{n}} \tag{3.19}$$

Fit parabola between point k and m as follows:

5. Find slope of the line between points m and u in Figure 3.6, using Equation (3.20)

$$m = \frac{p_u - p_m}{y_u - y_m} \tag{3.20}$$

6. Obtain the power of the parabolic section using Equation (3.21)

$$n = \frac{p_m}{m \cdot y_m} \tag{3.21}$$

7. Obtain the coefficient as follows, with Equation (3.22):

$$C' = \frac{p_m}{y_m^{\frac{1}{n}}} \tag{3.22}$$

8. Determine point k as in Equation (3.23).

$$y_k = \left(\frac{C'}{K_{py} \cdot z} \right) \tag{3.23}$$

9. Compute the appropriate number of points on the parabola using Equation (3.23).

Note: The step-by-step procedure is outlined, and Figure 3.6 is drawn, as if there is an intersection between the initial straight-line portion of the p-y curve and the parabolic portion of the curve at point k. However, in some instances there may be no intersection with the parabola. Equation (3.18) defines the p-y curve until there is an intersection with another branch of the p-y curve; if no intersection occurs, Equation (3.18) defines the complete p-y curve. This completes the development of the p-y curve for the desired depth. Any number of curves can be developed by repeating the above steps for each desired depth.

Triaxial compression tests are recommended for obtaining the friction angle of the sand. Confining pressures close to or equal to those at the depths being considered in the analysis should be used. Tests must be performed to determine the unit weight of the sand. However, it may be impossible to obtain undisturbed samples, and frequently the angle of internal friction is estimated from results of some type of in situ test.

Another method for predicting the p-y curves for sand is presented by the API in its manual on recommended practice (API RP 2A, 1987). The two main differences between the recommendations given above and the API recommendations concern the initial slope of the p-y curves and the shape of the curves.

The following procedure is for short-term static loading as described in API (RP 2A, 1987). The API recommendations were developed only for submerged sand, but the assumption is made that the method can be used for sand both above and below the water table, as was done for the recommendations above.

1. Obtain values for the internal friction angle ø, the soil unit weight γ, and the pile diameter b (note: use buoyant unit weight for sand below the water table and total unit weight for sand above the water table).
2. Compute the ultimate soil resistance at a selected depth z. The ultimate lateral bearing capacity (ultimate lateral resistance p_u) for sand has been found to vary from a value at shallow depths determined by Equation (3.24). At a given depth, the equation giving the smallest value of p_u should be used as the ultimate bearing capacity.

$$p_{us} = \left(C_1 \cdot z - C_2 \cdot b\right) \cdot \gamma \cdot z \tag{3.24}$$

$$p_{ud} = C_3 \cdot \gamma \cdot z \tag{3.25}$$

where C_1,C_2, and C_3 are coefficients determined from Figure 3.9.

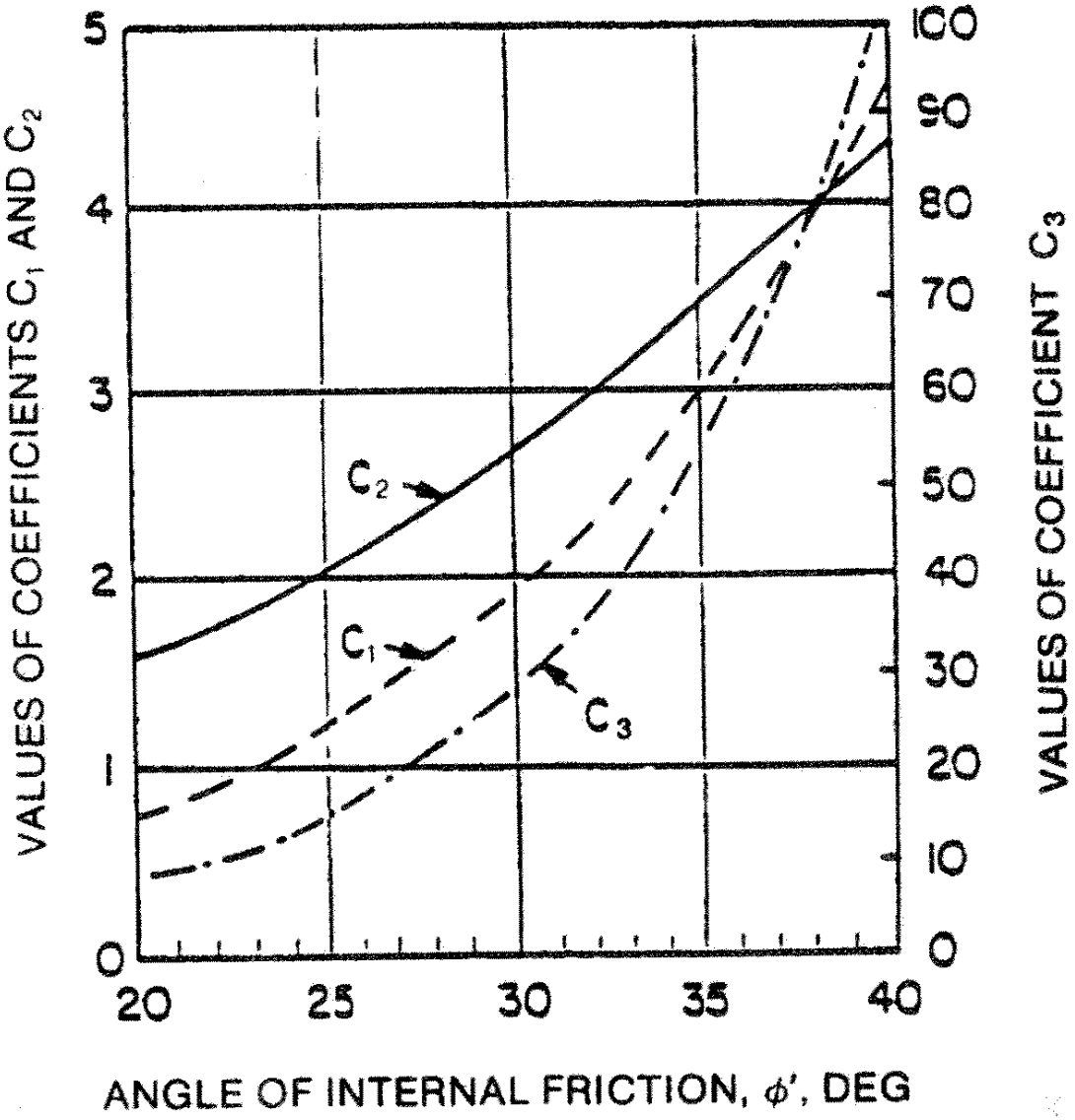

Figure 3.9: Coefficients $C_{1,2,3}$ as a function of ø. (Reese et al., 2006)

3. Develop the p-y curve based on the ultimate soil resistance p_u, which is the smallest value of p_u calculated in Step 2 and using Equations (3.24) and (3.25):

$$p = A_{ss} \cdot p_u \cdot \tan\left(\frac{E_{py\_max} \cdot z}{A_{ss} \cdot p_u}\right)^{-1}, \tag{3.26}$$

where coefficient A_s for sand ,A_{ss} ,is

$$\left(3 - 0.8 \cdot \frac{z}{b}\right) \geq 0.9 \tag{3.27}$$

for static loading, and K_{py} can be chosen from Table 3.3.

3.2.6 Gap between the Pile and Surrounding Soil

During a cyclic loading or installation of a pile, a gap may form between the pile and the surrounding soil. This phenomenon is modeled with p-y curves simply by shifting the curve with the width of the gap, y_0, as shown in Figure 3.10.

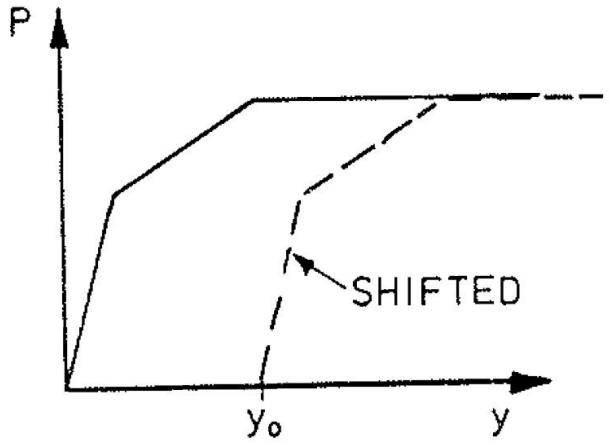

Figure 3.10: Shifting of p-y curve due to a gap. (Clausen, 1994)

3.2.7 Modifications for Inclined Piles

The effect of pile inclination on the behavior of laterally loaded piles was investigated by the use of experiments. The lateral soil-resistance curves for a vertical pile in a horizontal ground surface were modified by a constant to account for the effect of the inclination of the pile. The values of the modifying constant as a function of the batter angle were deduced from the result in the test tank (Awoshika and Reese, 1971) and from the results from full-scale tests (Kubo, 1965). The modifier to be used is shown by the solid line in Figure 3.11.

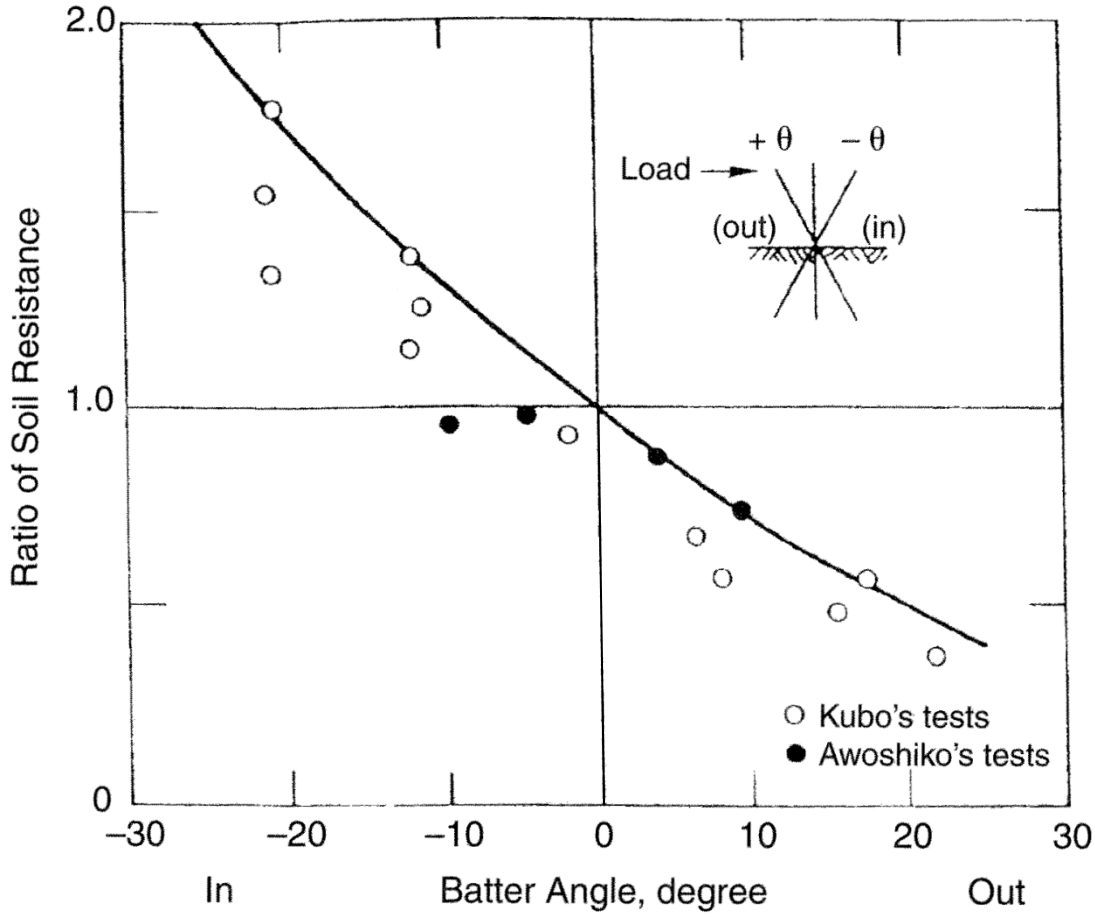

Figure 3.11: Modification of p-y curves for battered piles (after Kubo, 1964, and Awoshika and Reese, 1971)

This modifier is to be used to increase or decrease the value of p_u, which in turn will cause each of the p-values to be modified. While it is likely that the value p_u for the deeper soils is not affected by the batter, the behavior of the use of modifier for all depths is believed to be satisfactory.

As shown in Figure 3.11, the agreement between the empirical curve and the experiments for the in-batter piles (θ is positive) is somewhat better than that of the in-batter piles. The data indicate that the use of the modifier will yield somewhat questionable results; therefore, on an important project, the responsible engineer may wish to recommend full-scale testing. (Reese et al., 2006)

4 Modeling of Bending Moment due to Axial Skin Friction

4.1 Introduction

As was introduced in Chapter 1, a possible wedge on the passive side causes skin friction to the pile's surface. In addition a settling wedge might form on the pile's active side, which also causes skin friction to the pile surface. Particularly with firm soils, a gap behind a pile is more likely to occur rather than an active wedge. This sort of a soil slide may also take place due to a movement of the other piles in the pile group.

It is obvious that such minor skin friction doesn't only cause moment forces to the pile, but also some axial stresses. The effect of axial pile forces are not discussed in this thesis.

4.2 Modeling Technique

In order to represent the moment contribution due to the axial shear from surrounding soil of the pile, it is proposed that an additional rotational spring be attached at the pile centerline as shown in Figure 1.2. The moment force due to the shear transferred at the walls to the pile axis (M_s) is a function of the unit skin friction at the periphery of the pile, which varies around the pile's circumference.

To estimate the moment due to side shear, the pile's cross section is divided into slices as shown in Figure 4.1. For this idealization, the pile is loaded in direction A4-A2. All the points to the left of line A1-A3 move up, causing tensile skin friction (t_{tens}), while those on the right of A1-A3 are assumed to move down, causing compressive skin friction (t_{comp}). d_i is the distance from the center of the pile to the center of slice i. For example d_1, is distance from the center of the pile O to the point O1.

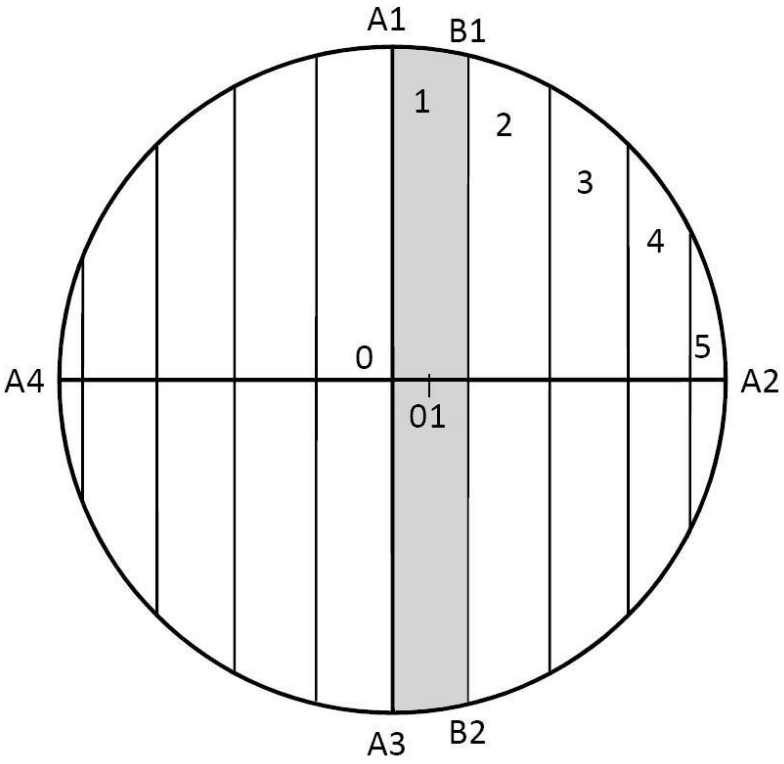

Figure 4.1: Pile cross-section divided into slices to calculate M_s (Niraula, 2004)

Next, the sum of arc length A1-B1 and A3-B2 is referred to as C_{sum1} where subscript 1 refers to the slice number 1. Note, both arcs are summed together, i.e. A1-B1 or A3-B2, since the shear stress, t, is assumed equal on both sides of the slices. The value of shear stress t_i, is a function of vertical displacement, z_i, which is a function of the rotation φ, wedge movement, and the distance d_i.

The relationship between z_i and t_i can be obtained from axial resistance versus axial displacement, t-z curve, as presented in Figure 4.2.

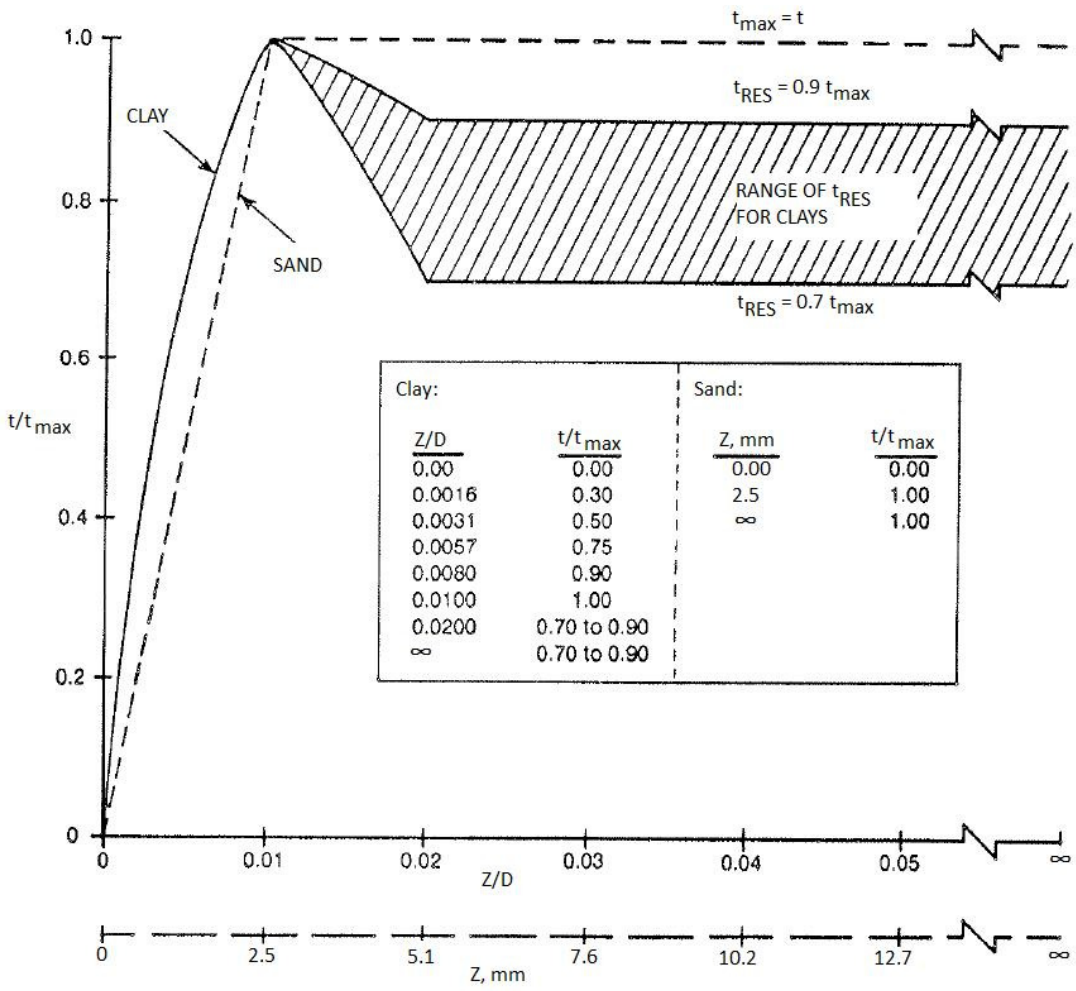

Figure 4.2: t-z curve for sand and clay. (API RP 2A, 1987)

If z_1 is the average axial displacement of slice 1 in Figure 4.1, and t_1 (obtained from t-z curve knowing z_1 due to the rotation φ and the wedge movement), then the side shear force/unit length, T_1, acting on slice 1 is given by equation (4.1).

$$T_1 = t_1 \cdot C_{sum1} \quad , \tag{4.1}$$

The moment M_{s1} per unit pile length about O, is found with equation (4.2).

$$M_{s1} = T_1 \cdot d_1 \quad , \tag{4.2}$$

The total moment per unit length may be found by summing the moments acting on all slices, as presented in equation (4.3).

$$M_s = \sum_{i=1}^{n} \left(t_i \cdot C_{sumi} \cdot d_i \right) \quad , \tag{4.3}$$

where n is the number of slices. (Niraula, 2004)

In the above estimation of M_s, it is assumed that the neutral axis (i.e. center of rotation) of the pile remains at the center of the cross section. This assumption naturally doesn't apply when the pile is also loaded axially, or when the pile yields.

It has been recommended on previous research that M_s-φ spring shouldn't be considered in conservative design. (Niraula, 2004)

5 Linearly Elastic Modeling of a Laterally Loaded Single Pile

5.1 Introduction

A pile subjected to lateral loading involves interaction of the surrounding soil and the structure. The aim of this chapter is to introduce the basics of finite difference computing method for laterally loaded beam on several elastic struts in half space. More advanced pile-soil interaction models are presented in following chapters, but before that the mechanics of a single pile needs to be introduced.

5.2 Computation Method

Horizontal loading (Q) and bending moment (M) to a pile head causes horizontal movement of the pile, which then creates a spring support (k_s) from soil, as illustrated in Figure 5.1 a). To analyze stresses within a pile, finite difference method is generally used. A pile and surrounding soil are combined to one structural model, which is then divided in to several elements. In that way a pile is modeled as an elastic beam fixed to several elastic struts as illustrated in Figure 5.1. b)

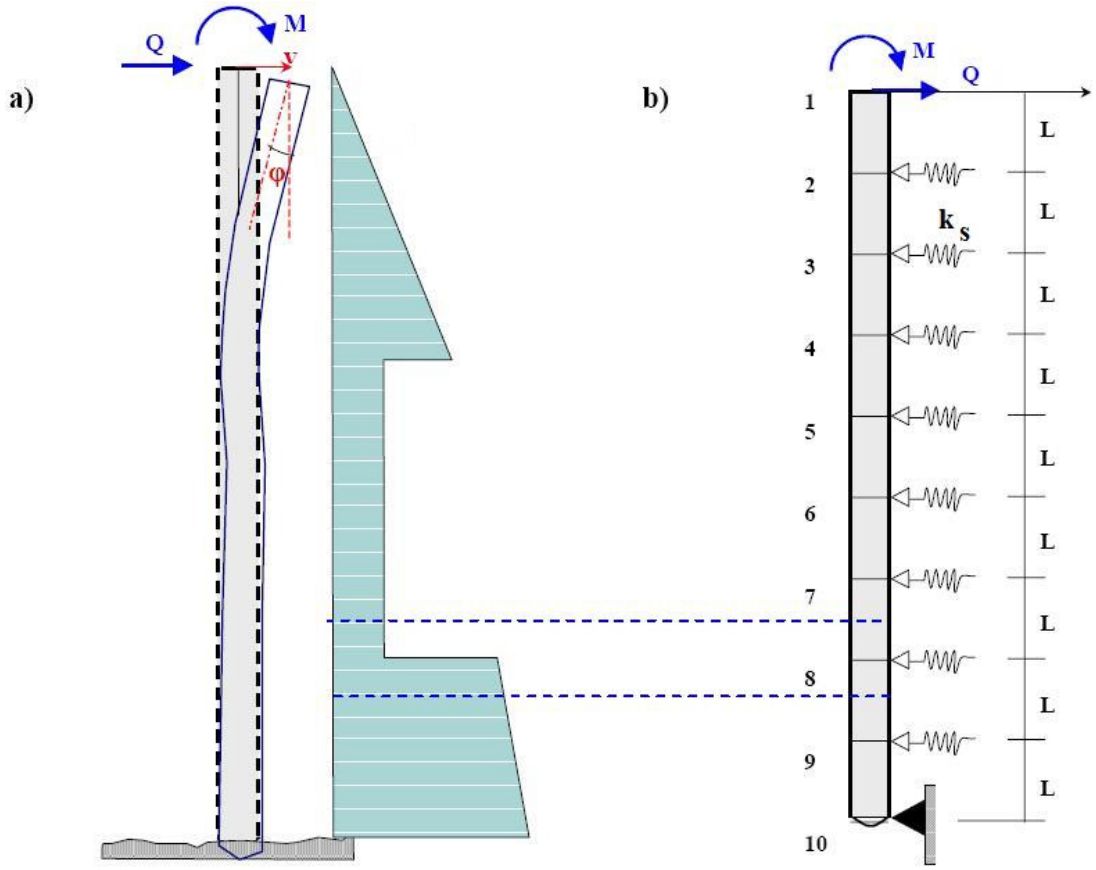

Figure 5.1: a) External loading of a pile and lateral side support from surrounding soil b) Structural model of lateral pile-soil interaction. (Salokangas, 2007)

Lateral spring constants are determined from p-y curves, by taking only an initial part of a curve in to account i.e. secant of the lateral stress-strain curve E_{py} and multiplying it with the element length L_i. Computing of the moment forces, introduced in Chapter 4, due to a skin friction can be modeled as rotational springs as was illustrated in Figure 1.2.

At each node point of the structural model, force equilibrium equations can be formed, as is done in Equation (5.1) and (5.2), for a single node number i. In Figure 5.2, forces and their directions acting to a single node number i are shown. Point force R_i in the figure, may be an external loading or soil pressures force resultant and bending moment force M_{si} due to the skin friction as was explained in Chapter 4.

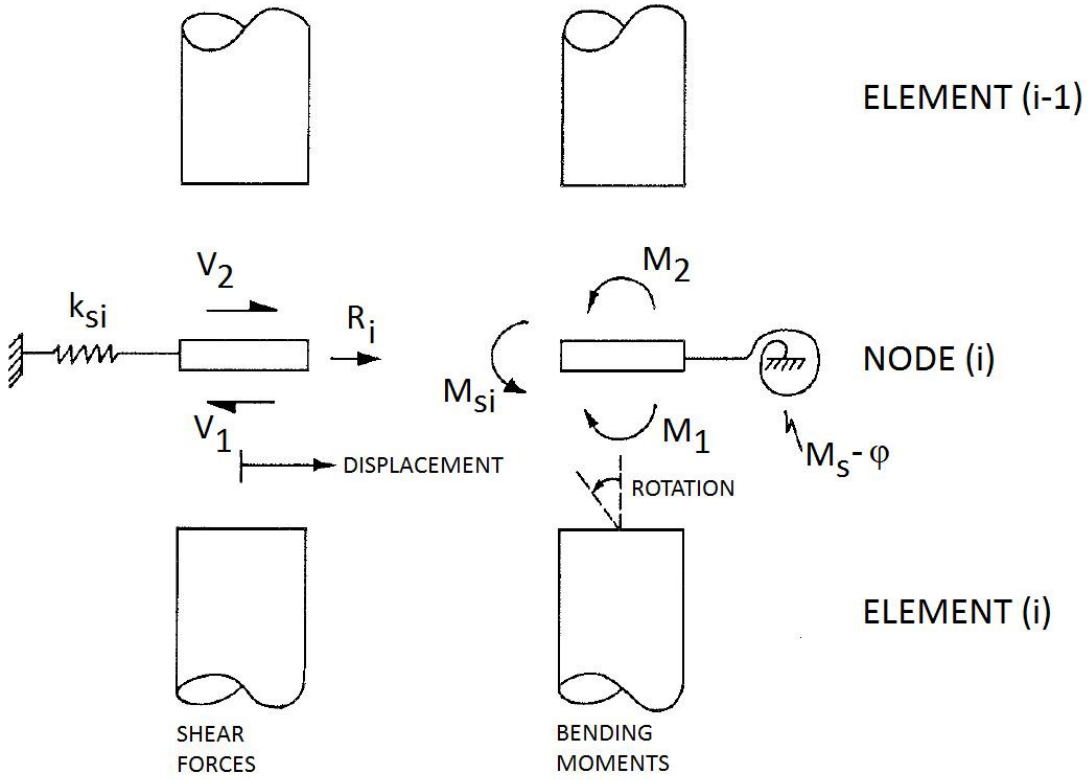

Figure 5.2: Illustrated force equilibrium of node i. (Clausen, 1994)

At each node point, horizontal and moment forces must be in equilibrium, therefore

$$V_2 - V_1 + R_i = 0 \tag{5.1}$$

and

$$M_2 - M_1 + M_{si} = 0 \tag{5.2}$$

When only bending moments and shear forces are taken in to account, correspondence between beam element's transitions and external forces can be written with Equation (5.3). Figure 5.3 a) represents the external forces and their positive directions in at beam element's ends, whereas Figure 5.3 b) does the same thing for horizontal transitions and rotations.

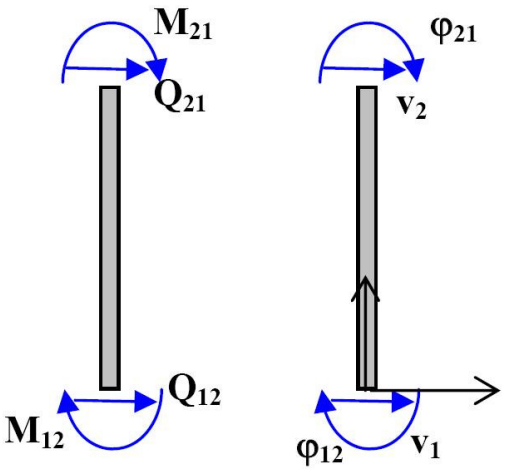

Figure 5.3: a) Forces acting on a beam element b) Beam element's transitions (Salokangas, 2007)

$$K_1 \cdot \begin{pmatrix} \upsilon_1 \\ \phi_{12} \\ v_2 \\ \phi_{21} \end{pmatrix} = \begin{pmatrix} V_{12} \\ M_{12} \\ V_{21} \\ M_{21} \end{pmatrix} \tag{5.3}$$

The stiffness matrix $[K_1]$ for a beam element 1, with even bending stiffness EI_1 and length of L_1 is

$$K_1 = \begin{pmatrix} \frac{12EI_1}{L_1^3} & \frac{6EI_1}{L_1^2} & -\frac{12EI_1}{L_1^3} & \frac{6EI_1}{L_1^2} \\ \frac{6EI_1}{L_1^2} & \frac{4EI_1}{L_1} & -\frac{6EI_1}{L_1} & \frac{2EI_1}{L_1} \\ -\frac{12EI_1}{L_1^3} & -\frac{6EI_1}{L_1^2} & \frac{12EI_1}{L_1^3} & -\frac{6EI_1}{L^2} \\ \frac{6EI_1}{L_1^2} & \frac{2EI_1}{L_1} & -\frac{6EI_1}{L_1^2} & \frac{4EI_1}{L_1} \end{pmatrix} \tag{5.4}$$

Lateral soil resistance is modeled in linear elastic analysis as a spring with a spring constant k_{si}, as shown in the Figure 5.4. In that way, when the horizontal transition v_i is known, also force R_i can be calculated with Equation (5.5).

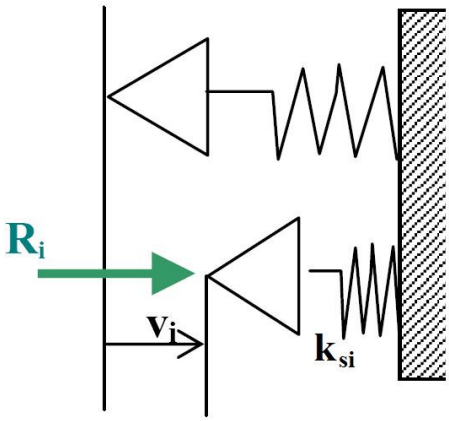

Figure 5.4: The spring force from the surrounding ground. (Salokangas, 2007)

$$k_{si} \cdot \upsilon_i = R_i \tag{5.5}$$

By forming stiffness matrixes for all elements (K_i) and spring constants k_{si}, the system stiffness matrix for the whole beam – soil–system, S, can be constructed.

Assembling of beam elements' stiffness matrixes is done by summing them from their corners, as is done in equation (5.6). The equation (5.6) is assembled only from 3 elements and by adding the number of elements to the system, global stiffness matrix expands.

The soil resistance factor k_{si}, is added those matrix elements that compensate that transition. In this 3 element case, if the pile is totally submerged in soil, lateral spring elements would be added to the matrix elements S_{11}, S_{33}, S_{55} and S_{77}.

If the skin friction due to bending of the pile is considered, the rotational spring constants are set, in this 3 element case, to stiffness matrix's elements S_{22}, S_{44}, S_{66}, S_{88}.

$$S = \begin{pmatrix} \frac{12EI_1}{L_1^3} & \frac{6EI_1}{L_1^2} & -\frac{12EI_1}{L_1^3} & \frac{6EI_1}{L_1^2} & 0 & 0 & 0 & 0 \\ \frac{6EI_1}{L_1^2} & \frac{4EI_1}{L_1} & -\frac{6EI_1}{L_1^2} & \frac{2EI_1}{L_1} & 0 & 0 & 0 & 0 \\ -\frac{12EI_1}{L_1^3} & -\frac{6EI_1}{L_1^2} & \frac{12EI_1}{L_1^3}+\frac{12EI_2}{L_2^3} & -\frac{6EI_1}{L_1^2}+\frac{6EI_2}{L_2^2} & -\frac{12EI_2}{L_2^3} & \frac{2EI_2}{L_2} & 0 & 0 \\ \frac{6EI_1}{L_1^2} & \frac{2EI_1}{L_1} & -\frac{6EI_1}{L_1^2}+\frac{6EI_2}{L_2^2} & \frac{4EI_1}{L_1}+\frac{4EI_2}{L_2} & -\frac{6EI_2}{L_2} & \frac{2EI_2}{L_2} & 0 & 0 \\ 0 & 0 & -\frac{12EI_2}{L_2^3} & -\frac{6EI_2}{L_2^2} & \frac{12EI_2}{L_2^3}+\frac{12EI_3}{L_3^3} & -\frac{6EI_2}{L_2^2}+\frac{6EI_3}{L_3^2} & -\frac{12EI_3}{L_3^3} & \frac{6EI_3}{L_3^2} \\ 0 & 0 & \frac{6EI_2}{L_2^2} & \frac{2EI_2}{L_2} & -\frac{6EI_2}{L_2^2}+\frac{6EI_3}{L_3^2} & \frac{4EI_2}{L_2}+\frac{4EI_3}{L_3} & -\frac{6EI_3}{L_3^2} & \frac{2EI_3}{L_3} \\ 0 & 0 & 0 & 0 & -\frac{12EI_3}{L_3^3} & -\frac{6EI_3}{L_3^2} & \frac{12EI_3}{L_3^3} & -\frac{6EI_3}{L_3^2} \\ 0 & 0 & 0 & 0 & \frac{6EI_3}{L_3^2} & \frac{2EI_3}{L_3} & -\frac{6EI_3}{L_3^2} & \frac{4EI_3}{L_3} \end{pmatrix} \quad (5.6)$$

The external forces acting to a beam are fitted to a force vector f_{tot} as shown in equation (5.7)

$$f_{tot} = \begin{pmatrix} V_1 \\ M_1 \\ V_2 \\ M_2 \\ V_3 \\ M_3 \\ V_N \\ M_N \end{pmatrix} \quad (5.7)$$

and equivalent global deflection vector (δ_{tot}) is assembled as shown in equation (5.8).

$$\delta_{tot} = \begin{pmatrix} v_1 \\ \phi_1 \\ v_2 \\ \phi_2 \\ v_3 \\ \phi_3 \\ v_N \\ \phi_N \end{pmatrix}. \tag{5.8}$$

To be able to determine the global deflection vector's elements, some boundary conditions must be set for the pile tip. A pile that is installed in to bedrock, with a rock shoe, is usually analyzed to be hinged from its tip, as shown in Figure 5.5 a). A pile tip installed in stiff moraine can be analyzed as rigidly fixed, illustrated in Figure 5.5 b).

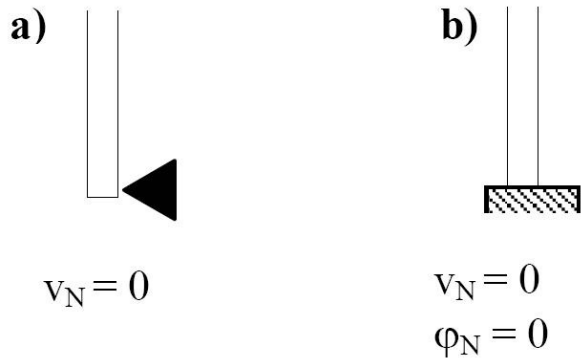

Figure 5.5: a) Hinged fixity b) Rigid fixity of a pile tip. (Salokangas, 2007)

As presented in Figure 5.5, when the pile tip is modeled as hinged, the lateral displacement of the pile tip is zero and when the tip is rigidly fixed, both lateral displacement and rotation are zero. These boundary fixities are included in the global deflection vector (δ_{tot}), to elements which corresponds with those transitions.

When the global stiffness matrix, S, global force vector f_{tot} are formed, and boundary conditions are set, the elements of the global deflection vector can be determined by using Equation (5.9).

$$\delta_{tot} = S^{-1} \cdot f_{tot} \tag{5.9}$$

With the global deflection vector δ_{tot}, the beam element's stresses and ground pressures can be solved.

In this chapter the pile computation procedure was presented for a pile in half space. An easy way to model a pile in three-dimensional space is to compute deformations and forces separately for both lateral directions and then combine the results.

6 Non-Linear Modeling of a Laterally Loaded Single Pile

6.1 Introduction

The deflection of a pile and lateral resistance of surrounding soil are interdependent. Therefore, because of the nonlinear nature of the soil and the pile, iterative techniques are almost always necessary to achieve reliable solutions.

This chapter presents a modeling of non-linear elasto-plastic soil-structure-soil interaction, as related to a laterally loaded single pile. While this chapter describes the nature of a single pile in non-linear soil and presents a method for computations, the following chapter introduces a fundamental method for analyzing piles in a group.

6.2 Computation Procedure

In non-linear finite difference analysis the initial step of the computation procedure is to assume a small displacement at the pile head. Then the deflections of the soil and the pile, caused by this initial step deflection are computed. For this first iteration step, the initial part of the p-y curve is used to form a spring constant to each node of the pile, as was done in Chapter 5.

When the whole pile is modeled, the computed pile forces at the pile head are compared with the external loading vector of the pile. If the computed forces from the initial step do not correspond with the external loading to the pile, a new loading vector is set to the pile head. The displacements (y_i) from the preceding iteration step are used to form the spring constants k_{si} of soil elements for the following step from the recommended p-y curves presented in Chapter 3. A new stiffness matrix for the pile is formed until the force vector acting at the pile head is met in sufficient accuracy.

6.3 Yielding of a Pile

In addition, a second non-linearity must be addressed. The value of bending stiffness EI_i of a pile element will be reduced as the bending moment along the pile is increased. For a pile of reinforced concrete, in particular, explicit expressions must be developed, based on the geometry of the cross section of the pile and the properties of the steel and concrete, yielding value of EI as a function of the applied bending moment. The method can be applied to piles with cross sections of other materials as well. Then a computing code must be written to determine the bending moment during a computation so that the value of EI_i can be modified as iteration process proceeds.

During an incremental iterative loading of a pile it may be experienced that the stress in the wall of a pile element becomes so high that yielding starts. In such cases a reduced stiffness should be used if the element is loaded further. The computer program SPLICE (version 1.0.4) handles such a situation in the following approximate manner (Clausen, 1994)

1. The yield stress σ_y has been specified as part of the pile cross section input data. In case σ_y = 0.0 MPa, the element is treated as linear elastic, independent of computed pile element stresses.
2. The element is assumed to be in a non-yielded state in load increment 1
3. For load increment number 2 or higher, the value of σ_y is compared to the last average maximum resulting pile element stress.
4. If the pile element stress is higher than σ_y , the element axial, torsional, bending and shear stiffness values are reduced to 1 % of the original value.

7 Group Effect with Piles in a Pile Group

7.1 Introduction

Bogard and Matloc (1983) present a method in which the p-y curves for a single pile are modified to take into account the group effect. The analyses of Brown et al. (1987) showed that the group effect could be taken into account most favorably by reducing the value of p for p-y curve of the single pile to obtain p-y curves for the pile group.

Brown et al. (1987) also concluded that the elasticity-based methods did not accurately predict the distribution of load within a pile group. In spite of that, both methods are discussed and compared in this thesis.

The curves in Figure 1.5 show that the factor f_m may be used to reduce the values of p_{sp} for the single pile to the value of p_{gp} for the pile group. The proposal makes use of other work in the technical literature, which are used in this chapter, (Prakash, 1962, Schmidt, 1981, 1985; Cox et al., 1984, Dunnavant and O'Neill, 1986; Wang, 1986; Lieng, 1988). Some of these results are based on model tests of pile groups.

7.2 Recommendations for Predicting p - multipliers

7.2.1 Side-By-Side Reduction Factors

The first pattern of the placement of piles in a group to be considered is for piles side by side. Values of reduction factor β_{ni} are found, termed β_a for this case and may be summarized, as shown later, to determine a composite factor of β_{ni} for each pile in the group. (Reese et al., 2006)

The pattern for the placement of the side-by-side piles is shown in Figure 7.1, with the arrows showing the direction of loading. The values of β_a may be found from the curve of equations given by the references previously cited. The value of β_a may be taken directly from the plot or may be found using the equation in the figure. As may

be seen, with s/b values of 3.7 or more, the value of β_a is unity. The smallest value of β_a for piles that touch is 0.5. A review of the plotted points reveals that the value of unity of β_a for s/b values of 3.7 or more is strongly supported. The value 0.5 for piles touch is found from mechanics. However, the first branch of the curve in Figure 7.1 is subject to uncertainty; this is not surprising, considering the variety of experiments that were cited.

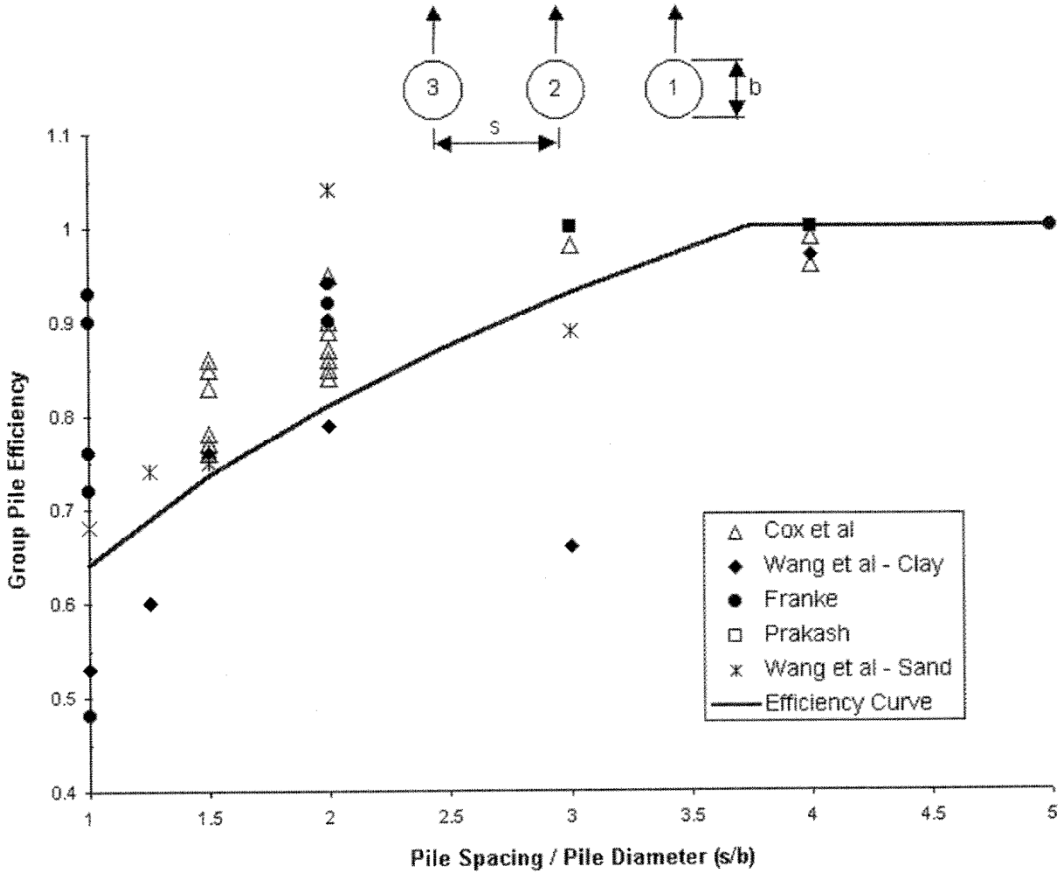

Figure 7.1: Curve giving reduction factors β_a for piles in a row. (Reese et al., 2006)

7.2.2 Line-By-Line Reduction Factors, Leading Piles

The next pattern of placement of the piles in a group to be considered is for piles placed in a line, as shown in Figure 7.2, with the arrow showing the direction of loading. The values of β_{bL} may be found from the curve of equations in Figure 7.2. The plotted points in the figure are identified by the reference previously citied. The suggested curve agrees well with the plotted points except for four points to the left of the curve indicating an efficiency of unity for close spacing.

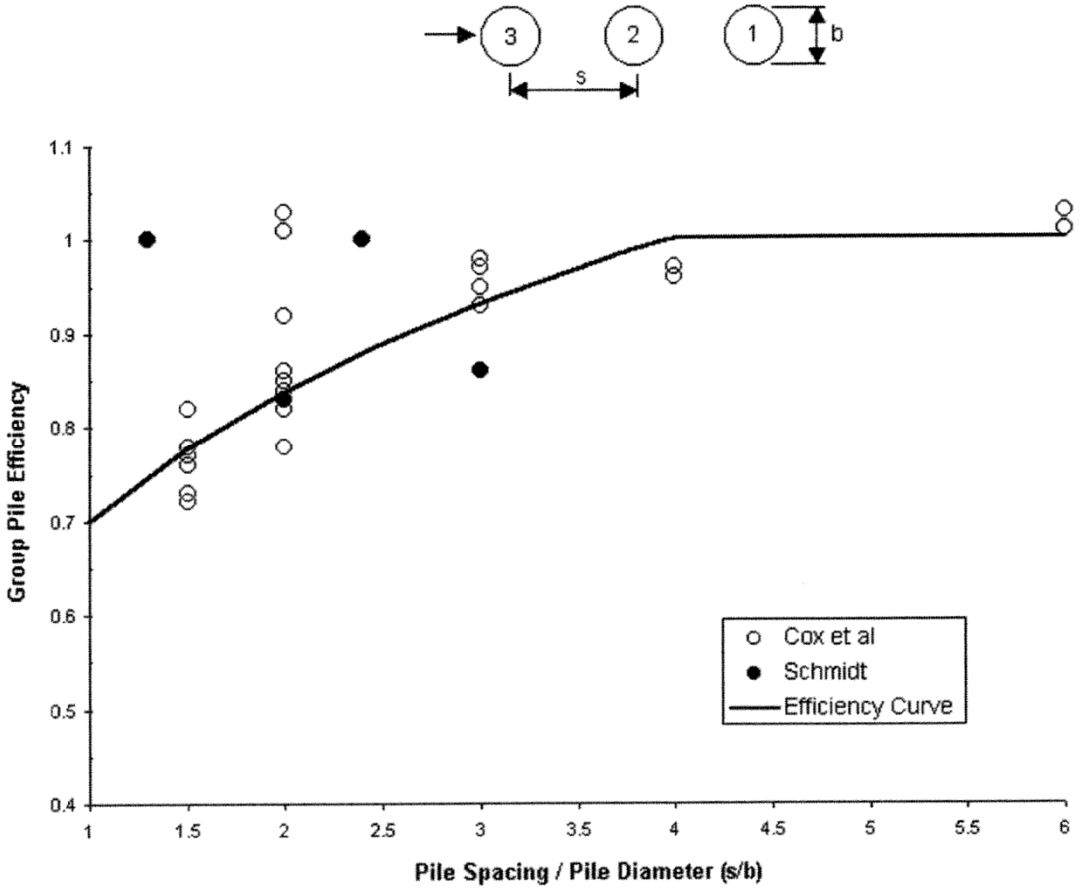

Figure 7.2: Curve giving reduction factors β_{bl} for leading piles in a line. (Reese et al., 2006)

7.2.3 Line-By-Line Reduction Factors, Trailing Piles

The experimental results, along with a suggested curve and equations, are given in Figure 7.3. The scatter of the plotted points indicates that the computed efficiency for the individual piles in a group is not likely to be precise. The scatter, as noted earlier, is not surprising in view of the many variables involved in the experiments. The use of values suggested in the curves and equations in Figure 7.1 through Figure 7.3 will yield to a much better result than ignoring the effect of close spacing.

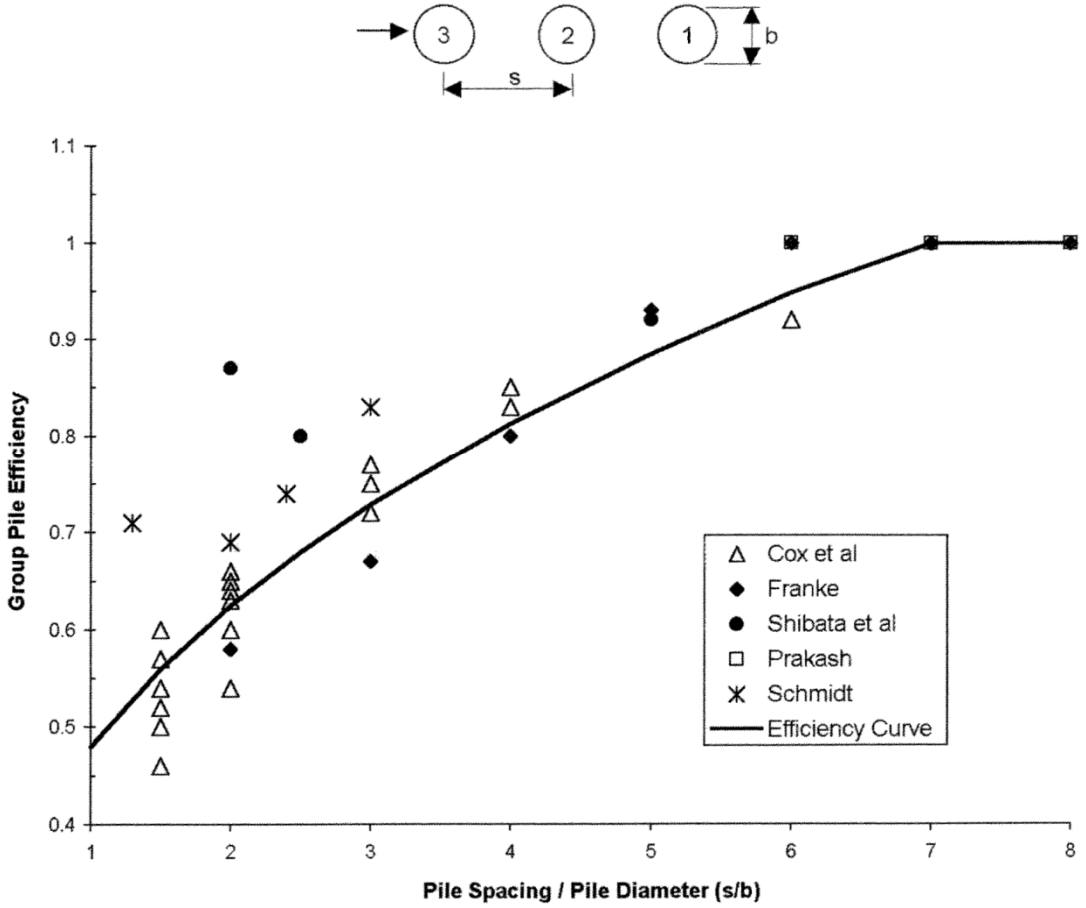

Figure 7.3: Curve giving reduction factors β_{bt} for trailing piles in a line. (Reese et al., 2006)

7.2.4 Skewed Piles

The experiments cited above did not obtain data on skewed piles, but provision for skewed piles is necessary. A simple mathematical expression for ellipse in polar coordinates was selected to obtain the reduction factor. The geometry of the two piles, A and B, is shown in Figure 7.4 (a). The side-by-side effect β_a may be found from Figure 7.1, where the spacing is r/b. The in-line effect β_b may be found from either Figure 7.2 or Figure 7.3, depending on whether Pile A or Pile B is being considered. The values of β_a and β_b are indicated in Figure 7.4 (b), and the value of β_b for the effect of skew may be found from the following equation (7.1):

$$\beta_s = \left({\beta_b}^2 \cdot \cos(\xi)^2 + {\beta_a}^2 \cdot \sin(\xi)^2 \right)^{0.5} \tag{7.1}$$

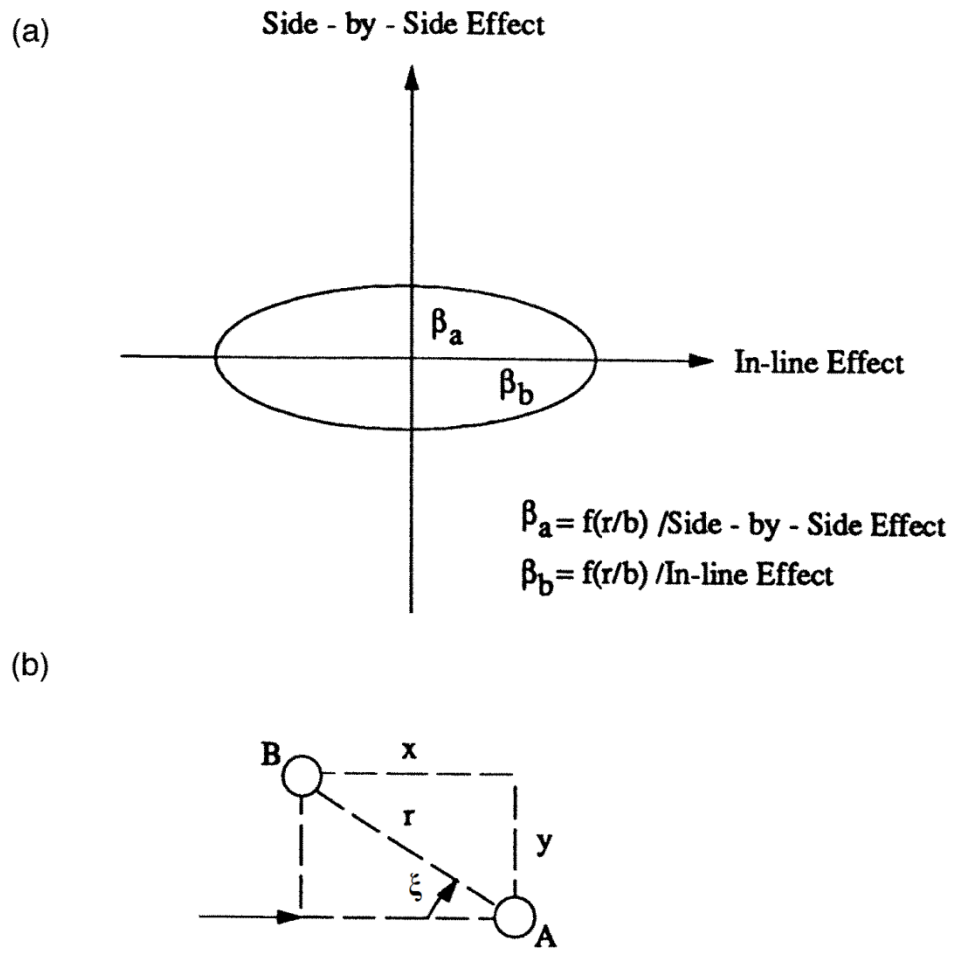

Figure 7.4: System for computing the reduction factor for skewed piles. (Reese et al., 2006)

For each pile i in a pile group that has n piles, the group reduction factor f_m may be computed by the following equation (7.2):

$$f_{mi} = \beta_{1i} \cdot \beta_{2i} \cdot \beta_{3i} \cdot\cdot \beta_{ni} \tag{7.2}$$

Computation of the factor to reduce the values p for the single pile to values for each pile in a group is tedious, but with properly written computer program it is easily performed.

7.3 Elastic Space -Technique

The effect of pile-soil-pile interaction can be alternatively computed with Mindlin's point force solutions. This method models the soil as elastic mass, where a

displacement of a single pile elements' node points causes stresses to the surrounding soil and thereby affect to the node points of the surrounding piles.

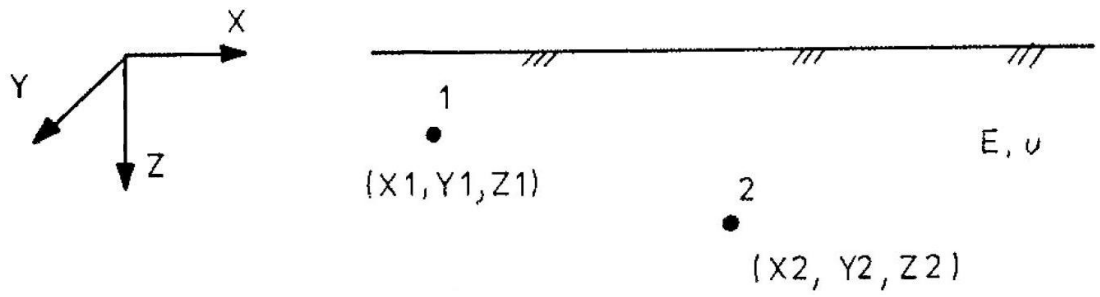

Figure 7.5: Two points in elastic half space. (Clausen, 1994)

Let point 2 (x_2, y_2 z_2) in Figure 7.5 be a soil element at a pile element's node point's immediate vicinity where the global displacements (ν_x, ν_y, ν_z) are wanted. These displacements are caused by a global increments force Q acting at point 1 (x_1, y_1 z_1) in Figure 7.6. This force is known from the last iterative solution of a single pile, as was discussed in Chapter 9.

When only lateral displacements of a pile at the point 1 are considered, displacements of the point 2 can be obtained with Equation (7.3).

$$\begin{pmatrix} \upsilon_x \\ \upsilon_y \\ \upsilon_z \end{pmatrix} = \begin{pmatrix} M_1 \\ M_2 \\ M_3 \end{pmatrix} \cdot Q \tag{7.3}$$

where each of the $M_{1,2,3}$-coefficients can be computed from Midlin's point force solutions Equations (7.4), (7.5), and (7.6). (Mindlin, 1936)

$$M_1 = \frac{1}{16 \cdot \pi \cdot G(1-\nu)} \left[\frac{3-4\nu}{R_1} + \frac{1}{R_2} + \frac{x^2}{R_1^3} + \frac{(3-4\nu)x^2}{R_2^3} + \frac{2 \cdot z_m \cdot z}{R_2^3} \cdot \left(1 - \frac{3 \cdot x^2}{R_2^2} \right) \ldots \right.$$
$$\left. + \frac{4 \cdot (1-\upsilon) \cdot (1-2 \cdot \upsilon)}{R_2 + z + z_m} \cdot \left(1 - \frac{x^2}{R_2 (R_2 + z + z_m)} \right) \right] \tag{7.4}$$

$$M_2 = \frac{x \cdot y}{16 \cdot \pi \cdot G(1-\upsilon)} \cdot \left[\frac{1}{R_1^3} + \frac{3-4\upsilon}{R_2^3} - \frac{6 z_m \cdot z}{R_2^5} - \frac{4(1-\upsilon)(1-2\upsilon)}{R_2 (R_2 + z + z_m)^2} \right] \tag{7.5}$$

$$M_3 = \frac{x}{16\cdot\pi\cdot G(1-\nu)}\cdot\left[\frac{z-z_m}{R_1^{\,3}} + \frac{(3-4\upsilon)\cdot(z-z_m)}{R_2^{\,3}} \ldots + \frac{4\cdot(1-\upsilon)(1-2\upsilon)}{R_2\cdot(R_2+z+z_m)} - \frac{6z_m\cdot z(z+z_m)}{R_2^{\,5}}\right] \tag{7.6}$$

where

$$R_1 = \left[r^2 + (z-z_m)^2\right]^{0.5} \tag{7.7}$$

$$R_2 = \left[r^2 + (z+z_m)^2\right]^{0.5} \tag{7.8}$$

and

$$r = \left(x^2 + y^2\right)^{0.5}. \tag{7.9}$$

z_m, r, Q, R_1, R_2, and z are illustrated in Figure 7.6.

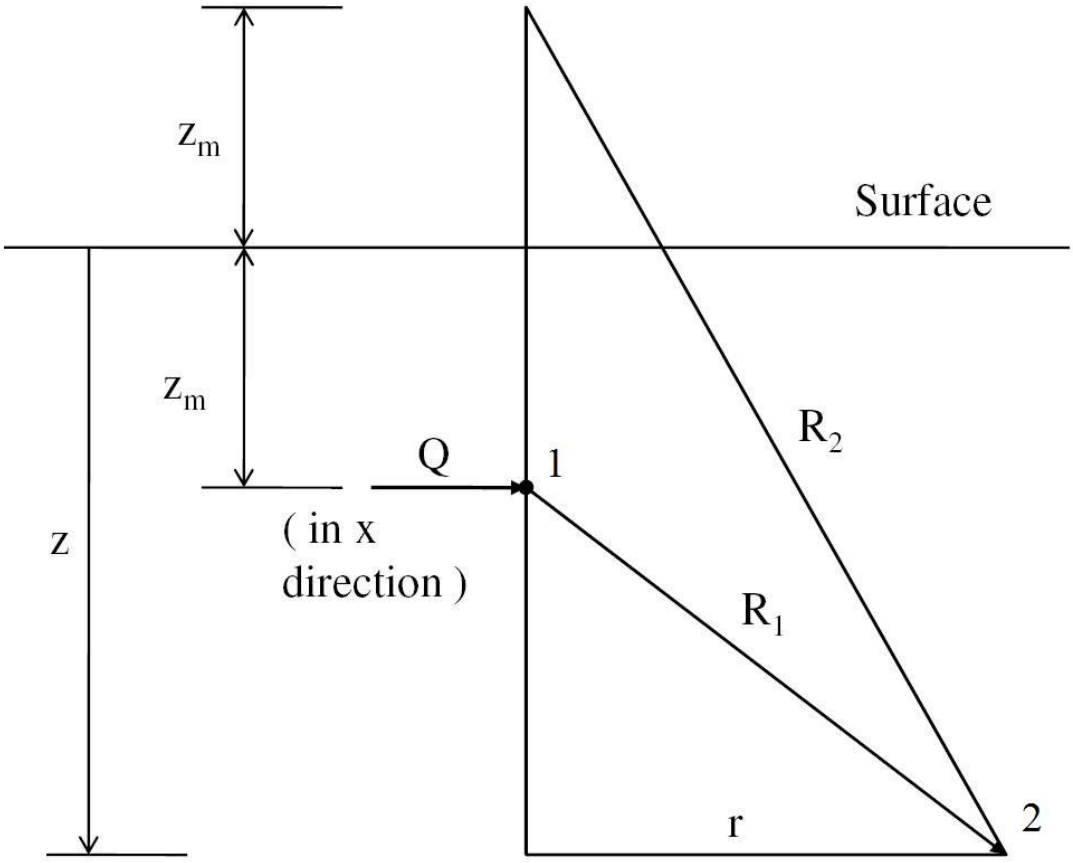

Figure 7.6: Lateral point load acting beneath the surface of a semi-infinite mass. (Mindlin, 1936)

The Mindlin's solution assumes a semi-infinite elastic half space of constant modulus of elasticity E. For many practical cases a modulus of elasticity that increases linearly with depth will be a more reasonable approximation, Equation (7.10) (Clausen, 1994).

$$E = E_0 + E_1 \cdot z \tag{7.10}$$

Shear modulus G can be calculated with Equation (7.11) for Equations (7.4),(7.5) and for (7.6).

$$G = \frac{E}{2(1+\upsilon)}\ , \tag{7.11}$$

where ν is the Poisson's value (Clausen, 1994).

After the displacements (ν_{x2}, ν_{y2}) are computed for soil point 2, forces due to the soil displacement should be added to the pile's total force vector f_{tot} (Equation (5.7)) with iterative process, so that a non-linear p-y curve is used. The initial point at the p-y curve, at which the additional forces due to displacements are computed, should be obtained from the last computed iterative step of the pile next to the soil point 2.

As the soil point 2 moves axially along the pile's side, it causes skin friction, which causes bending moments to the pile. This phenomenon can be modeled with the M_s-φ spring- technique that was introduced in Chapter 4.

The pile group modeling program SPLICE uses Mindlin's elastic half space equations to simulate pile-soil-pile interaction. SPLICE does the group effect computation process only for one equivalent depth, z_e, for each pile. The estimation of the depth z_e is presented in the report by Clausen, (1983).

8 Linear Elastic Modeling of a Pile Group

8.1 Introduction

This chapter introduces a linearly elastic computing procedure of a pile group, presented by H. Bredenberg and B. Broms (1983). The computation process is based on a finite difference method, where a single pile head is modeled as a group of springs and a pile group is a formation of these spring clusters.

For more advanced soil and pile models iteration procedure becomes more crucial, which is presented in the following chapter 9. Figure 8.1 illustrates the computing flowchart of a linear elastic pile group program.

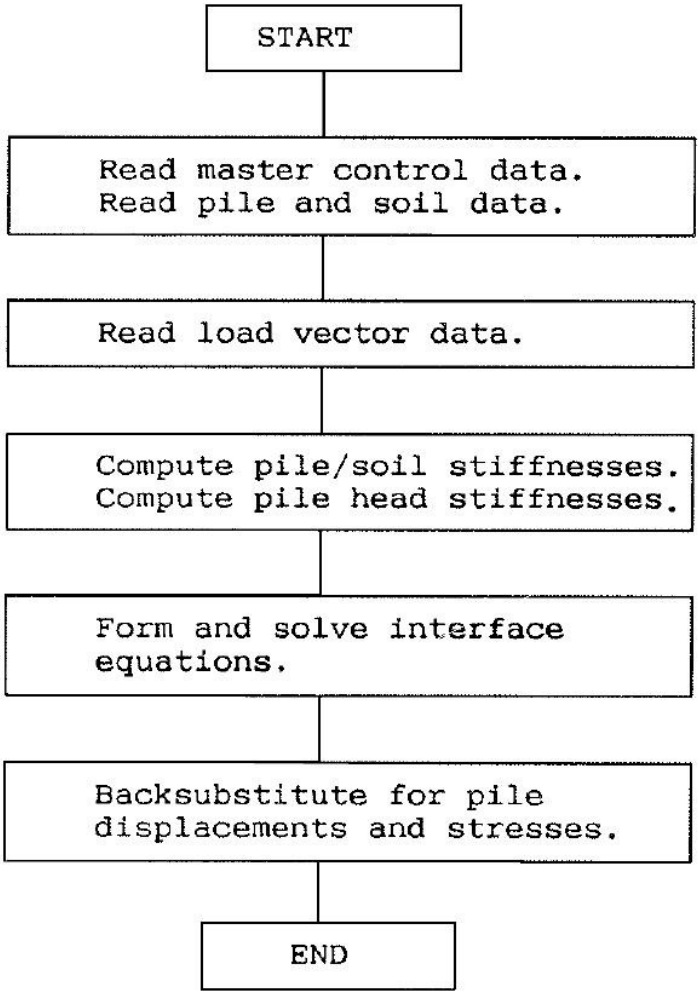

Figure 8.1: Flowchart for linearly elastic modeling of a pile group. (Clausen, 1994)

8.2 Single Pile Head's Stiffness

Figure 8.2 a) presents directions of elements in a single pile head's load vector, F_q, and Figure 8.2 b) presents corresponding displacement directions X_q. Both of the coordinate systems are orthogonal.

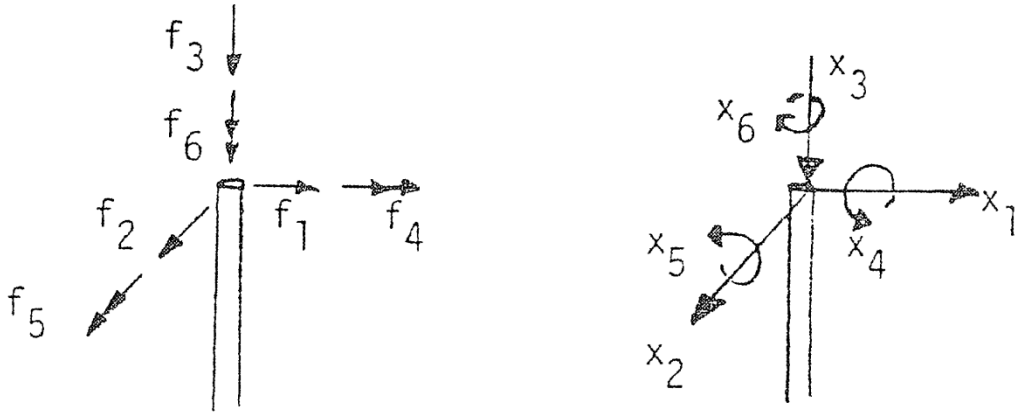

Figure 8.2: a) Directions of a single pile head's load vector's elements. b) Directions of a single pile head's displacement vector's elements. (Bredenberg and Broms, 1983)

Linear elastic correlation between a single pile head's loadings and deflections are

$$F_q = K_q \cdot X_q \quad , \tag{8.1}$$

where

$$F_q = \begin{pmatrix} f_1 & f_2 & f_3 & f_4 & f_5 & f_6 \end{pmatrix}^T \tag{8.2}$$

$$K_q = \begin{pmatrix} k_{11} & 0 & 0 & 0 & k_{15} & 0 \\ 0 & k_{22} & 0 & k_{24} & 0 & 0 \\ 0 & 0 & k_{33} & 0 & 0 & 0 \\ 0 & k_{42} & 0 & k_{44} & 0 & 0 \\ k_{51} & 0 & 0 & 0 & k_{55} & 0 \\ 0 & 0 & 0 & 0 & 0 & k_{66} \end{pmatrix} \tag{8.3}$$

$$X_q = \begin{pmatrix} x_1 & x_2 & x_3 & x_4 & x_5 & x_6 \end{pmatrix}^T \tag{8.4}$$

Directions of f_1-f_6 and x_1-x_6 are show in Figure 8.2 a) and b). K_q is the stiffness matrix of a single pile head. (Bredenberg and Broms, 1983)

8.3 Determination of a Single Pile Head's Stiffness Matrix

8.3.1 Introduction

In linearly elastic analysis presented by Bredenberg and Broms (1983), lateral pile head's stiffness is analyzed by calculating the bending length of the pile. The bending length L_d is a function of pile's bending stiffness, EI, and stiffness of surrounding soil.

8.3.2 Pile in Friction Soil

The bending length of a pile in frictional soil L_{df} can be calculated with equation (8.5).

$$L_{df} = 1.8 \cdot \sqrt[5]{\frac{EI}{K_{py}}} \quad , \tag{8.5}$$

where the horizontal ground constant K_{py}, may be chosen from Table 8.1. Equation (8.5) is valid only with piles longer than $4L_{df}$.

Table 8.1: Ground constant K_{py} (Terzaghi,1955)

Relative density (D_r)	Loose	Normal	Dense	
Unsubmerged	2,5	7,0	18	MN/m^3
Submerged	1,5	4,5	11	MN/m^3

Single pile head's stiffness matrix elements in Equation (8.3), can be formed from Equation (8.6) through (8.15), when the modeled pile is in frictional soil.

$$k_{11} = k_{22} \tag{8.6}$$
$$k_{44} = k_{55} \tag{8.7}$$
$$k_{15} = k_{51} \tag{8.8}$$
$$k_{24} = k_{42} \tag{8.9}$$
$$k_{42} = -k_{15} \quad , \tag{8.10}$$

where

$$k_{11} = (1 + 3m)\frac{3 \cdot EI}{L_{df}^{3}} \tag{8.11}$$

$$k_{44} = \frac{4m \cdot EI}{L_{df}} \tag{8.12}$$

$$k_{15} = \frac{6 \cdot m \cdot EI}{L_{df}^{2}} \tag{8.13}$$

$$k_{33} = \frac{A \cdot E}{L} \tag{8.14}$$

$$k_{66} = \frac{m \cdot J \cdot G}{L} \quad , \tag{8.15}$$

where

m is 0 for hinged, and 1 for rigid pile head - pile cap fixity

A is the cross section area of the pile

L is the pile length

J is the pile's torsional bending stiffness

EI is the pile's bending stiffness

For a pile with square cross section the torsional bending stiffness J is $0.14b^4$ and for round $0.098b^4$, where b is pile's width. Shear modulus G can be estimated to be 40 % of pile's elastic modulus E. (Bredenberg and Broms, 1983)

8.3.3 Pile in Cohesion Soil

The bending length of a pile in cohesive soil, L_{dc}, is calculated as a function of the pile's bending stiffness EI, undrained shear strength of surrounding soil c_u and a time factor λ.

Time factor λ is a constant that considers time dependent resistance decrease in cohesive soil due to consolidation. It can be chosen from 20 to 80; 80 for short-term and 20 for long term situation. Time dependence factor λ versus time curve is shown in Figure 8.3.

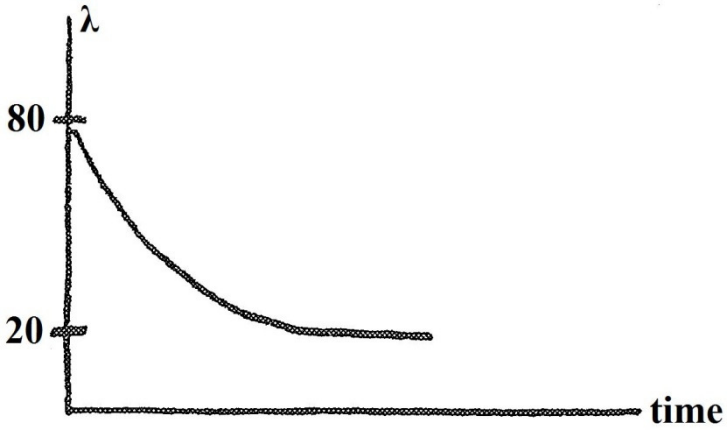

Figure 8.3: Time – λ – correspondence. (Bredenberg and Broms, 1983)

Deflection length of a pile in cohesive soil, L_{dc} is

$$L_{dc} = \sqrt[4]{\frac{4EI}{\lambda \cdot c_u}} \quad . \tag{8.16}$$

Single pile head's stiffness matrix's elements in Equation (8.3) , for a pile in cohesive soil are otherwise written as was for a pile in frictional soil, but

$$k_{11} = (1 + m) \cdot \frac{2 \cdot m \cdot EI}{L_{dc}} \tag{8.17}$$

$$k_{44} = \frac{2 \cdot m \cdot EI}{L_{dc}} \tag{8.18}$$

$$k_{15} = 2 \cdot m \cdot \frac{EI}{L_{dc}^{\,2}} \quad . \tag{8.19}$$

8.3.4 Pile Partially in Soil

For piles that are only partially in soil, the following elements of a single pile head's stiffness matrix have to be modified with terms

$$k_{11} = \frac{3 \cdot \left(1 + m\left(1 + 2L_r\right)\right)e}{L_a^{\,2}} \tag{8.20}$$

$$k_{44} = \frac{m\left(3 + 6 \cdot L_r + 6 \cdot L_r^{\,2} + 2 \cdot L_r^{\,3}\right) \cdot e}{L_a^{\,2}} \tag{8.21}$$

$$k_{15} = \frac{3 \cdot m\left(1 + 2 \cdot L_r + L_r^{\,2}\right) \cdot e}{L_a^{\,2}} \quad , \tag{8.22}$$

where

$$L_r = \frac{L_f}{L_a} \tag{8.23}$$

and

$$e = \frac{2EI}{3 + 6L_r + 6L_r^2 + 2(1 + m)\,L_r^3 + mL_r^4}. \tag{8.24}$$

L_a is L_{df} or L_{dc}, depending if the pile is partially in a cohesive or partially in a frictional soil. L_f is the free length of the pile. (Bredenberg and Broms, 1983)

8.3.5 Free Pile Rigidly Fixed to the Pile Cap

For a pile group where side resistance from surrounding ground is not considered, the stiffness matrix K_q is formed with following terms.

$$k_{11} = k_{22} \tag{8.25}$$

$$k_{22} = \frac{3EI}{L^3} \tag{8.26}$$

$$k_{44} = k_{55} \tag{8.27}$$

$$k_{44} = \frac{3EI}{L} \tag{8.28}$$

$$k_{15} = 0 \tag{8.29}$$

Terms k_{33} and k_{66} can be solved as was done before.

8.3.6 Group Effect

When piles are installed close to each other, their individual efficiency will decrease, as was discussed in Chapter 7. This effect can be taken into account by reducing the ground resistance with a multiplier f_m presented in Figure 8.4. (Bredenberg and Broms, 1983)

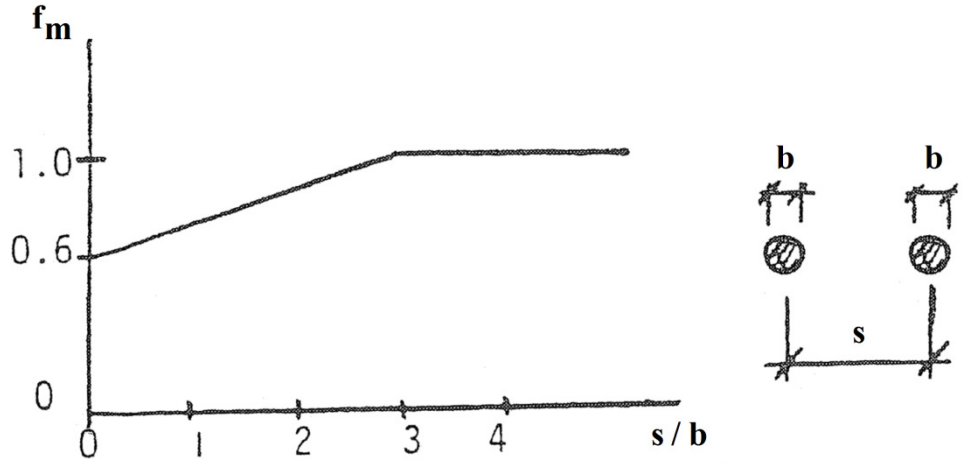

Figure 8.4: Correspondence between factors f_m and s/b. (Bredenberg and Broms, 1983)

As was discussed in Chapter 7 the group effect is not similar to both horizontal axis k_{sx} and k_{sy}, as illustrated in Figure 8.5. This causes a single pile's stiffness matrix to be unsymmetrical, and equations $k_{11}=k_{22}$, $k_{24}=k_{42}$, $k_{15}=k_{51}$, $k_{24}=k_{15}$, $k_{55}=k_{44}$ do not apply any longer. The soil resistance must be reduced separately for both directions.

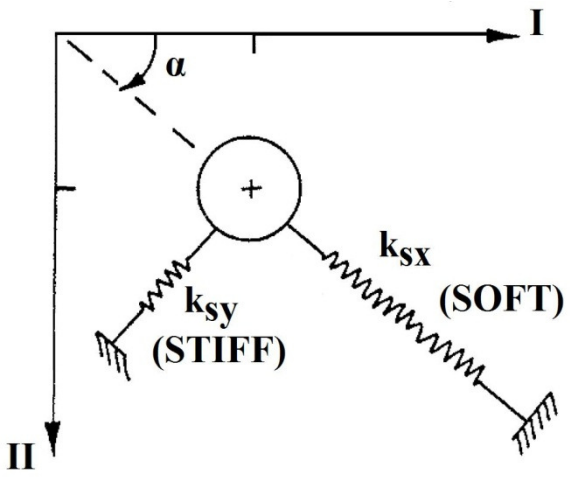

Figure 8.5: Different lateral stiffness due to the group effect. (Clausen, 1994)

8.4 Effect of a Pile Inclination

When a pile is inclined, its local coordination system 1-2-3 is inclined with the global coordinate system, I-II-III, fixed to the pile cap. That's why the pile's local coordinate system has to be rotated to coordinate system 1'- 2'- 3', which is parallel to the global coordinate system.

α is the lateral rotation angle and β is the inclination angle between pile's installation direction and vertical axis 3'. In other words, α is the angle from plan view of the system, and β is the inclination angle seen from the side of the pile group. Angles α and β are presented in the Figure 8.6.

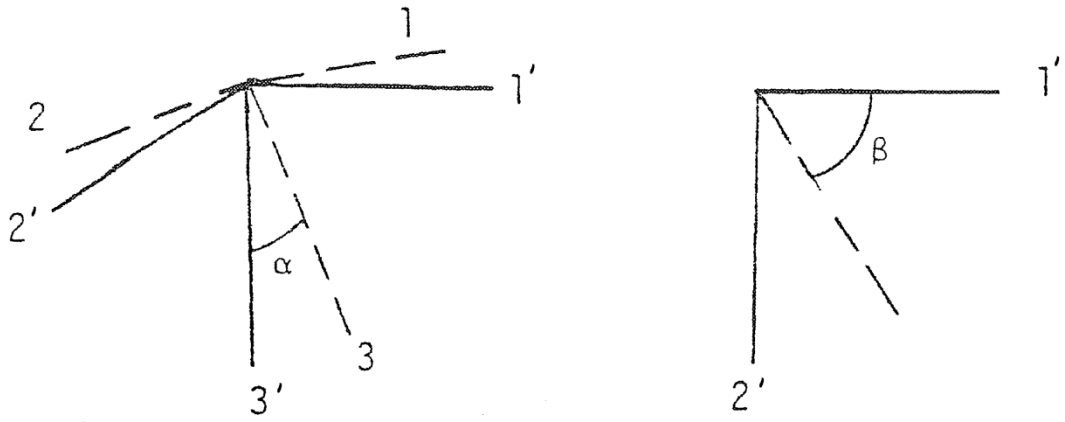

Figure 8.6: Angles α and β, (Bredenberg and Broms, 1983)

A single pile's force vector, F_q, can be converted to a force vector parallel to the pile cap, F'_q, by multiplying it with matrix A_q, (8.30).

$$A_q = \begin{pmatrix} A' & 0 \\ 0 & A' \end{pmatrix}, \tag{8.30}$$

where

$$A' = \begin{pmatrix} \cos(\beta)\cdot\cos(\alpha) & -\sin(\alpha) & \sin(\beta)\cdot\cos(\alpha) \\ \cos(\beta)\cdot\sin(\alpha) & \cos(\alpha) & \sin(\beta)\cdot\sin(\alpha) \\ -\sin(\beta) & 0 & \cos(\beta) \end{pmatrix}. \tag{8.31}$$

The relation of a pile head's displacement vector between these two coordinate systems is

$$X_q = A_q^T \cdot X'_q \quad . \tag{8.32}$$

When equations (8.1) and (8.32) are combined, the force vector F'_q (in parallel coordinate system with the global coordinate system) can be formed with Equation (8.33). (Bredenberg and Broms, 1983)

$$F'_q = A_q \cdot K_q \cdot A_q^T \cdot X'_q \tag{8.33}$$

8.5 Effect of a Pile Head's Position

The global coordinate system I-II-III is fixed to a pile cap as shown in Figure 8.7.

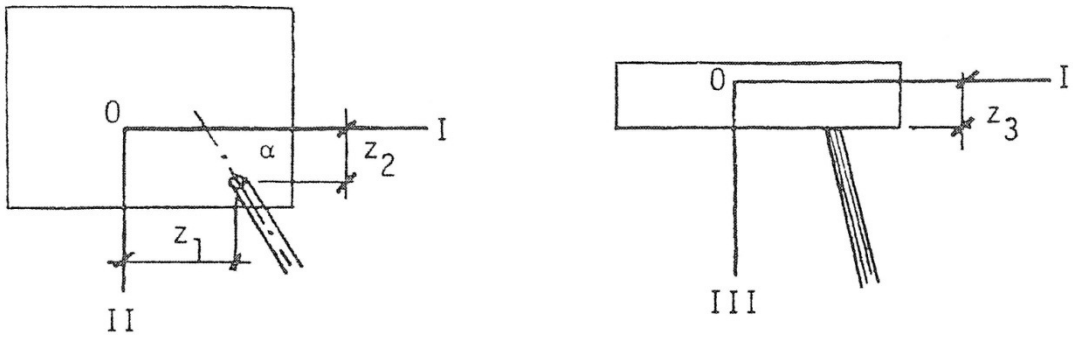

Figure 8.7: a) Pile cap coordination system from above b) Pile cap coordination system from the side. (Bredenberg and Broms, 1983)

At the Figure 8.7 a) and b), the single pile head's coordinates, z_1, z_2 and z_3 in global coordinate system are illustrated.

Single pile's loading vector P_q in the global coordination system is

$$P_q = C_q \cdot F'_q \quad , \tag{8.34}$$

where

$$C_q = \begin{pmatrix} 1 & 0 & 0 & 0 & 0 & 0 \\ 0 & 1 & 0 & 0 & 0 & 0 \\ 0 & 0 & 1 & 0 & 0 & 0 \\ 0 & -z_3 & z_2 & m & 0 & 0 \\ z_3 & 0 & -z_1 & 0 & m & 0 \\ -z_2 & z_1 & 0 & 0 & 0 & m \end{pmatrix} . \tag{8.35}$$

Relationship between pile head's force vector $F`_q$ and loading vector P_q is shown in Figure 8.8.

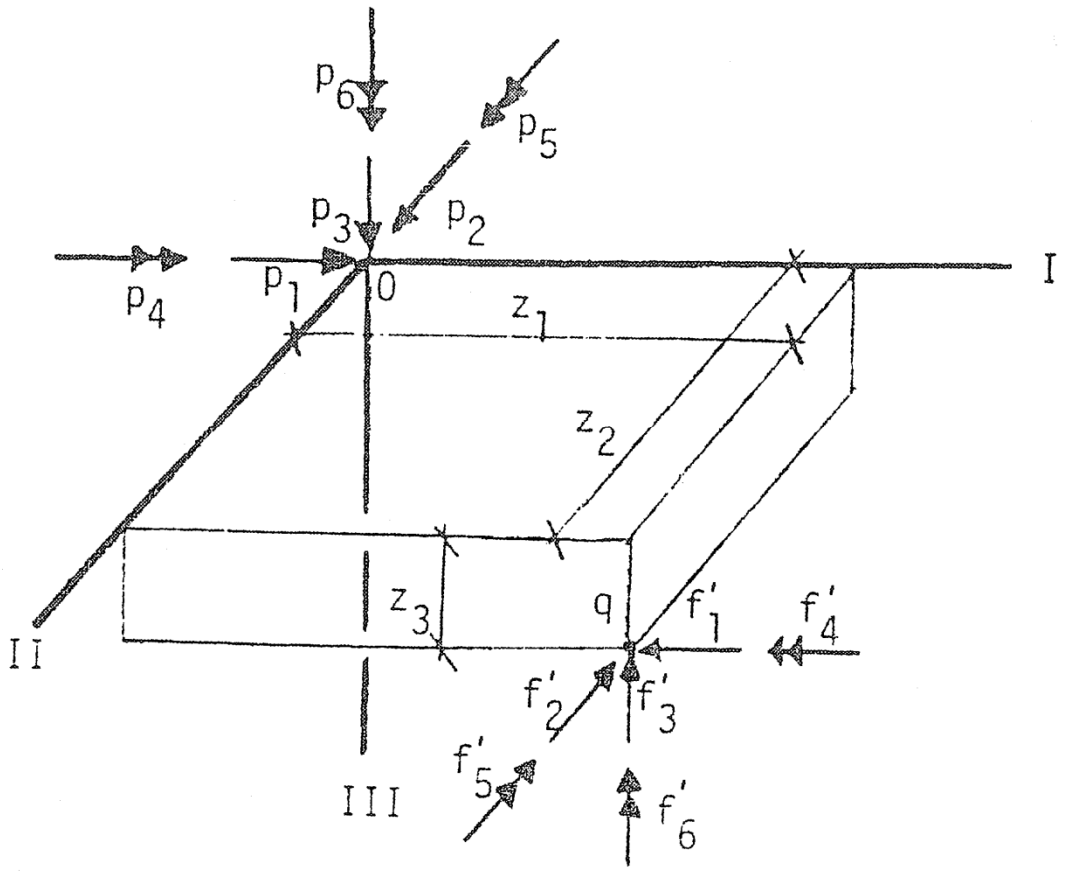

Figure 8.8: Correspondence between F`q, Pq and origin. (Bredenberg and Broms, 1983)

8.6 Gathering of the System Stiffness Matrix

When effects by inclination, placement and stiffness of a pile are gathered, the individual pile's global stiffness matrix in global coordination system, S_q, can be formed with Equation (8.36).

$$S_q = D_q \cdot K_q \cdot D_q^T \quad , \tag{8.36}$$

where

$$D_q = C_q \cdot A_q \quad . \tag{8.37}$$

When this global stiffness matrix is formed for each of piles in a group, the system's stiffness matrix S can be formed by summation of the single piles' stiffness matrixes.

8.7 Forming of Loading and Transition Vectors

The vector of external forces, R's, elements and their directions are shown in Figure 8.9. As shown in the figure, all forces are deducted to a pile cap's origin.

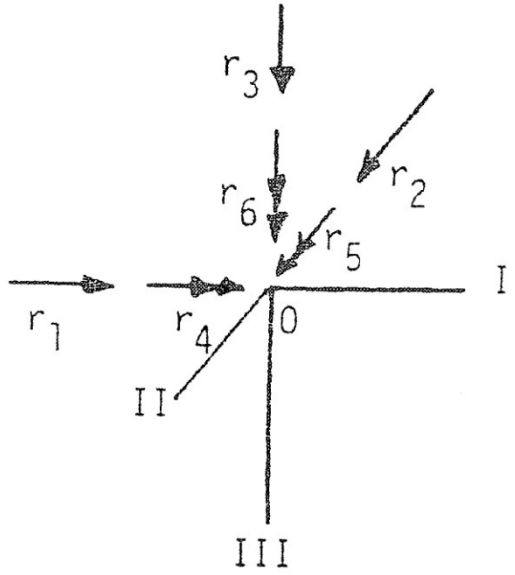

Figure 8.9: Directions of a global loading vector's elements. (Bredenberg and Broms, 1983)

Elements of a global displacement vector U are illustrated in the Figure 8.10.

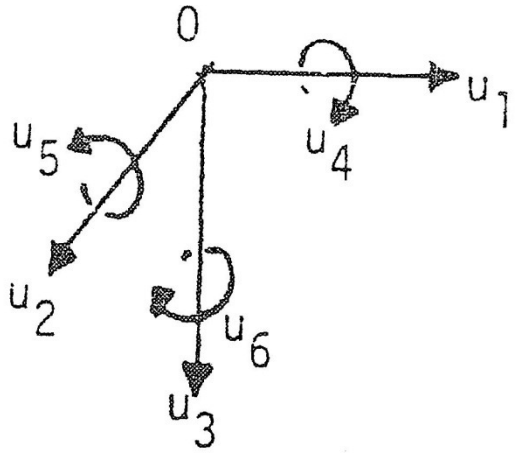

Figure 8.10: Directions of a displacement vector's (U) elements. (Bredenberg and Broms, 1983)

The summation of individual pile's loading vectors has to be equal to the global loading vector, Equation (8.38), so that the system is in equilibrium.

$$R = \sum_{q=1}^{n} P_q \quad . \tag{8.38}$$

This equation becomes significant especially with the iterative process, which will be introduced in Chapter 9.

8.8 System Transitions

Correspondence between pile group's loadings, R, and transitions U, can be written as

$$R = S \cdot U, \tag{8.39}$$

where S is the system's stiffness matrix.

8.9 Gathering of the Results

When the force vector F_q and the transition vector X_q are formed for each pile, the axial forces, largest bending moments, largest shear forces, and torsional bending moments can be solved.

Each pile's force vector is F_q (Equation (8.40)), with vector's elements' directions illustrated in Figure 8.2 a).

$$F_q = \begin{pmatrix} f_1 \\ f_2 \\ f_3 \\ f_4 \\ f_5 \\ f_6 \end{pmatrix} \tag{8.40}$$

In this vector (8.40), f_3 represents the pile's axial force from a pile to the pile cap.

The largest shear force f_V can be calculated with equation

$$f_V = \sqrt{f_1^2 + f_2^2} \quad . \tag{8.41}$$

The largest bending moment f_M and its depth can be solved with the equations presented on Table 8.2.

Table 8.2: Computing of the largest bending moment. (Bredenberg and Broms, 1983)

Soil Type	Fixation to the pile cap	Max. Bending moment [kNm]	Depth from the ground surface [m]
Friction	Hinged	$0.43f_VL_{df}$	$0.8L_{df}$
	Rigid	$(f_4^2+f_5^2)^2$	+/-0
Cohesion	Hinged	$0.32f_VL_{dc}$	$0.8L_{dc}$
	Rigid	$(f_4^2+f_5^2)^2$	+/-0

The force vector's element f_6 is the element for the pile's torsional bending moment. The largest ground pressure between a pile and soil can be computed with equations presented on Table 8.3.

Table 8.3: Computing of the largest pile-soil pressure. (Bredenberg and Broms, 1983)

Soil Type	Fixation to the pile cap	Max. Ground pressure [kPa]	Depth from the ground surface [m]
Friction	Hinged	$1.75f_V/(L_{df}D)$	$0.44L_{df}$
	Rigid	$1.15f_V/(L_{df}D)$	$0.54L_{df}$
Cohesion	Hinged	$2f_V/(L_{dc}D)$	+/- 0
	Rigid	$f_V/(L_{dc}D)$	+/- 0

9 Non-Linear Modeling of a Pile Group

9.1 Modeling Technique

The solution of the complete superstructure-pile-soil system is obtained through the use of different modeling techniques: (Clausen, 1994)

1. The superstructure is assumed to be linear elastic i.e., it is possible to establish a unique relationship between the six displacement components of each of the superstructure support points and the corresponding six forces acting at the support points, Equation (8.1). This procedure was explained in Chapter 8.
2. The piles are modeled as finite elements. Each pile is subdivided into a number of elements that are rigidly interconnected at nodal points. Each node has six degrees of freedom. In this thesis only lateral loading of a pile group is considered, so the degree of freedoms is reduced to four. This method was presented in Chapter 5.
3. A linear variation of pile-soil contact stresses is assumed over the length of each element, Figure 5.1 a).
4. At each pile node, the incremental change in pile-soil contact stress is equal to the relative displacement, pile node displacement minus soil displacement, times a secant stiffness value in the direction considered. These secant stiffness values are dependent upon the magnitude of the relative displacement values, both resulting and incremental values. This modeling step is a combination of Chapters 3, 4 and 5.
5. The pile-soil secant stiffness values are computed from known or assumed relative displacement values using computed p-y load displacement data as was introduced in Chapter 3.
6. The soil profile is divided into a number of layers. Each layer is assumed to have constant geotechnical properties.
7. Pile-soil-pile interactions are computed from elastic half-space theory by using Mindlin's equation, in Chapter 7.3, or by reducing the soil stiffness's around the pile with computed multipliers as was described in Chapter 7.2.

8. Loading of the system may be a number of load vectors divided into one or several load increments. For each load increment a number of iterations may be performed in order to meet a specified convergence criterion, as is shown in Figure 9.1.

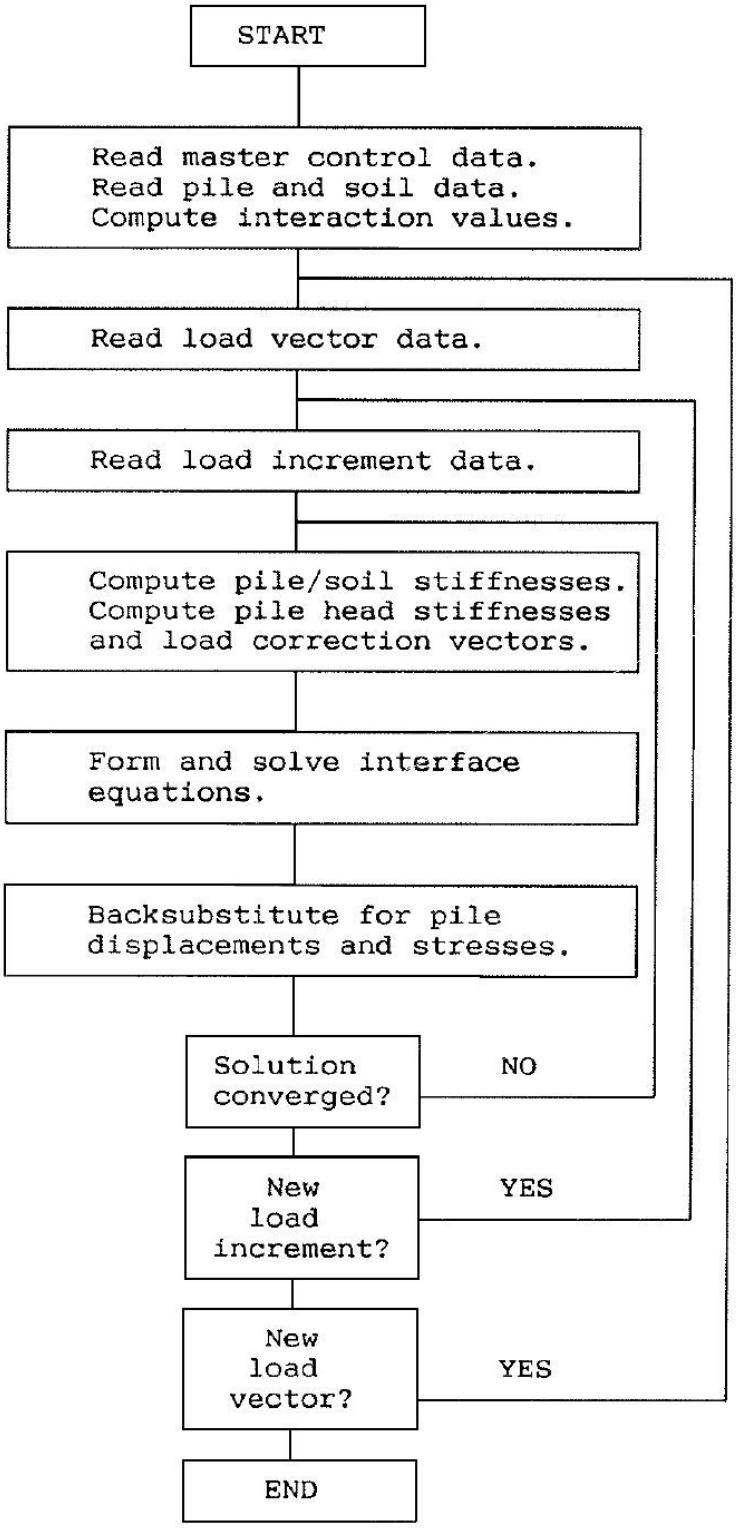

Figure 9.1: SPLICE Main Control Flow. (Clausen, 1994)

9.2 Single Pile Solution

In computer program SPLICE, a pile head is assumed to be rigidly fixed to the pile cap. This gives an additional option for a single pile tip to be modeled as free. On the other hand it naturally reduces the option for pile head- pile cap fixity to be modeled as hinged. The initial step of the iteration procedure of a single pile in Chapter 6.2, was to assume an initial deflection at the pile head in order to compute the pile deflections and soil displacements. In SPLICE the initial deflection is set to the pile tip and pile forces are back calculated from tip to head. (Clausen, 1994)

1. The displacements of the pile tip are assumed to be known.
2. From the pile tip boundary stiffness values, the corresponding pile tip forces can be computed.
3. The displacements of the soil surrounding at all nodes are assumed to be known, so that elastic springs can be set to every pile node.
4. With known displacements and forces at a pile element bottom and known soil displacements, the displacements and the forces at the top of the pile can be computed.
5. When the head has been reached, the computed forces are the forces required at the pile head in order to develop the displacement assumed at the pile tip. The computed pile head displacements are the displacements associated with the computed pile head forces.

This solution procedure assumes linear elastic conditions, at which is the case within each iteration step. It follows that the problem of solving a single pile, once the pile tip displacements are known, has been reduced to that of expressing displacements and forces at the top of a pile element in terms of those at the element bottom and other quantities.

9.3 Pile Group Solution

These solution procedures are used twice within SPLICE, for each iteration step: (Clausen, 1994)

1. To form pile head stiffness values for Equation (8.3) and load correlation vectors.

2. To solve the piles for actual forces and displacements after the superstructure and pile interface equations has been formed (Equation (8.1))

The above procedure assumes that there is a reasonable degree of coupling between the pile head and the pile tip, i.e. unit forces acting at the pile head will result in displacements at the (free) pile tip different from zero.

10 Static Loading Test of a Pile Group

10.1 Introduction

The pile group loading test, conducted by J. Walsh (2005), was oriented on a 3 x 5 pile configuration with row spacing 3.92 pile diameters center-to-center in the direction of loading. A single pile loading test was also conducted at the site for obtaining reference data. This chapter describes briefly the test layout, instrumentation and the testing procedure.

10.2 Test Layout

The pile group piles were organized into five rows of three piles each. In the direction of loading, piles were spaced a distance of 3.92 pile diameter or 1.27 m on centers. Perpendicular to loading, piles were spaced 3.29 diameters or 1.07 m on centers. Figure 10.1 is a photograph of the pile group and the single pile.

Two reinforced concrete shafts (1.22 m diameter) were installed 7.92 meters north of the front or northernmost row of the 15-pile group. These shafts served as the loading point against which the pile group was reacted (Figure 10.3).

Figure 10.1: Photograph taken from the west of the overall layout of the 15-pile group and the single pile. (Walsh, 2005)

All the piles were conformed to ASTM A252 Grade 3 specification. The outer diameter of each pile was 423 mm and the wall thickness was 9.5 mm. In conjunction with I-15 reconstruction project, Geneva Steel performed tests on 192 piles of the same type as used at the airport site. Using 0.2 percent offset method, the average yield strength of the piles was determined as 404 592 kPa with a standard deviation of 15 168 kPa. The average tensile strength was found to be 584 087 kPa with standard deviation of 17 659 kPa. Calculations are performed on the same type resulted in a yield moment of 350 kNm. Because the center pile of each row had angle irons attached to protect strain gages as presented in Figure 10.2.

The properties of these center piles were identical to those of the additional single pile, in that moments of inertia were 1.43×10^8 mm^4 about the axis perpendicular to loading. The outside piles of each row had a moment of inertia of 1.16×10^8 mm^4. All piles had a modulus of elasticity of 207 GPa.

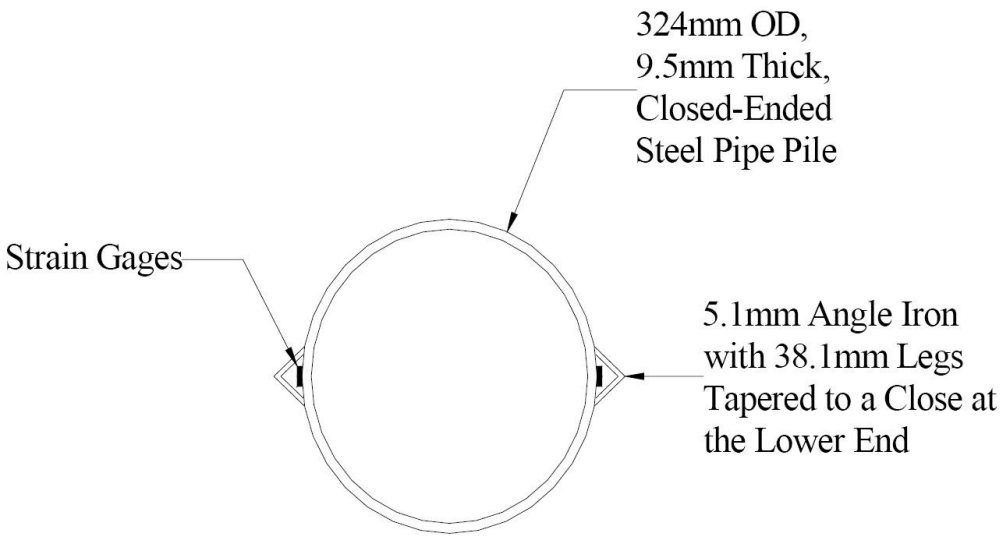

Figure 10.2: Cross-sectional view of a pile with additional angle iron (Snyder, 2004)

Figure 10.3 is a plan view of the test site and diagrams the locations of the 15-pile group, its companion single pile, and the drilled shafts used as a reaction foundation.

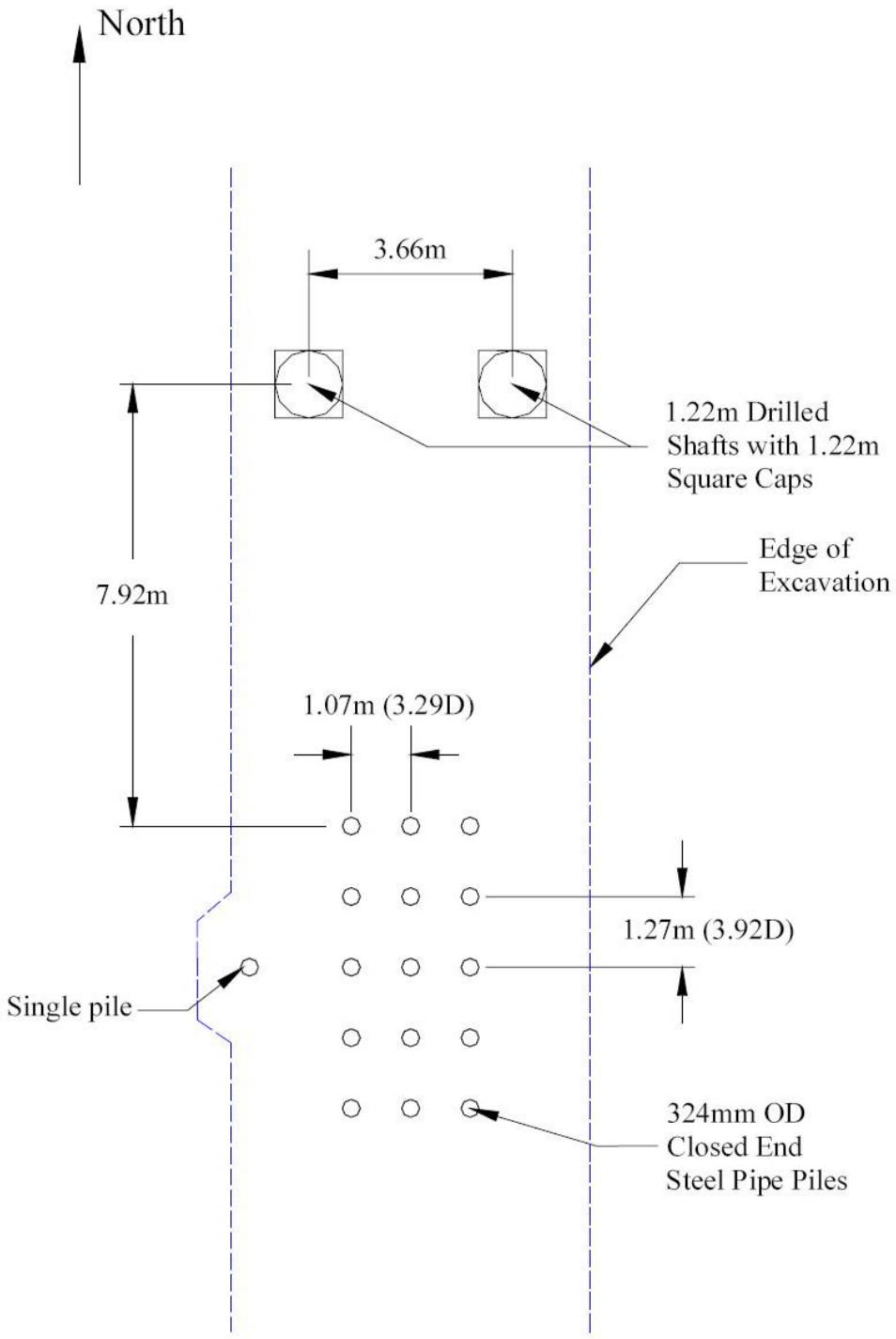

Figure 10.3: Plan view of the test site including locations of the 15-pile group its companion single pile, and the drilled shafts. (Snyder, 2004)

The layout of the loading system is provided in plan and profile views in Figure 10.4 and Figure 10.5, respectively. Two 1.34 MN hydraulic jacks loaded the group against

the two drilled shafts. A pump that could develop a maximum pressure of 69 MPa powered these jacks. A loading beam (AISC Shapes W760x248) was placed beside the two drilled shafts. Hemispherical swivel heads were placed between each jack and the beam and between each jack and the corresponding drilled shaft to prevent eccentric loading.

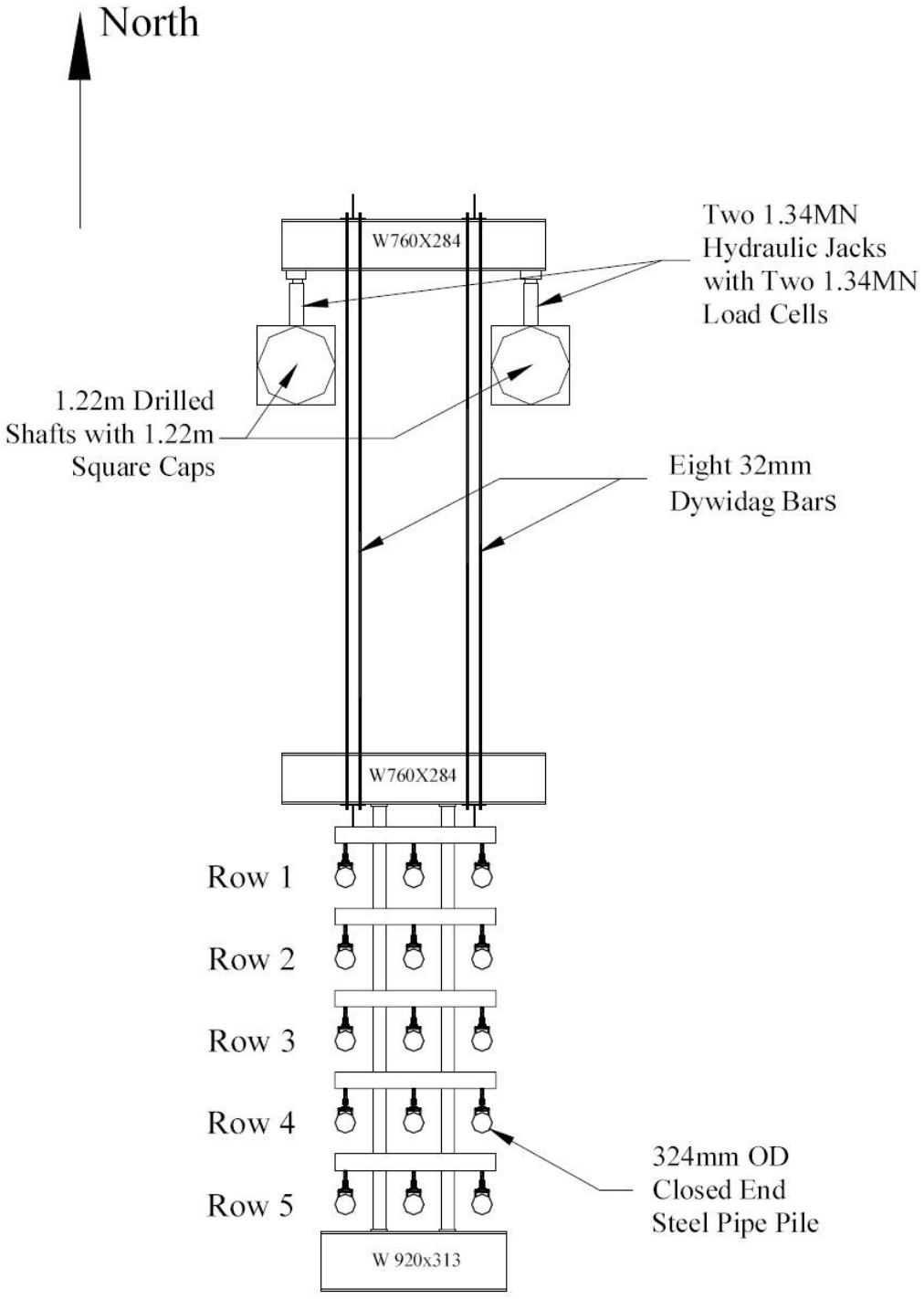

Figure 10.4: Plan view of the loading system for the 15-pile group and numbering of the pile rows. (Snyder, 2004)

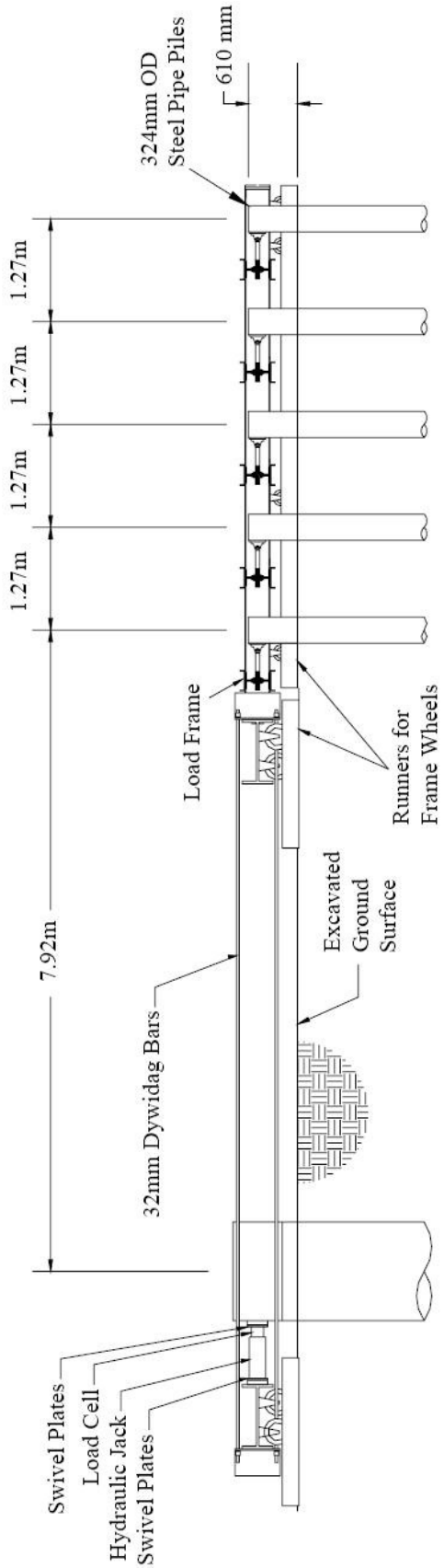

Figure 10.5: Profile of 15 piles test setup as viewed from east, looking west. (Walsh, 2005)

10.3 Instrumentation

Test-site instrumentation measured the lateral loads exerted against and the lateral displacement of each pile. They also measured the strains developed along the length of each pile so that the bending moment profiles could be computed.

The tie rods that connected each pile to the load frame served as loads cells. A pair of strain gages was attached to each tie rod. Combining strain gage data with known properties of the tie rod yielded lateral loads felt in each tie rod. Additionally, each hydraulic jack had an associated load cell that measured the load exerted through it the rest of the system. Thirteen string potentiometers (accurate to 0.25 mm) and two linear variable differential transformers (LVDTs) (accurate to 0.127 mm) measured the lateral displacement of each pile head. Two additional string potentiometers were used for both drilled shafts. A fixed frame separate from and raised above the loading system provided an independent reference point for the various measurement devices. Additionally, small aluminum channels with protruding hooks were glued to each pile or shaft at load point elevations, thus supplying a connection point between the piles/shafts and the reference frame. LVDTs and string potentiometers attached between these hooks and the reference frame recorded deflection data during the test. Figure 10.6 is a picture of instrumentation at the head of each pile.

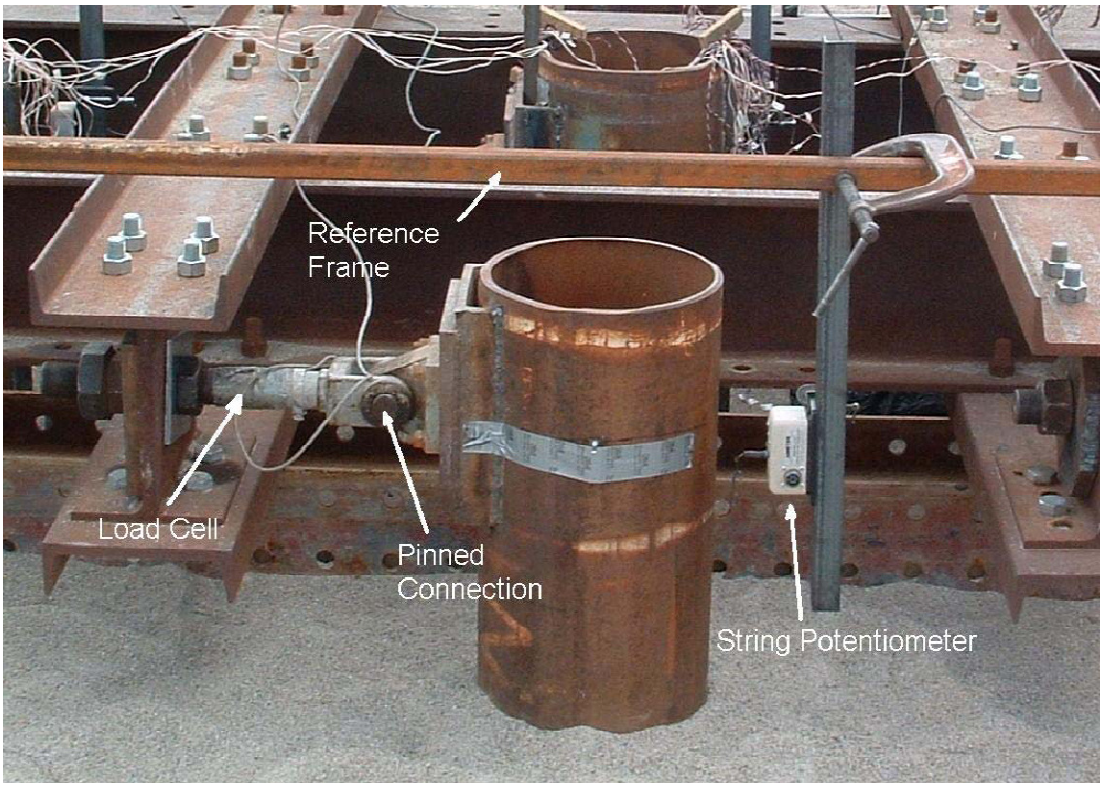

Figure 10.6: Setup for the pile-head deflection and loads. (Walsh, 2005)

10.4 Test Procedure

The 15-pile test was performed on five different days between July 29 and August 10, 2004. Target deflections were selected as 6, 13, 19, 25, 38, 51, 64 and 89 mm. The system was loaded until the specific target deflection was reached for a predetermined string potentiometer. Because all piles deflected slightly different amounts, this string potentiometer was not necessarily equal to the average deflection of the group as a whole. Consequently, average group deflections discussed in the following section did not peak at the exact target deflection they represent.

During the first day of testing, cyclic loading was carried out up to the 28 mm target deflection without incident. However, as the pile group was being loaded to the 51 mm target deflection, the hydraulic jacks rapidly rotated upward causing the reaction beam to slip out of place and suddenly move up and over the drilled shafts. Subsequent tests suggested that this occurrence resulted from a minor misalignment of the load cells on the spherical end-plates, which developed as the deflection levels increased.

This incident made it necessary to reposition and carefully realign the frame for subsequent testing. Because testing was conducted over a period of a week and a half, problems arose in merging the data sets from different days.

Results for target deflections of 63 and 68 mm were successfully zeroed out by integrating measurements taken during instrument checks with data collected during testing, so adjusted data agreed with trends developed for lower target deflections and likewise coincided with computed results (discussed in Chapter 11). While deflection data corrected this way provided information regarding pile group displacements for higher loads, strain data for higher target deflections could not easily be corrected. Consequently, J. Wash's rapport includes plots of load versus deflection and load distribution among piles and rows for target deflections up trough 68 mm, but bending moments versus depth curves are only provided up to the 38 mm deflection level.

11 Computer Analysis of the Loading Test

11.1 Introduction

Three different computer programs are used to simulate this pile group field loading test.

1. J. Walsh (2005) analyzed this field test in his master‘s thesis by using nonlinear computer program GROUP Version 4.0 with back-calculated p-multipliers.

2. Another nonlinear computer program SPLICE (Version 1.04) is used to analyze this pile group. SPLICE uses Mindlin’s elastic soil model for analyzing group effect.

3. Linear elastic computations are conducted with the method introduced by Bredenberg and Broms (1983) (Chapter 8), with the back-calculated p-multipliers presented by J. Walsh (2005). Also the horizontal ground resistance K_{py} is back calculated.

11.2 Input Parameters for Computations

11.2.1 Input Parameters for GROUP

As was explained in Chapter 10, J. Walsh (2005) conducted a single pile loading and 15-pile group loading tests separately. The single pile was analyzed with nonlinear computer program LPILE and GROUP was used to model 15-pile group test.

Calculations performed in GROUP are essentially identical to the one in LPILE with addition of p-multipliers. Because GROUP and LPILE share the same computational methodology, the soil profile to model the single pile test in LPILE could likewise be used to model the 15-pile group test in GROUP. The soil profile was kept constant and p-multipliers were back-calculated so by matching the measured load-deflection curves for each row with the curves computed using GROUP.

The back calculated p-multipliers are presented on Table 11.1 and preliminary results of this back calculation are shown in Figure 11.1, where average group deflection versus loading curves of field test and GROUP computations are to be seen.

Table 11.1: Back calculated p-multiplier (J. Walsh, 2005)

	Row 1	Row 2	Row 3	Row 4	Row 5
p-multiplier	1	0.5	0.4	0.3	0.4

Just for a comparison, p –multipliers were also computed with the method presented in Chapter 7.2, giving the results on Table 11.2.

Table 11.2: Calculated p-multipliers

	Western pile	Center pile	Eastern pile
Leading row 1	0.95	0.90	0.95
Trailing rows 2 - 5	0.63	0.52	0.63

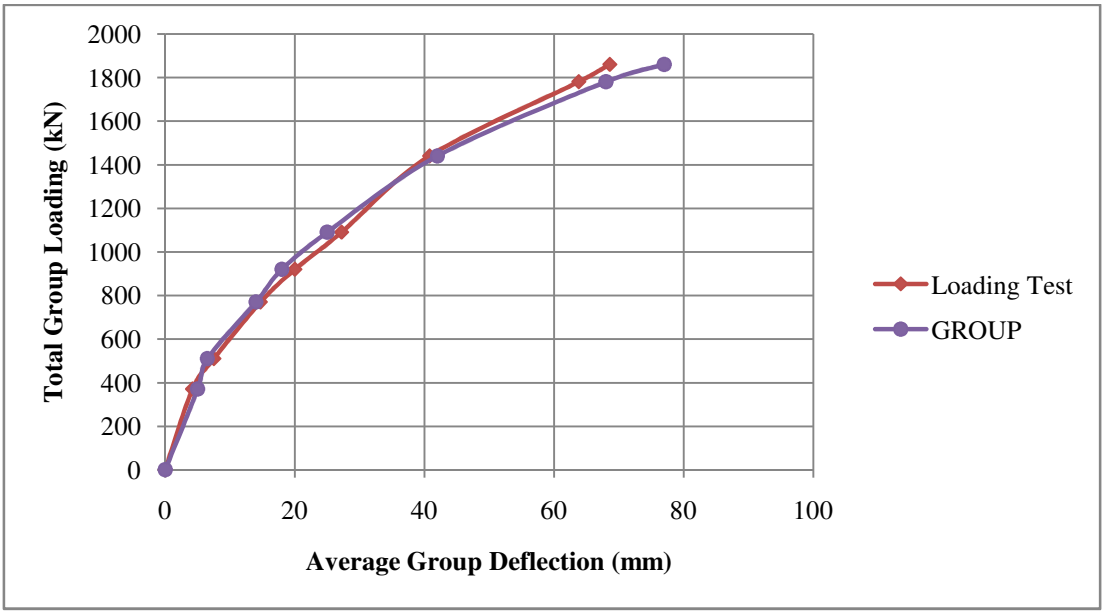

Figure 11.1: Load - deflection curve from loading test and from GROUP computation, J. Walsh (2005)

11.2.2 Input Parameters for SPLICE

Input parameters for SPLICE were chosen to be as similar as possible with the soil and pile profiles used by J. Walsh (2005), because calculation results of J. Walsh seemed to compensate quite accurately with the measured data. In that way the two different pile-soil-piles -interaction modeling methods, could be compared. Input soil parameters for SPLICE are shown on Table 11.3 and input pile data on Table 11.4.

In addition to soil input parameters used in GROUP, there are several parameters that needed to be set for SPLICE computations. Some of those parameters have relative little to do with the results of these computations, because they are used only with axial pile loading analyzes.

As was discussed in Chapter 9.3, in computer program SPLICE, there must be some level of fixity between a pile head and a pile cap. In the field test conducted by J. Walsh (2005), the pile heads were hinged to the loading frame, and there were no moment forces at the pile heads. To be able to model this sort of a problem with SPLICE, the piles had to be divided into two segments. The upper segment models a hinged fixity between the pile cap and the pile head (Table 11.4., segment 1), so it has a very short length and low bending stiffness. The lower segment of the pile models the pile itself (Segment 2).

Table 11.3: Soil parameters for SPLICE computations

Layer	Depth	γ	s_u	ø	ε_{50}	J_e	t_{comp}	t_{tens}	t_{res}/t_{max}	t_{zres}	q_{tip}	z_{tip}/D
	[m]	[kN/m^3]	[kPa]	[deg]	[---]	[---]	[kPa]	[kPa]	[---]	[mm]	[kPa]	[---]
Sand 1	0-2.4	16.7	0	40	0.01	0.5	38	19	1.0	2.5	7660	0.01
Clay 1	2.4-2.7	19.1	41	0	0.01	0.5	41	41	0.8	2.5	372	0.01
Clay 2	2.7-3.7	19.1	50	0	0.01	0.5	50	50	0.8	2.5	450	0.01
Clay 3	3.7-4.6	19.1	40	0	0.01	0.5	40	40	0.8	2.5	360	0.01
Sand 2	4.6-6.3	18.1	0	38	0.01	0.5	29	15	1.0	2.5	5743	0.01
Clay 4	6.3-8.0	19.1	57	0	0.01	0.5	57	57	0.8	2.5	512	0.01
Sand 3	8.0-15	16.7	0	33	0.01	0.5	23	12	1.0	2.5	4599	0.01
Water table below the ground surface 2.13 m.												

Table 11.4: Pile parameters for SPLICE computations

	Segment number	Length	Unit weigth	Outer diameter	Wall thickness	Yield strength	E-modulus	EI	EA	Tip code
		[m]	[kN/m^3]	[m]	[mm]	[MPa]	[GPa]	[kNm^2]	[MN]	
Side row piles	1	0.001	28	0.324	9.5	405	207	0.1	1943	
	2	13.299	28	0.324	9.5	405	207	24010	1943	Free
Middle row piles	1	0.001	28	0.324	9.5	405	207	0.1	2104	
	2	13.299	28	0.324	9.5	405	207	29600	2104	Free
Loading point for each pile 0.483 m above the ground surface.										

$J_{e,}$ which effects to the form of p-y curves, was chosen to be 0.5 for each layer, as was recommended by Matlock (1970) and discussed in Chapter 3.2.2.

Parameters used to model axial skin friction in compression, t_{comp} were chosen for each layer from the reference thesis of J. Walsh (2005). But the ultimate skin friction in tension t_{tens}, was chosen to be the same as in compression for clays and a half of the initial value for sands, due to decreasing of horizontal soil pressure by soil elevation.

Residual skin friction in proportion to ultimate skin friction, t_{res}/t_{max} , values were chosen from Figure 4.2. The very same figure was also used for values of t_{zres}, axial deflection of a pile where the residual skin friction is achieved.

The factor relating deflection at max tip bearing with pile diameter, z_{tip}/D, were chosen to be 0.01 for each layer, which correspond 3.2 mm axial displacement with the piles used.

Terms $t_{comp,}$ t_{zres}, t_{res}/t_{max}, tz_{res}, z_{tip}/D doesn't have significant effect to results, because SPLICE doesn't consider skin friction due to the lateral transition or bending of a pile that was presented in Chapter 4.

The SPLICE uses Mindlin's elastic model to analyze pile-soil-pile interaction. Elastic modulus E_0 was chosen from Table 11.5 to be 25 000 kPa for the ground surface and increasing constant versus depth E_1/z 2000 kPa. In that way, the ground surface is modeled as relatively loose sand, and the deeper layers are hardening approximately until a value of 51 000 kPa at the pile tip, which corresponds a value of dense sand on Table 11.5.

Table 11.5: Representative Values of E and ν. (Girsang, 2001)

Soil Type	Elastic Modulus	Poisson's Ratio
	[kPa]	[---]
Loose Sand	10 350 - 27 600	0.2 - 0.4
Medium Sand		0.25 - 0.4
Dense Sand	34 500 - 69 000	0.3 - 0.45
Silty Sand		0.2 - 0.4
Soft Clay	1 380 - 3 450	0.15 - 0.25
Medium Clay		0.2 - 0.5
Hard Clay	5 865 - 13 800	

The distance of shadowing effect was calculated to be 3.8 m, with Rankine assumption for frictional soil, Figure 11.2. The depth of the influence zone was assumed to be the depth of the sand layer at the top of the soil profile, 2.4 m.

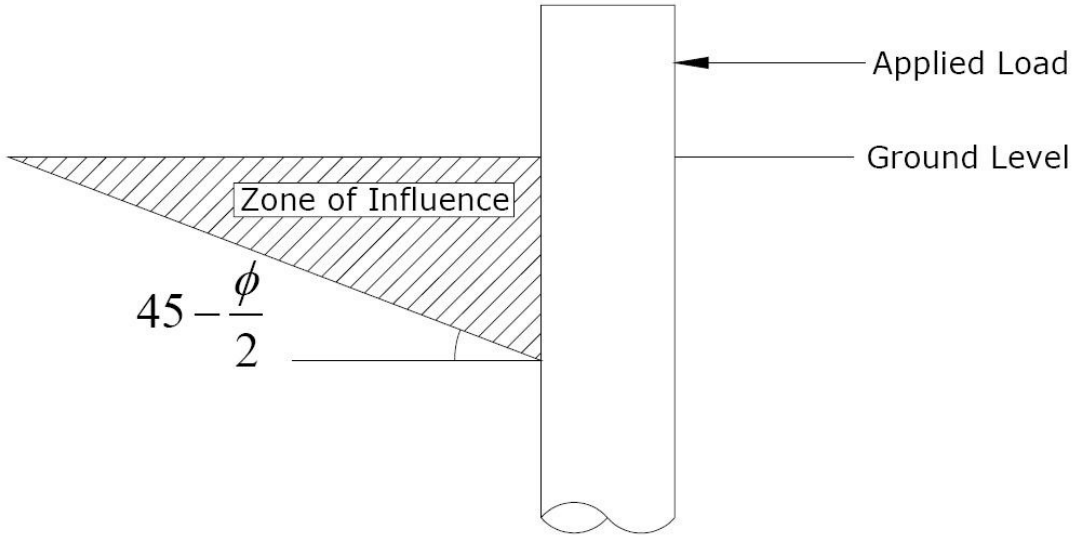

Figure 11.2: Rankine assumption of passive zone that develops in front of a laterally loaded pile. (Rankine, 1857)

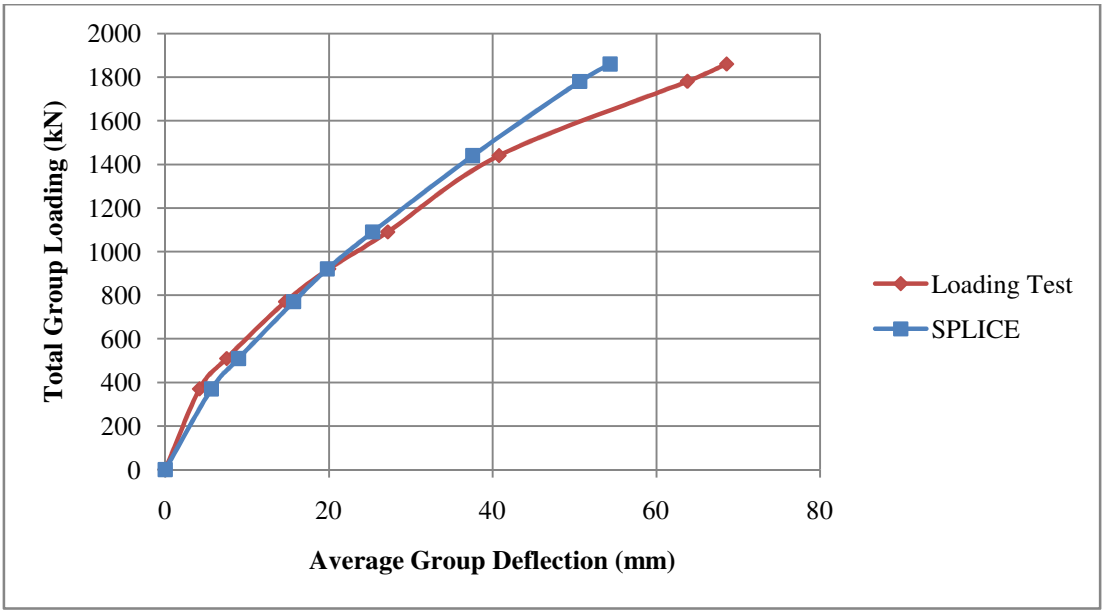

Figure 11.3: Load-deflection curves from field test and from SPLICE computations

11.2.3 Input Parameters for Linear Elastic Computation Program

The back-calculated p-multipliers presented by J. Walsh (2005) (Table 11.1) were used to analyze the 15-pile group linear elastically. The soil input data for this type of analyses is given only by horizontal ground coefficient K_{py}. This value was back-calculated by iterative process, so that the group loading- group deflection curve was parallel with the measured data (target deflections smaller than 38 mm). This procedure gave K_{py} a value of 2080 kN/m^3 as shown in Figure 11.4. The received value of K_{py} corresponds in Table 8.1 for loose sand.

The pile data presented for SPLICE in Table 11.4 was also used for linear elastic calculations. The main difference with linear elastic pile input data to SPLICE pile data, was that in linear elastic computation process, the pile head- pile cap fixity could be computed as hinged, so there was no need for the hinge segment 1. The downside was that the piles had to be modeled as fully submerged to the ground.

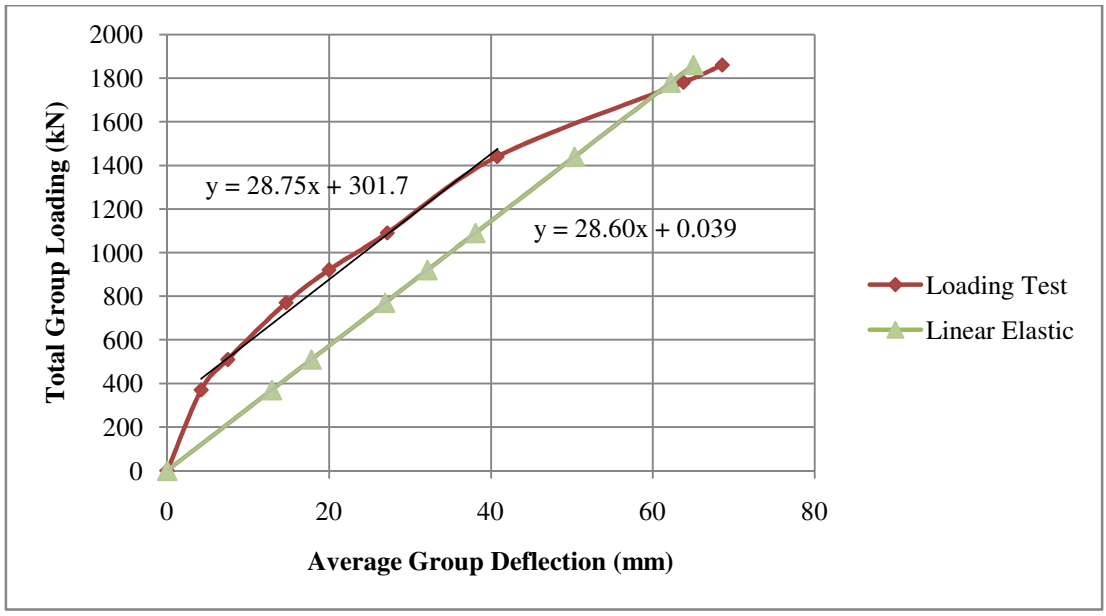

Figure 11.4: Load-deflection curves from field test and from linear elastic analysis, with K_{py} a value of 2080 kN/m^3.

11.3 Loading versus Deflection per Each Row

11.3.1 GROUP Computation Results, J. Walsh (2005)

With back calculated p-multipliers, GROUP calculations gave the results shown from Figure 11.5 through Figure 11.9.

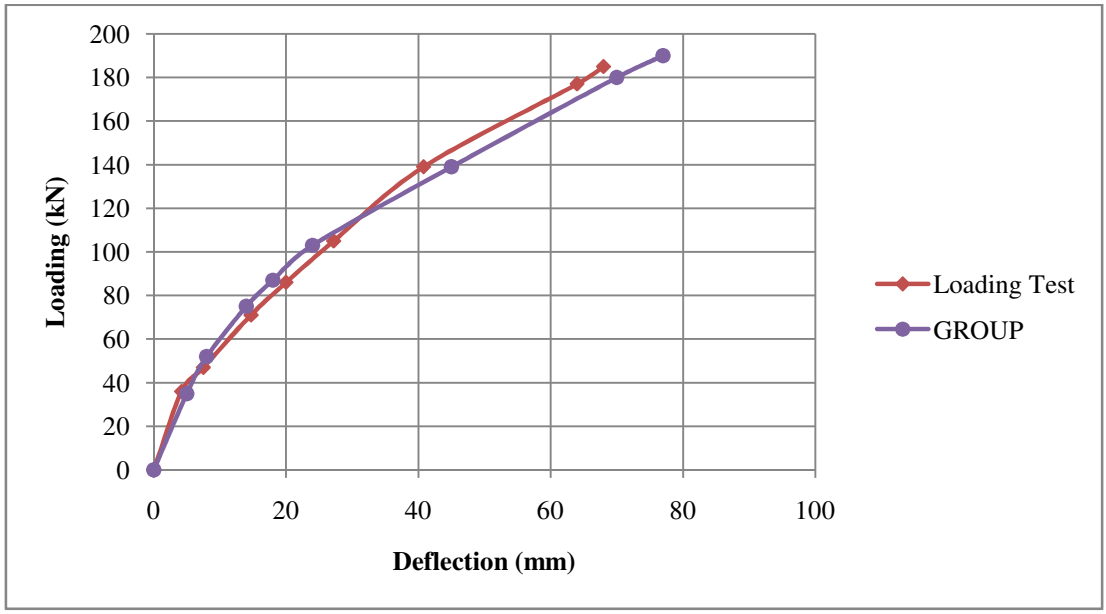

Figure 11.5: Computation results from GROUP and measured load - deflection curve for row 1. (Walsh, 2005)

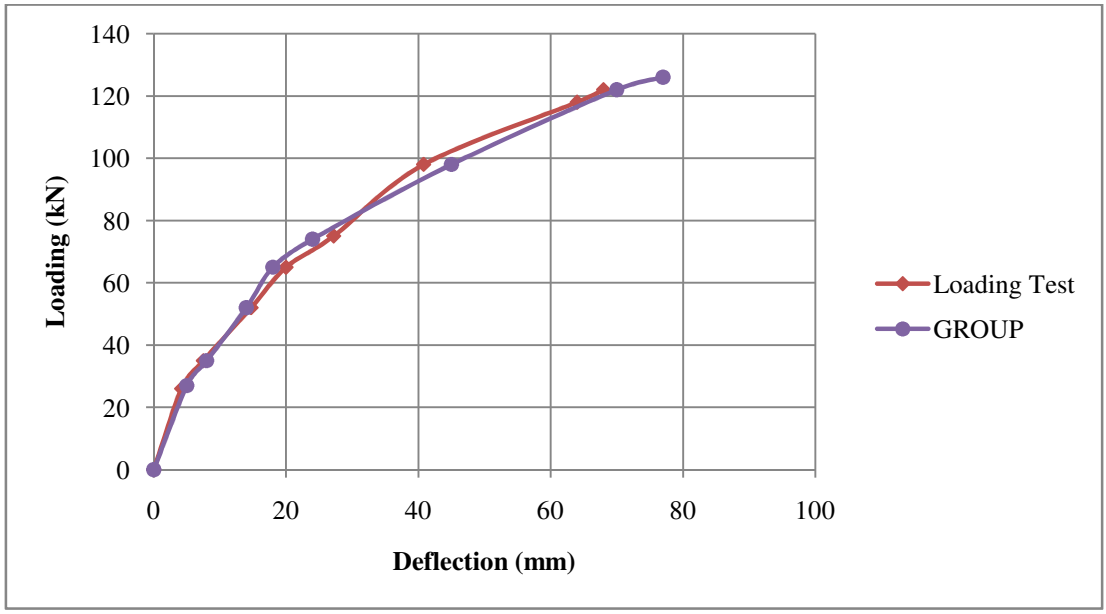

Figure 11.6: Computation results from GROUP and measured load - deflection curve for row 2. (Walsh, 2005)

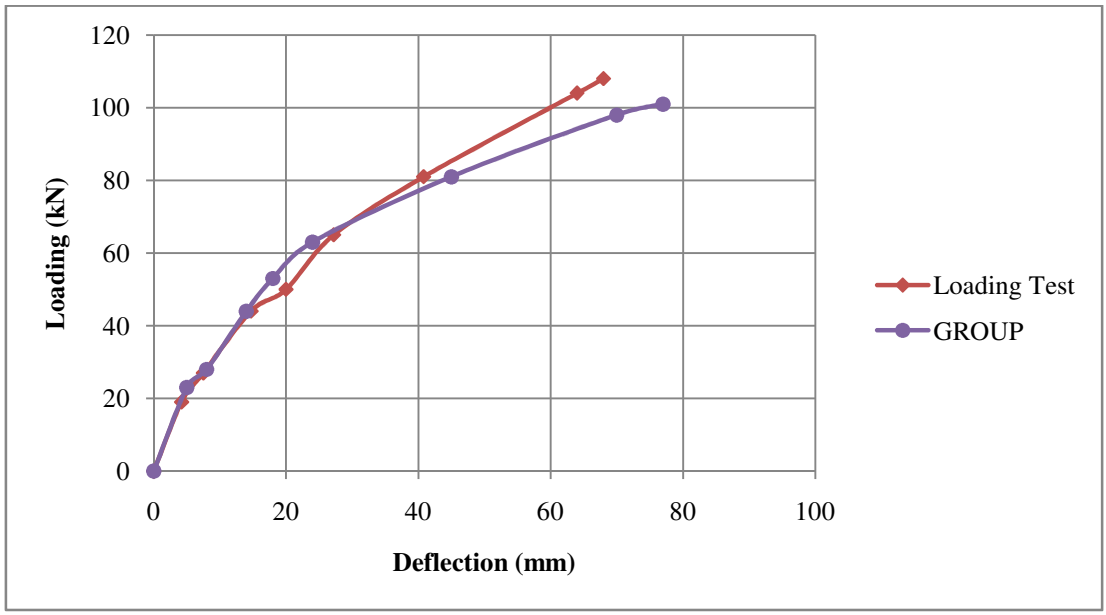

Figure 11.7: Computation results from GROUP and measured load - deflection curve for row 3. (Walsh, 2005)

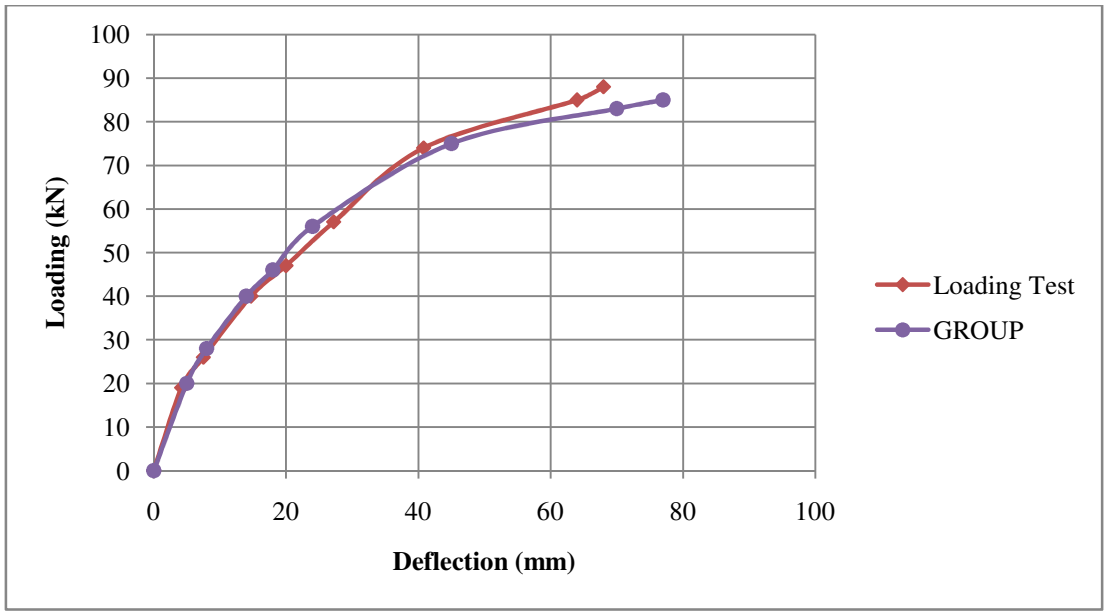

Figure 11.8: Computation results from GROUP and measured load - deflection curve for row 4. (Walsh, 2005)

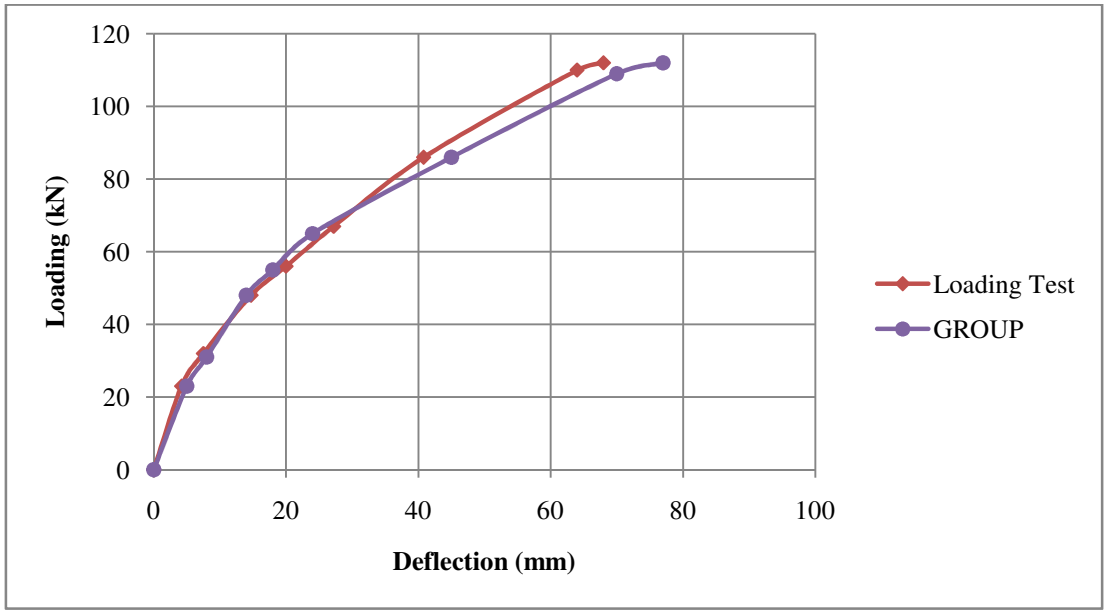

Figure 11.9: Computation results from GROUP and measured load - deflection curve for row 5. (Walsh, 2005)

11.3.2 SPLICE Computation Results

With the elastic modulus at ground surface, $E_{0,}$ a value of 25 000 kPa and E_1/z a value of 2000 kPa/m and calculated shadow effect distance of 3.8 m, SPLICE calculations gave pile load - pile deflection results shown from Figure 11.10 trough Figure 11.14.

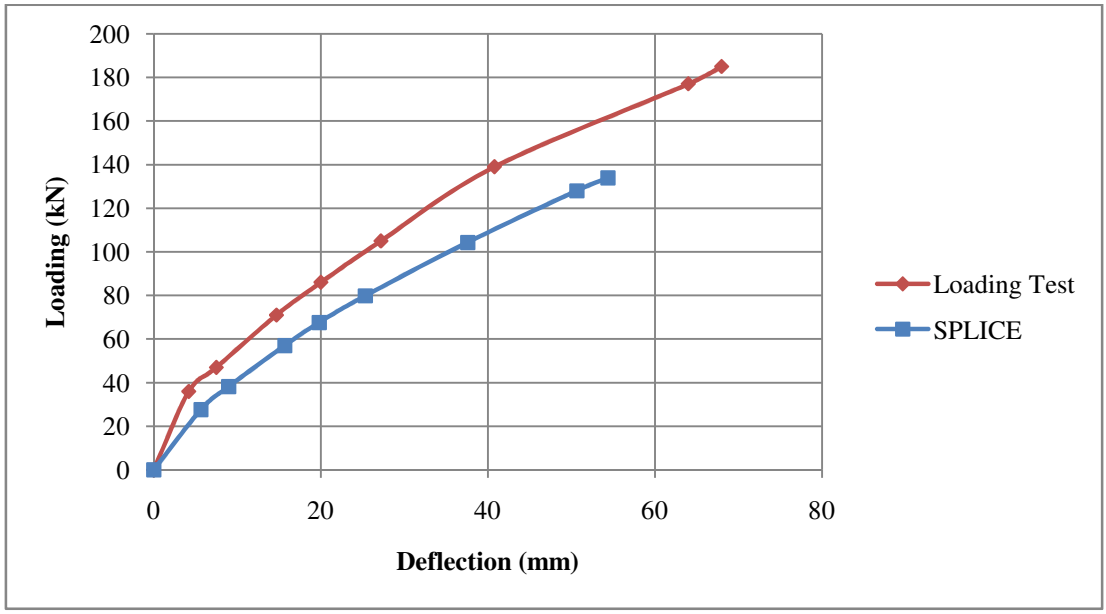

Figure 11.10: Computation results from SPLICE and measured pile load - pile deflection curve for row 1

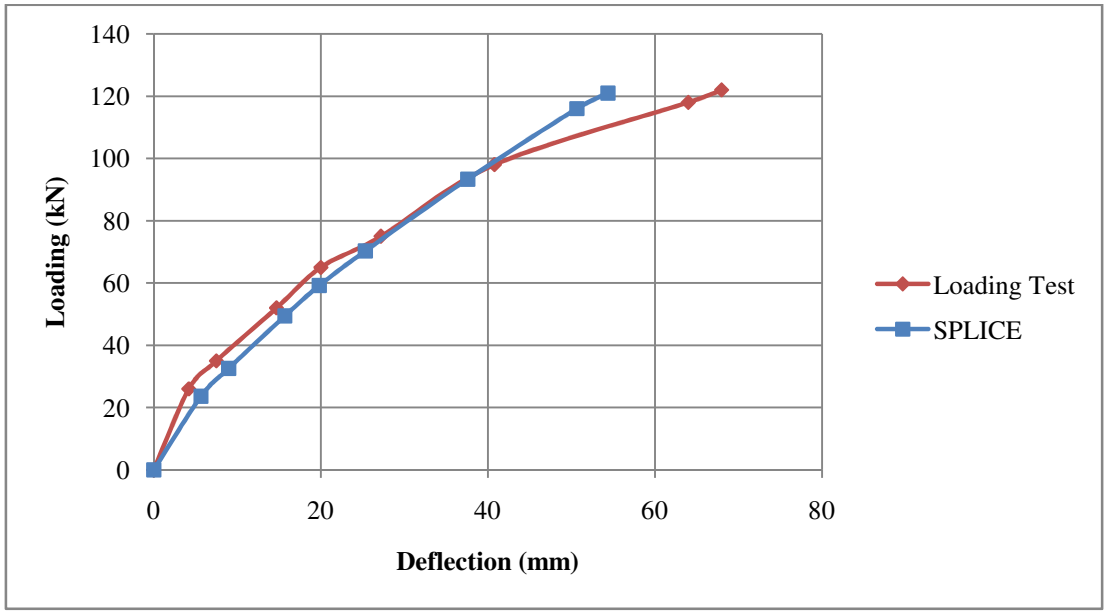

Figure 11.11: Computation results from SPLICE and measured pile load - pile deflection curve for row 2

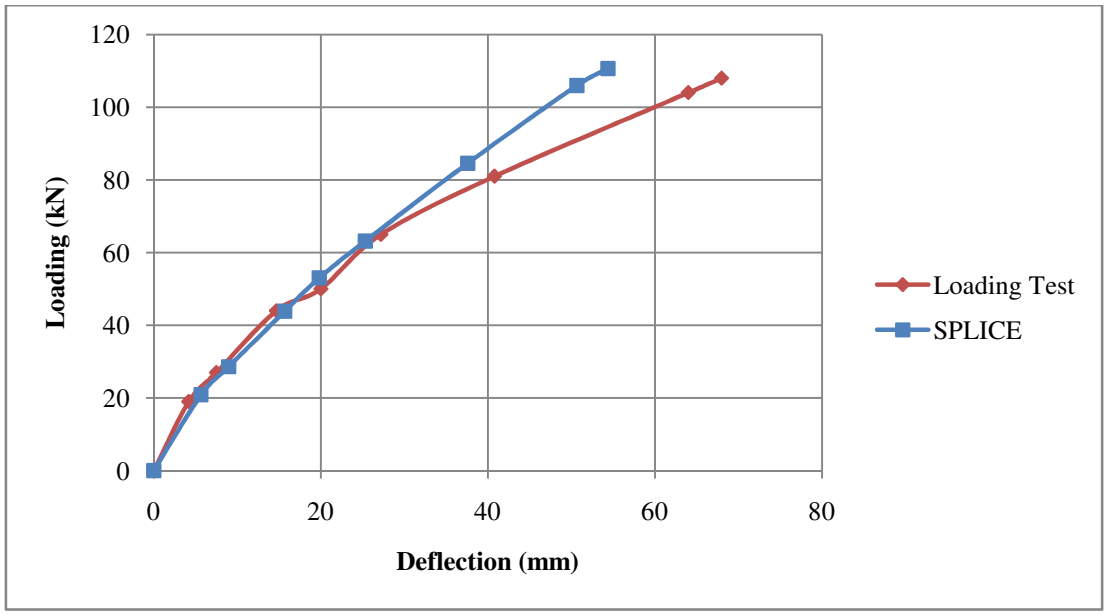

Figure 11.12: Computation results from SPLICE and measured pile load - pile deflection curve for row 3

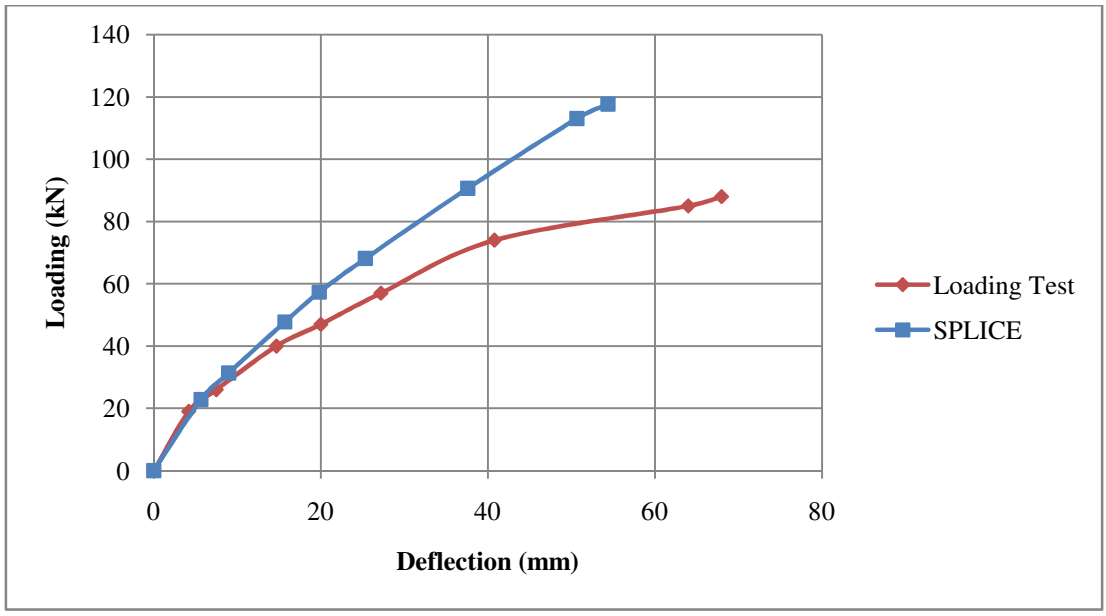

Figure 11.13: Computation results from SPLICE and measured pile load - pile deflection curve for row 4

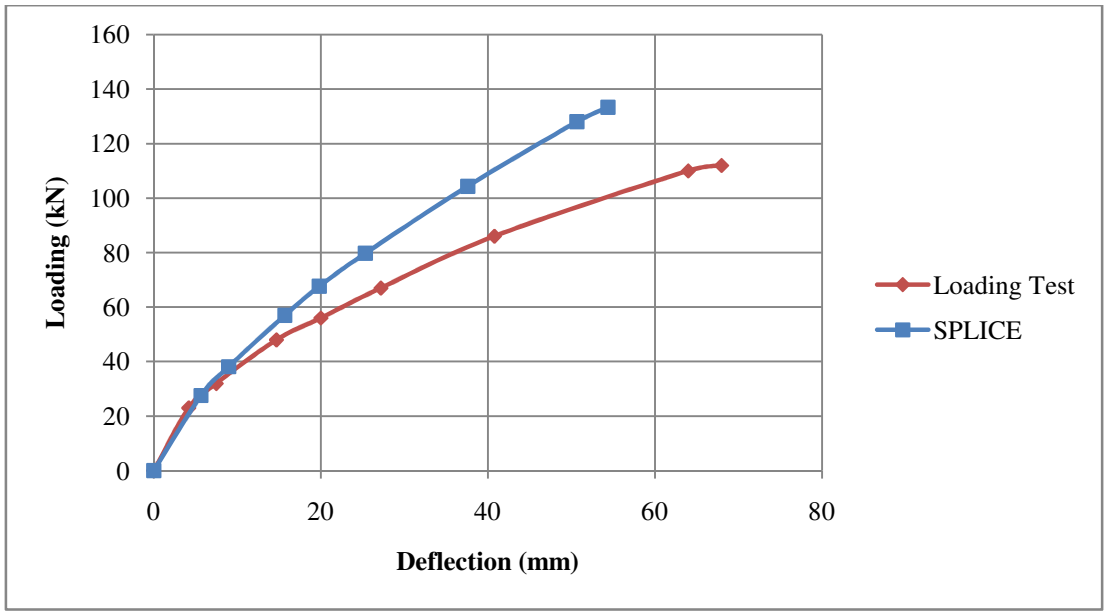

Figure 11.14: Computation results from SPLICE and measured pile load - pile deflection curve for row 5

11.3.3 Results with Linearly Elastic Computation Method

Whit back calculated p-multipliers from Table 11.1 and horizontal ground constant K_{py} a value of 2080 kN/m^3, linearly elastic calculation method gave the pile load - pile deflection results shown from Figure 11.15 trough Figure 11.19.

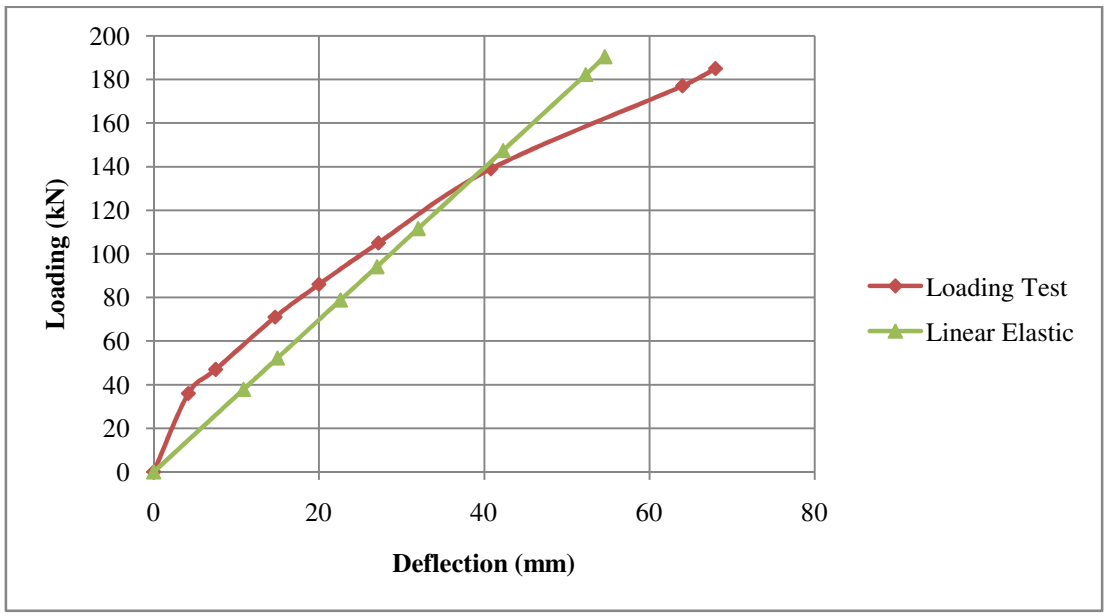

Figure 11.15: Results from linearly elastic computation method and measured pile load - pile deflection curve for row 1.

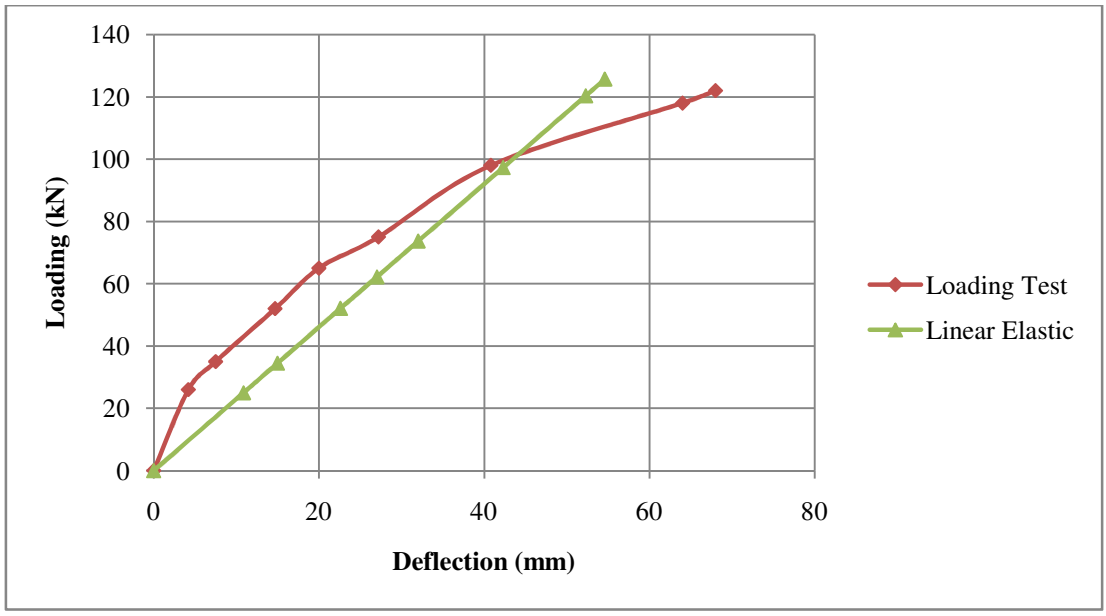

Figure 11.16: Results from linearly elastic computation method and measured pile load - pile deflection curve for row 2.

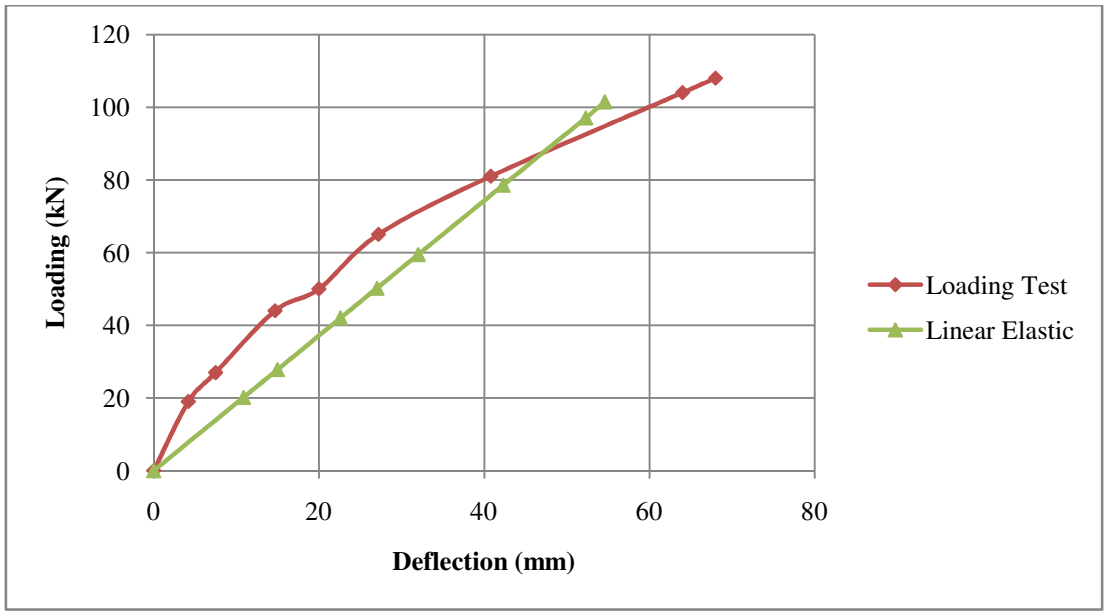

Figure 11.17. Results from linearly elastic computation method and measured pile load - pile deflection curve for row 3.

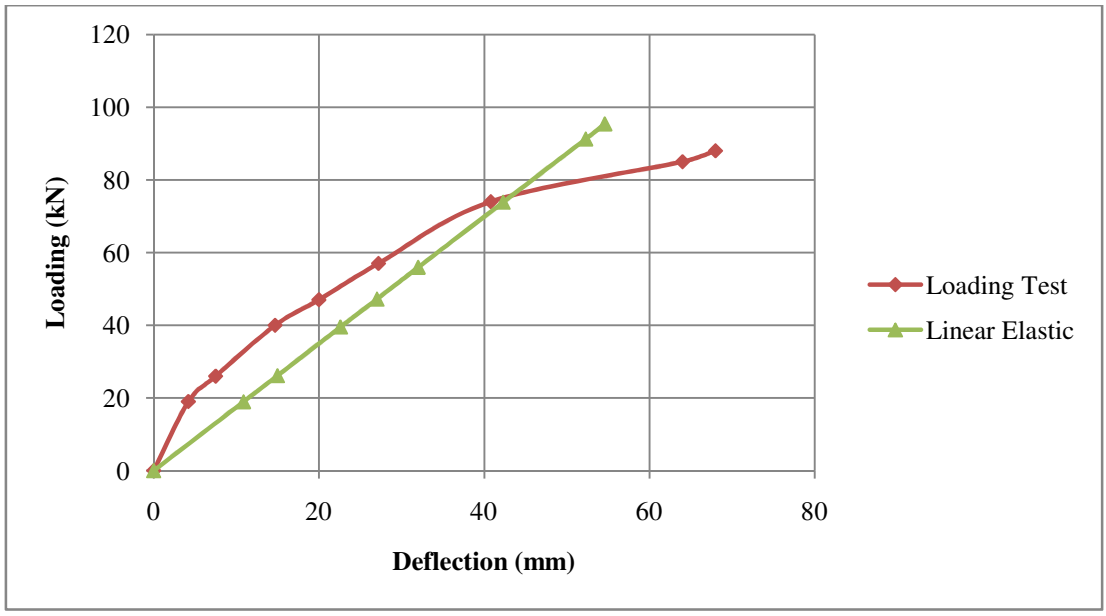

Figure 11.18: Results from linearly elastic computation method and measured pile load - pile deflection curve for row 4.

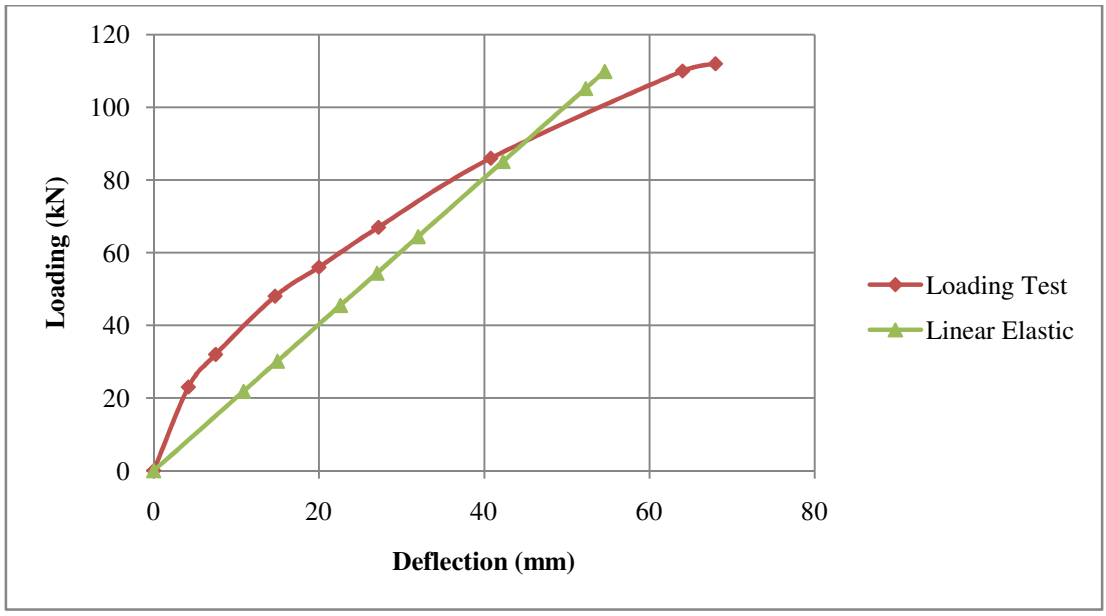

Figure 11.19: Results from linearly elastic computation method and measured pile load - pile deflection curve for row 5.

11.4 Load versus Bending Moment for Each Row

The measurement equipment for bending moment calculations sustained only until target deflection level 38 mm, so moments were not gathered beyond that deflection level. From Figure 11.20 trough Figure 11.34, computed and measured bending

moments versus depth results are shown. In those figures a purple dot represents the maximum bending moment and its depth from GROUP computations (J. Walsh, 2005), whereas a green triangle does the same for linear elastic calculations. Full bending moment versus depth curves from GROUP calculations, are presented in Appendix 1 – 5.

Because strain gage measurements were performed only for the center pile of the pile rows, bending moment results only of those piles are presented. The rows are numbered as in Figure 10.4.

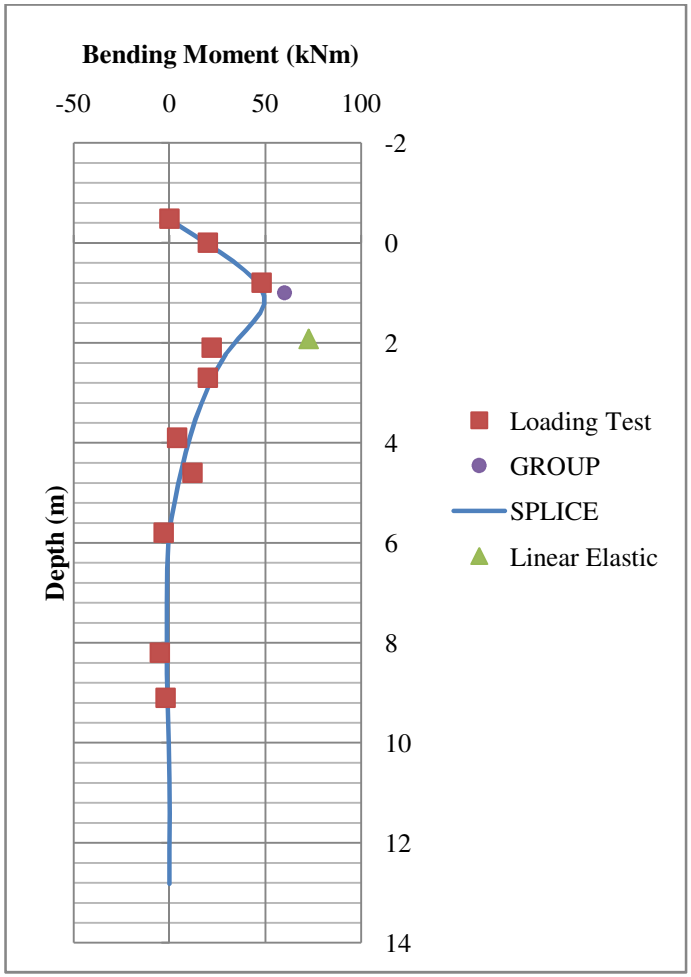

Figure 11.20: Bending moment results of center pile in Row 1, with the pile group loading of 510 kN.

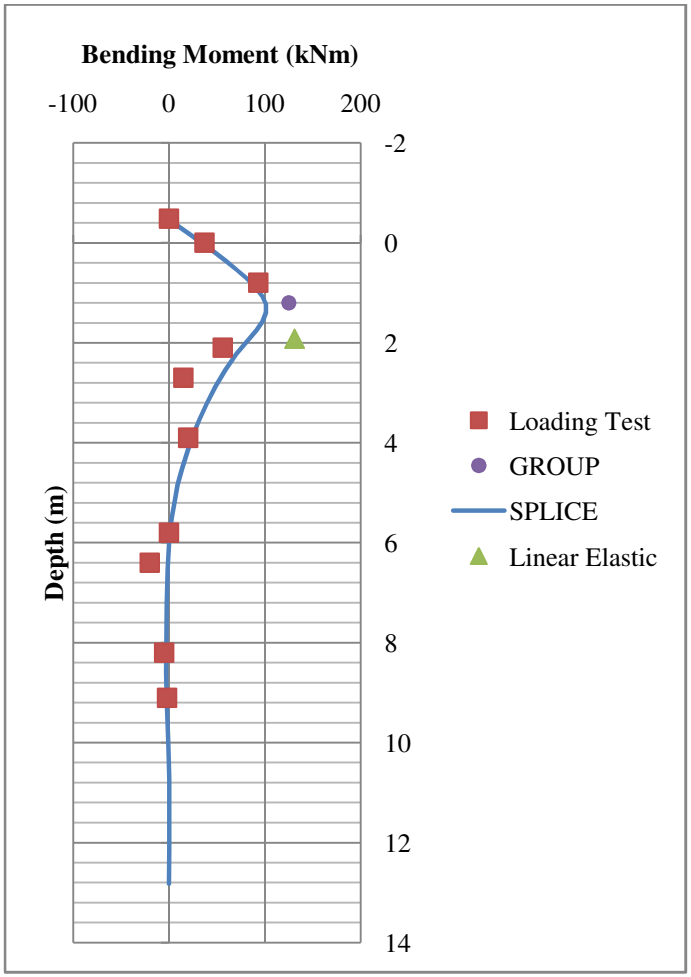

Figure 11.21: Bending moment results of center pile in Row 1, with the pile group loading of 920 kN.

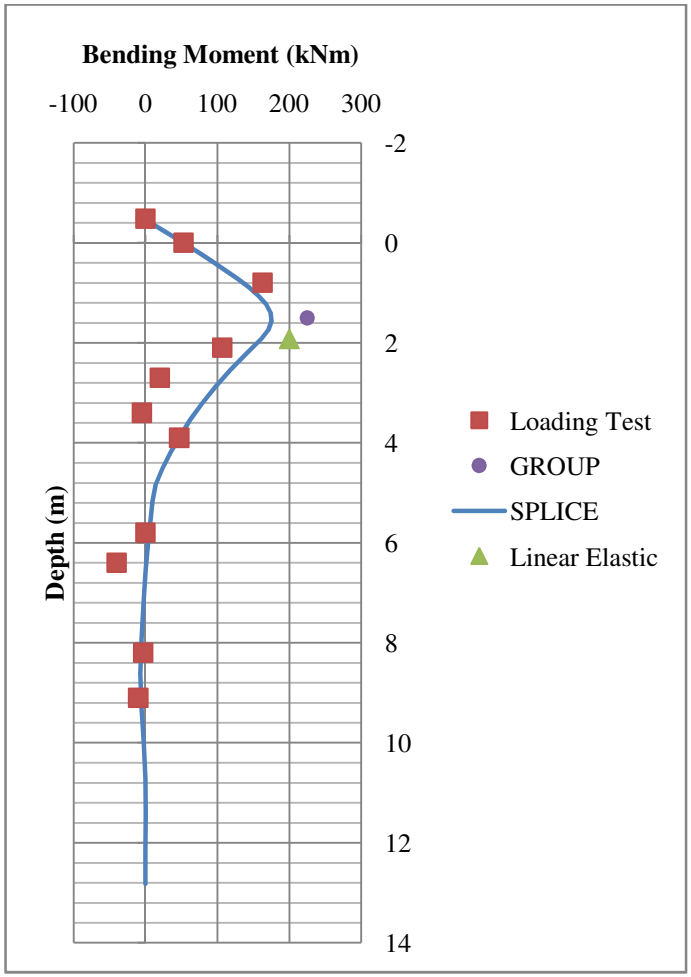

Figure 11.22: Bending moment results of center pile in Row 1, with the pile group loading of 1440 kN.

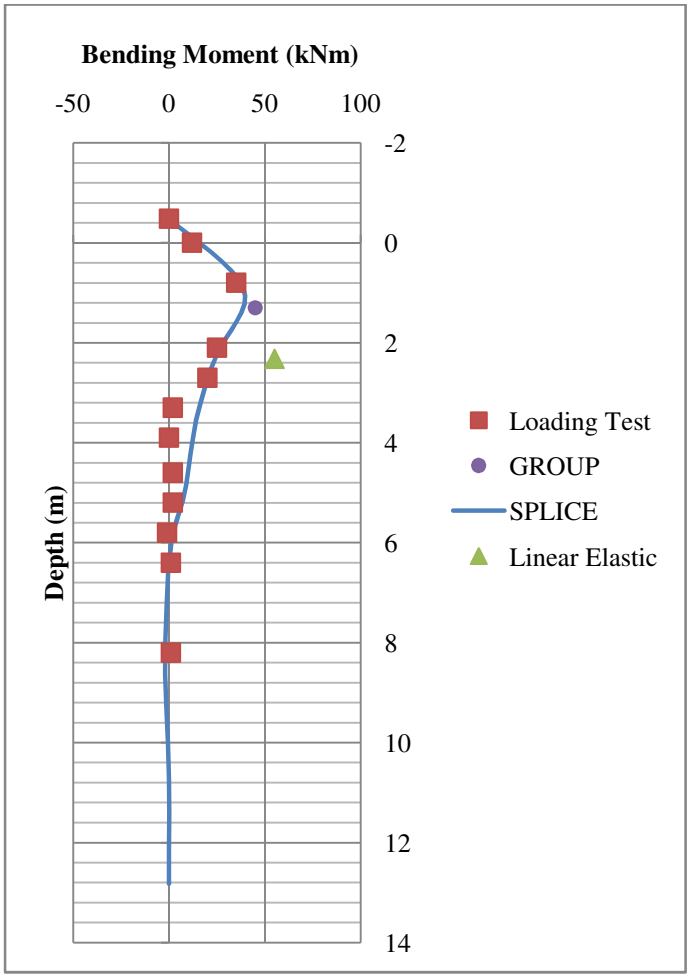

Figure 11.23: Bending moment results of center pile in Row 2, with the pile group loading of 510 kN.

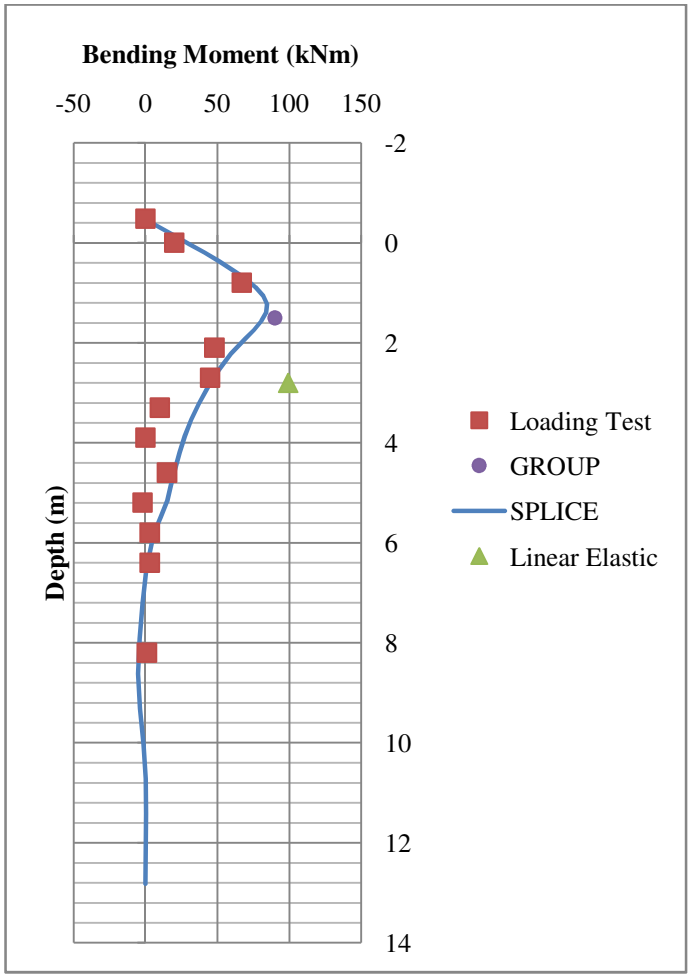

Figure 11.24: Bending moment results of center pile in Row 2, with the pile group loading of 920 kN.

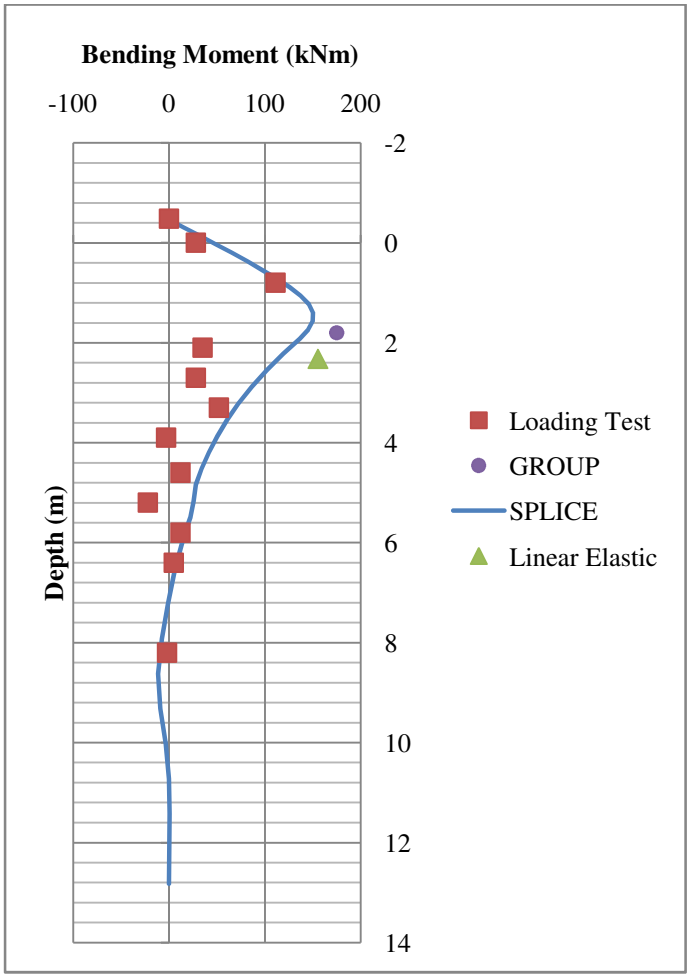

Figure 11.25: Bending moment results of center pile in Row 2, with the pile group loading of 1440 kN.

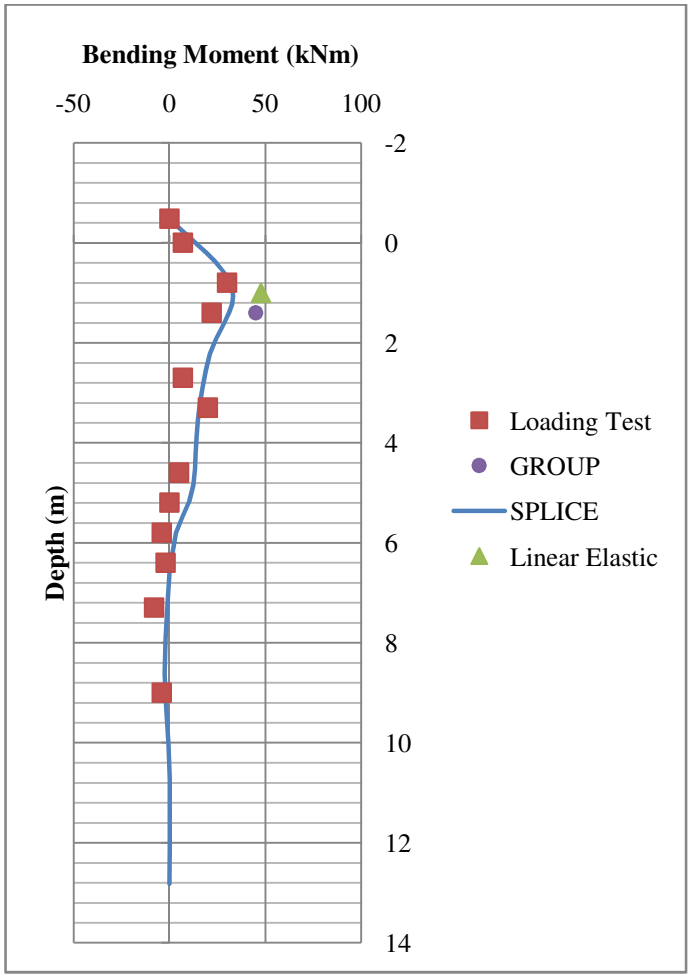

Figure 11.26: Bending moment results of center pile in Row 3, with the pile group loading of 510 kN.

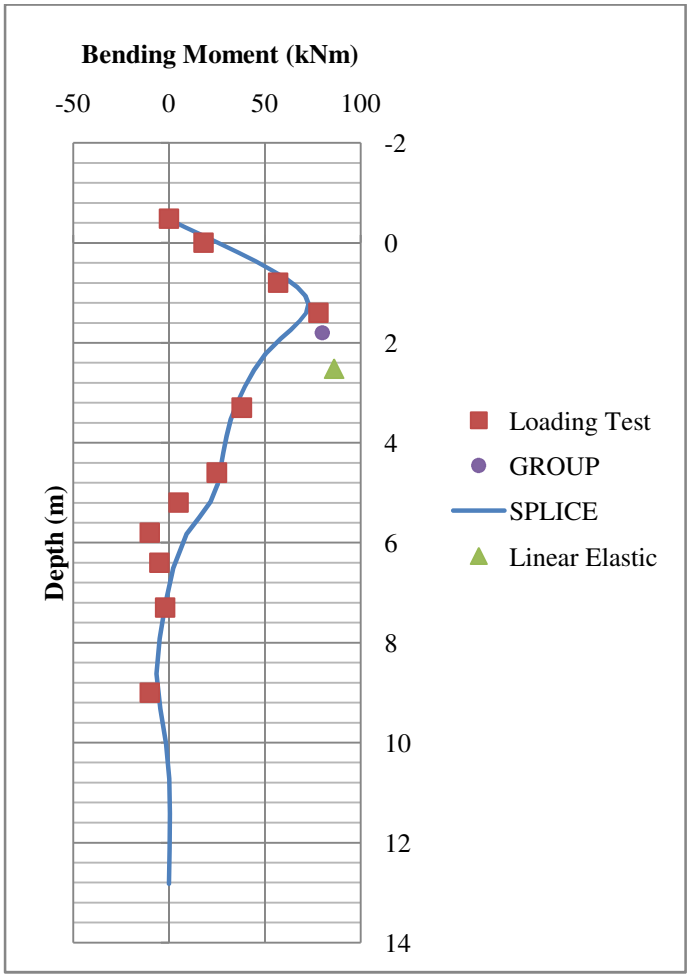

Figure 11.27: Bending moment results of center pile in Row 3, with the pile group loading of 920 kN.

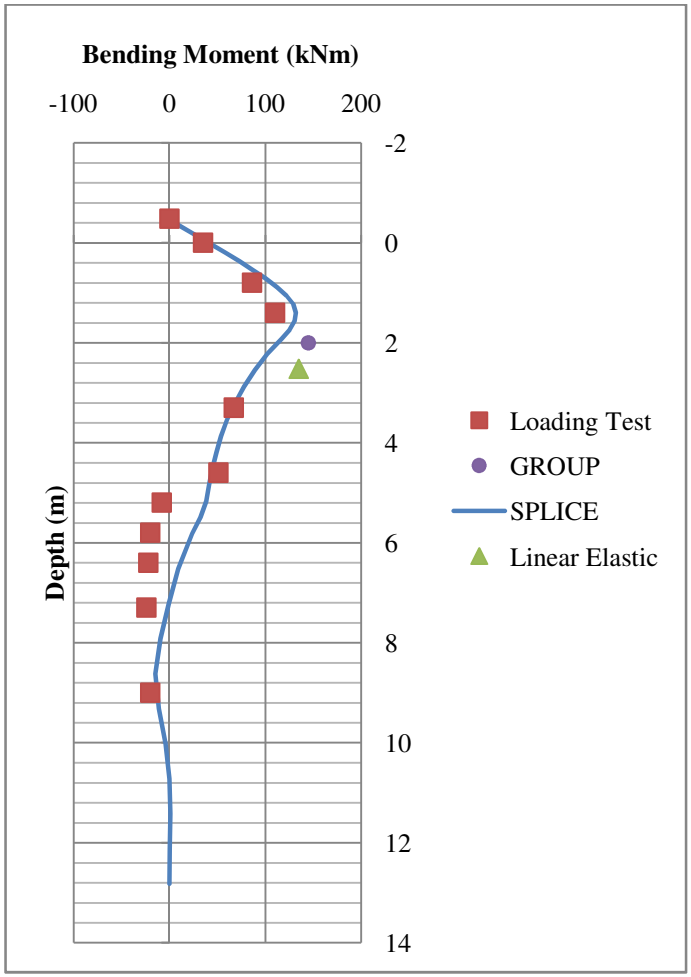

Figure 11.28: Bending moment results of center pile in Row 3, with the pile group loading of 1440 kN.

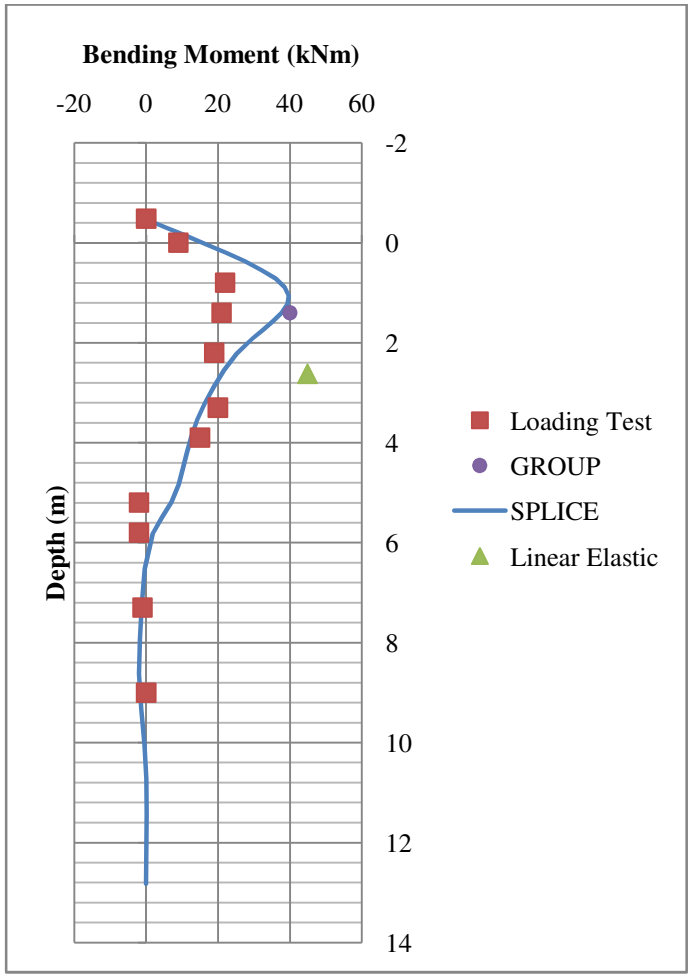

Figure 11.29: Bending moment results of center pile in Row 4, with the pile group loading of 510 kN.

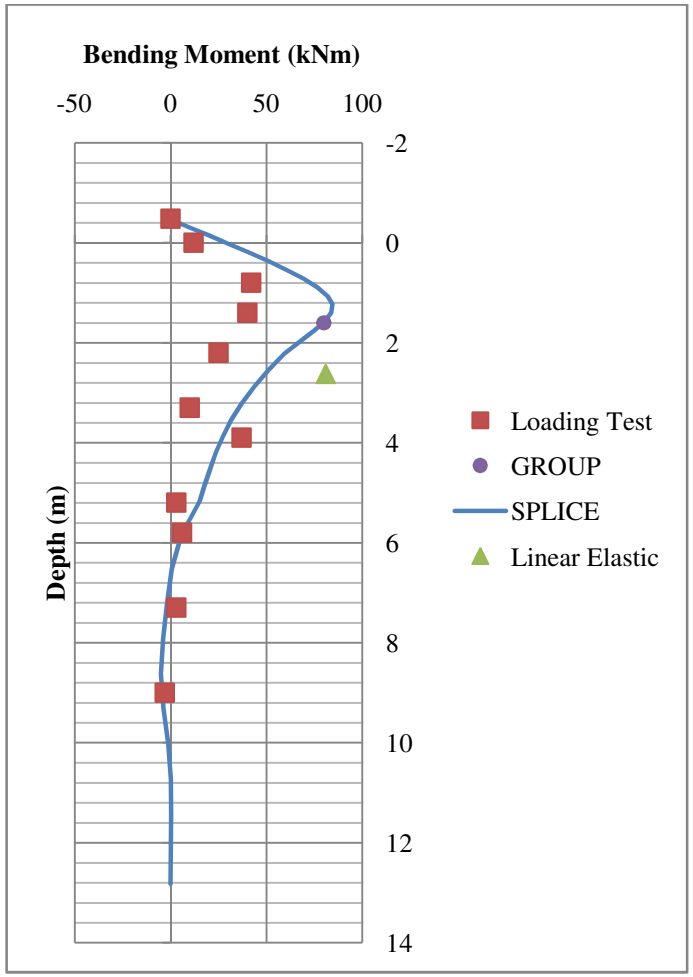

Figure 11.30: Bending moment results of center pile in Row 4, with the pile group loading of 920 kN.

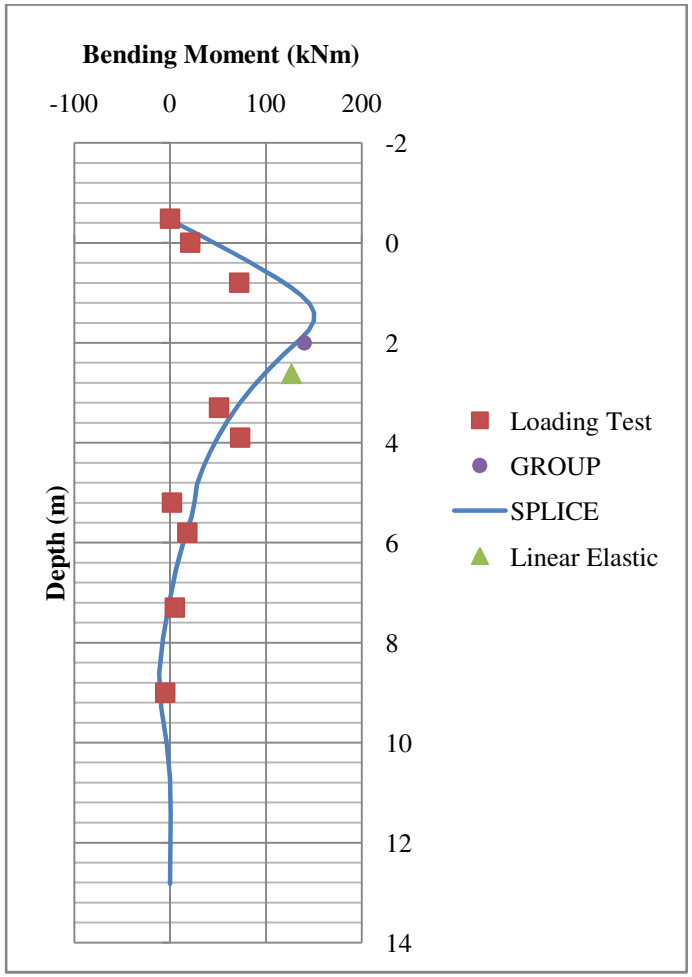

Figure 11.31: Bending moment results of center pile in Row 4, with the pile group loading of 1440 kN.

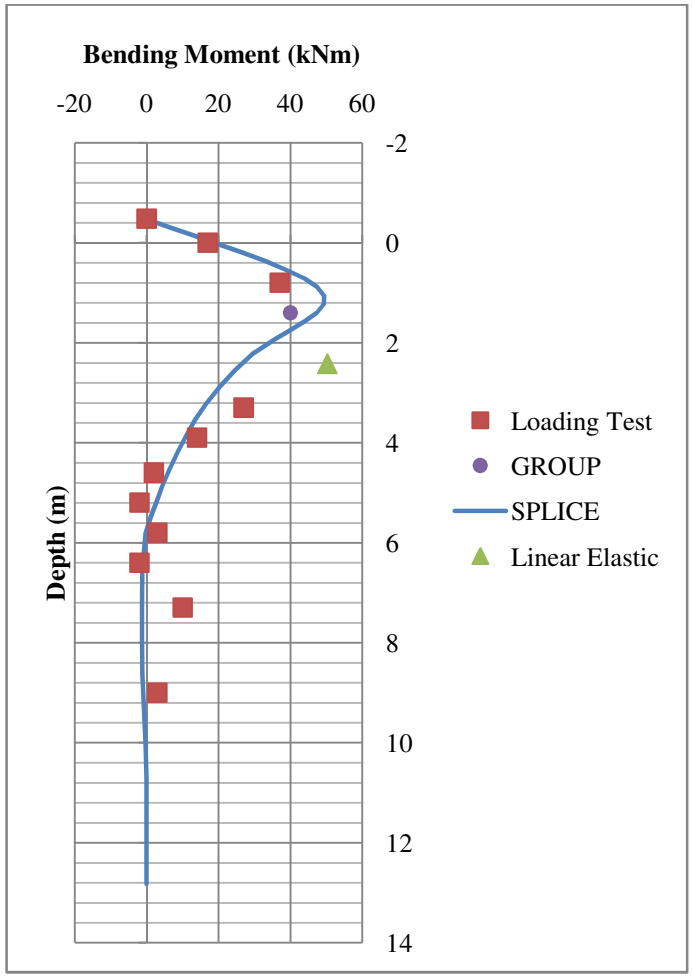

Figure 11.32: Bending moment results of center pile in Row 5, with the pile group loading of 510 kN.

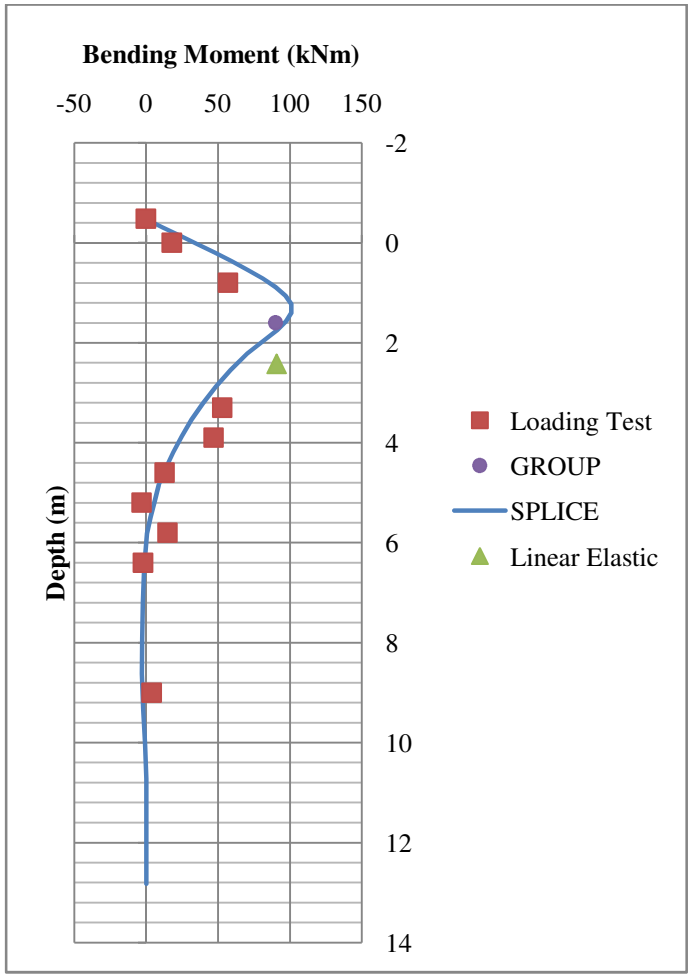

Figure 11.33: Bending moment results of center pile in Row 5, with the pile group loading of 920 kN.

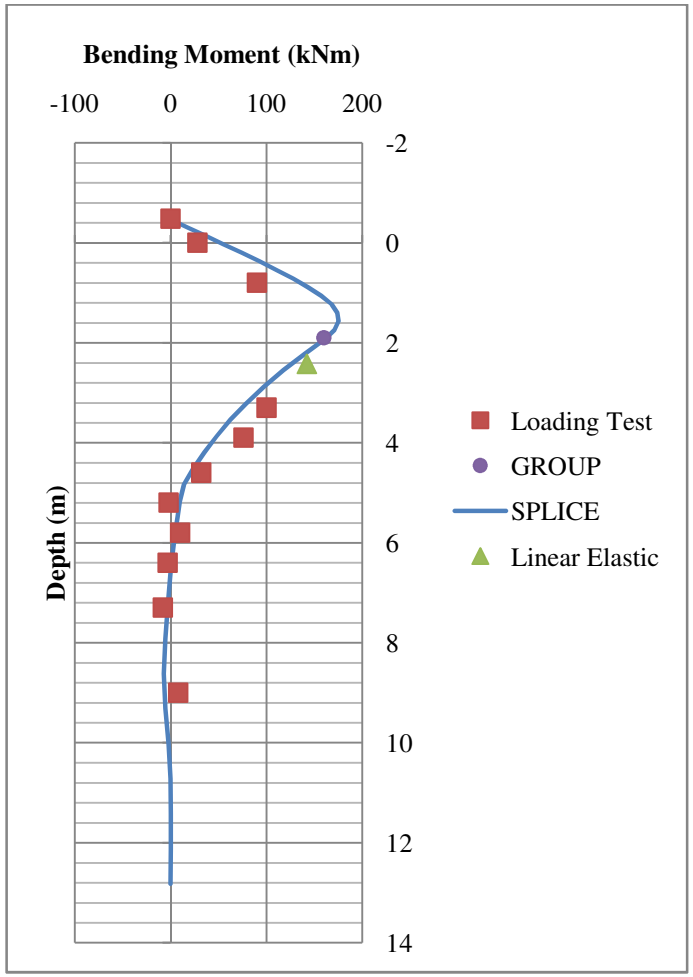

Figure 11.34: Bending moment results of center pile in Row 5, with the pile group loading of 1440 kN.

11.5 Summary of the Computer Analyses

11.5.1 GROUP Analysis

In the computation results presented by J. Walsh (2005), there is a good correlation between the loading of each row and a row deflection as shown from Figure 11.10 to Figure 11.14. Especially the middle row number 3 has an excellent correspondence with the measured results. More summarization of the GROUP computation results is presented in his Master's thesis.

The weakness of this type of computation method is the p-multipliers, which are hard to predict as is obvious if values on Table 11.1 and on Table 11.2 are compared. P-multipliers have a significant effect to the results for getting the right loading value to each pile in a group. However, it can be seen from the result curves that also computed deflections are in quite good correlation with the measured results, which is obvious because p-multiplier technique lowers the efficiency of soil to resist lateral deflection with a given value.

As a result of this investigation, the conclusion number 11 that was concluded from previous research, in Chapter 2.12, did not hold good. With user-defined p-multipliers that are determined from design curves (p-multipliers vs. pile spacing) based on previous full-scale tests, don't predict pile group behavior accurately.

11.5.2 SPLICE Analysis

The soil profile to test computer program SPLICE was obtained from J. Wash's master's thesis (2005) and modified to fit in SPLICE.

The influence of group effect is significant for this type of investigation, which can be seen from Figure 11.10 trough Figure 11.14. The group loading - group deflection curve is quite similar with the measured data in Figure 11.3, until the two highest loading group loading levels. Load deflection curves computed for each rows have a significant discrepancies with the measured data. The discrepancy is noticeable

especially with higher loading levels and gable rows. Results from SPLICE calculations load-deflection curves for each row are too similar with each other i.e. the effect of pile – soil - pile interaction is not affecting enough. Lateral group loading of 1860 kN, gave the loading for each row from 120 kN to 140 kN with SPLICE, where the loading were measured approximately from 90 kN to 190 kN whit this specific group loading. This type of an error is most probably caused by the used group effect technique, because the piles are behaving in calculations more like isolated single piles, than piles in a pile group.

The first row load - deflection curve was acting in SPLICE too alike with the trailing ones, and the effect is considerable. But as it should be, the first pile row is taking the most loads of the rows.

SPLICE computation results from row 2 and 3, until group loading 1440 kN, the results are almost congruent with measured ones, so it seems that the soil and pile parameters were chosen correctly.

Rows 4 and 5 seem to act similarly incorrectly with the measured data. With smaller loading values the surrounding soil seems to be too loose and the piles are taking too much load. As the deflections increase, Rows 4 and 5 act too stiffly and they take too much load compared to deflections.

Loadings between piles in a same row were quite equal within a row. Due to the higher bending stiffness of the center line piles, those piles took a little bit more loading, as was also measured in the field test, by J. Walsh (2005).

In general, SPLICE seemed at least somewhat effective indicating the depths of maximum moments as presented from Figure 11.20 trough Figure 11.34. The magnitudes of the maximum bending moments were not accurate with higher loading levels, because the pile loads didn't match with the measured data. This is difficult to establish, as some data at maximum bending moments are missing, but trends above and below where maximum moments are expected. With lower loadings the discrepancies are not that clear, but the error increases with the group loading.

Bending moment figures from SPLICE also illustrates the effect of stiffer soil layer at the depth of 4.5 m- 5.5 m. The stiffer layer shows in moment curves as bumps. SPLICE was also effective at predicting depths at which moments returned to zero. Measured results available, matched with SPLICE computation results fairly closely.

When the computation results between GROUP and SPLICE are compared, it is obvious that the GROUP results are more accurate. This applies for load-deflection curves as well as to the bending moment - depth curves. It should be also noticed, that if the bending moments would have been measured for even higher deflections, the discrepancy between measured and calculated results with SPLICE would have probably increased.

Brown et al. (1987) concluded that the elasticity-based methods did not accurately predict the distribution of load within a pile group and that empirical modification factors were necessary. This conclusion qualifies also to this investigation, but with correlations presented in next chapter 12, the elastic method might become more accurate and thereby more reliable.

11.5.3 Linear Elastic Analysis

From Figure 11.15 through Figure 11.19, load – deflection curves show that the used linear elastic calculation method doesn't really correspond with the measured data, but if only loadings between the rows are compared the method is quite accurate. Anyhow, these similarities between loads at each row with measured loads is due to the back calculated p-multipliers. The purpose of p-multipliers is to divide the loading correctly between rows and because they were back calculated, the right results did not come as a surprise.

The accuracy of calculated bending moments and their depth compared with the measurement results are relatively high. Especially if the simplicity of the method used to compute the maximum bending moment and its depth is considered (Table 8.2).

The error in some maximum bending moment depths may be caused by the specified ground level. In general as simple computation method as was introduced in Chapter 8 gave quite accurate results and the results are on the “safer” side of the measured bending moment data.

The input values for linear elastic computations needed back calculation with parameters that are quite hard to predict and have a significant impact on results. The arduousness is noticed when the back calculated and hand calculated p-multipliers in Table 11.2 and Table 11.2 are compared.

12 Summary and Conclusions

The 3 x 5 pile group field loading test conducted by J. Walsh (2005) was analyzed with three different pile group programs. Computer program GROUP calculations were done by J. Walsh (2005), with back calculated p-multipliers. Computer program SPLICE calculations were conducted, which analyses pile-soil-pile effect with Mindlin's equations. Also linear elastic computations, with back calculated p-multipliers and soil resistance factor were conducted.

In order to obtain reliable results from computer programs, needed input parameters ought to be assuredly measureable. P-multipliers used by some of the pile group programs are really hard to measure from the field or to calculate assuredly with existing recommendations. Probably the only way of gathering reliable p-multipliers is to conduct a full scale field load test at the construction site. The p-multiplier formation method presented in Chapter 7.2 assumes that the group efficiency is only dependent of the pile spacing, which is obviously not true.

The alternative computation method used, analyzes group effect with Mindlin's elastic half space equations, where the soil is presumed to behave as elastically homogeneous mass, with elastic stiffness increasing linearly with the depth. The results from this computation method didn't give very reliable results. The errors are most probably due to that the group effect is calculated only from one specific depth z_e. If the group effect would be considered from the whole length of a pile, the results would be more relying on the group effects and might become more accurate.

The group effect is a significant for obtaining reliable results. The input parameters set in SPLICE E_0 and E_1/z are not that hard to predict with comparatively accurately, especially if the alternative method is to predict p-multipliers. There should be an option in computer program for a user to set the elastic modulus and Poisson's ratio for each layer manually, so that the non linear stiffness alternations could be more accurately modeled. Additionally, the user should be able to set a depth of a rigid

boundary (bedrock), under which the pile nodes would not be affected by the pile-soil-pile interaction of the upper layers (Mosher and Dawkins, 2000).

The additional forces to each pile elements' node points due to the group effects should be computed with calculated additional deflections set to the "non-linear springs" that are set to each pile element's node. The initial spring constant should be set to the last value that was computed from the latest iteration step and the additional deflections should be added iteratively, so that the spring constant would vary throughout the process when the group effect load to the pile is added, as was explained in Chapter 7.3.

Linear elastic computation method presented in Chapter 8 is a too simple method for analyzing the elasto-plastic behavior of the pile group. Harshly accurate results obtained with this method needed back-calculated p-multipliers and back calculated soil parameter and even then the results were unreliable, but the results were still on the safer side.

It is also seen from the bending moment results of rows 1 to 4 in thesis of J. Walsh (2005) (Appendix 1 - 4), that with the highest loading level measured, the peak of the bending moment curves are at shallower depth and smaller than GROUP computations imply. The divergence might be due to the bending moments caused by the skin friction. If the skin friction would have been considered, the bending moment curves would be closer to the ground surface and the peak values would also be smaller. The lack of this phenomenon in Row 5 (Appendix 5) might be because there is no pile row pushing soil against its back, the pressure that would cause the skin friction is missing, or at least lower. The bending moments due to skin friction are naturally increasing with higher deflection levels, which were not measured, thus the effect of this phenomenon requires additional testing and analysis.

Even if the calculation procedure seems complex and computation process time consuming, the SPLICE did the computations within 1-2 seconds. Thus the additional computations recommended here would not make the calculations too

heavy for a modern computer. The main obstacle might be at getting the programming work economically efficient.

The field load test selected to this thesis is not a usual construction situation. There aren't many cases where a pile group, hinged to the pile cap, is only loaded laterally. As a reference case for testing and valuating modeling programs it suited well, even if some of the measurement data was missing.

13 References

American Association of State Highway and Transportation Officials (AASHTO) (2000), “Bridge Design Specifications,” Washington, D.C.

American Petroleum Institute (1987) ”API Recommended Practice for Planning, Design and Constructing Fixed Offshore Platforms,“ Report RP-2A, 17th Edition, April

Awoshika, K., and Reese, L.C. (1971a), “Analysis of Foundations with Widely Spaced Batter Piles,” Research Report 117-3F, Project 3-5-68-117, Center Highway Research, University of Texas at Austin, February

Bogard, D. Matlock, H. (1983), “Procedures for analysis of laterally loaded pile groups in clay,” Proceeding of the Speciality Conference on Geotechnical Engineering in Offshore Practice, ASCE, pp. 499-535

Bredenberg Håkan, Bengt Broms (1987, Reviewed 1983), “Rapport 54, Pålgrupper med sidomotstånd och instpänning,” Comission on Pile Research, Royal Swedish Academy of Engineering sciences.

Brown D.A., Reese L.C., and O’Neill M.W. (1987), “Cyclic lateral loading of a large-scale pile group,” Journal of Geotechnical Engineering, ASCE, Vol. 103, No. 11, pp. 1326-1343

Brown, D.A., and Shie, C-F. (1991), “Modification of p-y curves for group effect on laterally loaded piles,” Geotechnical Special Publication, ASCE, Vol. 1, No. 27, pp. 479-490

Brown, D.A., Reese, L.C.. (1988), “Lateral load behavior of pile group in sand,” Journal of Geotechnical Engineering, ASCE, Vol. 114, No. 11, pp. 1261-1276

Chen Yung-Tsang (2004), ”Lateral load analysis of single piles,” University of California

Christensen D. S. (2006), "Full scale static lateral load test of a 9 pile group in sand," Thesis, Master of Science in Civil Engineering, Brigham University

Clausen, C.J.F. (1983) "SPRINT, A Computer Program for Analysis of a Rigid Three-Dimensional Structure supported by an Elastic Half Space." Report 8207-1, Copenhagen, 22nd February

Clausen C. J. F. (1994), "Documentation of Computer Program Package for Structure/Pile/Soil Interaction analysis," Engineering Documentation, Report 8407-4, Computer Program SPLICE, July

Cox, W.R., Reese, L.C., and Crubbs, B.S. (1984), "Lateral Load Tests of 25.4 mm Diameter Piles in Very Soft Clay in Side-by-Side and In-line Groups," Laterally Loaded Deep Foundations: Analysis and Performance, SPT 835. American Society for Testing and Materials

De Gennaro Vincenzo, Roger Frank (2005), "Finite element modeling of the pile-soil interaction," Bulletin des laboratories des Ponts et Chaussees- 256-257; July – August-Sebtember, pp. 107-133

Desai Chandrakant S, John T. Christian (1977), "Numerical Methods in Geotechnical Engineering," ISBN 0-07-016542-4, McGraw-Hill Book company

Dunnvant, T.W., and O'Neill, M.W. (1986), "Evaluation of Design-Oriented Methods for Analysis of Vertical Pile Groups Subjected t Lateral Load," Numerical Methods in Offshore Piling, Institute Française du Petrole, le Laboratoire Central des Pontes et Chaussees, pp. 303-316

Feagin, L. B. (1937), "Lateral pile-loading tests," Transactions, ASCE, Vol. 102, Paper No. 1959, pp. 236-254

Girsang, C. H., (2001), "A Numerical Investigation of the Seismic Response of the Aggregate Pier Foundation System," Thesis, Master of Science in Civil Engineering, Virginia Polytechnic Institute and State University, December, http://scholar.lib.vt.edu/theses/available/etd-12212001-133242/unrestricted/17Appendix_A.pdf, pp. 12, Table A.5

Hoit, M., Hays, C., and McVay, M. (1997), "The Florida Pier Analysis Program Methods and Models for Pier Analysis and Design," Transportation Research Record 1569, Transportation Research Board, National Research Council, Washington, D.C., pp.1-7

Kim, J.B., and Brungraber, R.J. (1976), "Full scale lateral load tests of pile groups," Journal of the Geotechnical Engineering Division, ASCE, Vol. 102, No. GT1, pp. 87-105

Kim, J.B., L.P., Singh, and Brungraber, R.J. (1979), "Pile cap soil interaction from full-scale lateral load tests," Journal of Geotechnical Engineering, ASCE, Vol. 105, No. 5 pp. 643-653

Kubo, K. (1965), "Experimental Study of the Behavior of Laterally Loaded Piles," Proceedings, Sixth International Conference on Soil Mechanics and Foundation Engineering, Vol. II, Montreal, pp. 275-279

Lieng J. T. (1988), "Behavior of Laterally Loaded Piles in Sand – Large Scale Model Tests," Ph.D. Thesis, Department of Civil Engineering, Norwegian Institute of Technology, ISBN 82-7119-078-4

Martin Geoffrey R. (2005), "Geotechnical modeling and capacity assessment," Seismic Retrofit of Highway bridges, A pilot training course / Workshop; December 5-7, 2005; Portland, Oregon

Matlock, H. (1970), "Correlations for Design of Laterally Loaded Piles in Soft Clay," Proceedings, Offshore Technology Conference, Houston, Texas, Paper No. 1204, pp. 307-594

Matlock, H., Ingmar, W, B., Kelley, A. E., and Bogard, D. (1980), "Field Tests of Lateral Load Behavior of Pile Groups in Soft Clay," Proceedings, Twelfth Annual Offshore Technology Conference, OTC 3871, Houston Texas, Paper No. 1204, pp. 577-594

Meimon, Y., Baguelin, F,. and Jezequel, J.F. (1986), "Pile group behavior under long time lateral monotonic and cyclic loading," Proceedings, Third International

Conference on Numerical Methods on Offshore Piling, Inst. Francais du Petrole, Nantes, France, pp. 285-302

Mindlin, R.D., (1936), "Force at a point in the interior of a semi-infinite solid," Jnl.Appl.Phys., Vol.7, No. 5, pp. 188-204

Mosher, R.L. and Dawkins, W.P. (2000), "Theoretical Manual for Pile Foundations," ERDC/ITL TR-00-5, US Army Corps of Engineers, Engineering Research and Development Center, November

Niraula, L. D., (2004), "Development of Modified t-z Curves for Large Diameter Piles/Drilled Shafts in Limestone for FB-Pier," Thesis, Master of Science in Civil Engineering, Brigham University of Florida, http://etd.fcla.edu/UF/UFE0006988/niraula_l.pdf, 22.11.2007, pp. 41 – 57

Pikley Walter D.(2002), "Analysis and Design of Elastic Beams, Computational Methods," ISBN 0-471-38152-7, pp. 88-98, pp. 122-128

Poulos H. G., E.H. Davis (1974), "Elastic Solutions for Soil and Rock Mechanics," John Wiley & Sons, Inc, ISBN 0-471-69565-3

Prakash, S.(1962), " Behavior of Pile Groups Subjected to Lateral Load," Ph.D. Dissertation, Department of Civil Engineering, University of Illimois

Rajashree S. S, T.G. Sitharam (July 2001), "Nonlinear finite-element modeling of batter piles under lateral load," Journal of Geotechnical and Geoenvironmental Engineering

Ramachandran Jayram (2005)," Analysis of pile foundations under seismic loading," CBE Institute

Rankine, W. J. M., (1857), "On the Stability of Loose Earth," Philosophical Transactions of the Royal Society of London, Vol. 147

Reese L.C. and Wang S.T. (1996),"Technical manual of documentation of computer program GROUP 4.0 for Windows," Ensoft, Inc., Austin, Texas.

Reese Lymon C., William F.Van Impe (2001), "Single Piles and Pile Groups Under Lateral Loading," ISBN 90-5809-340-9, pp. 14-16, Chapter 5 pp. 125-185

Reese Lymon C., William M. Isenhower, Shin-Tower Wang (2006), "Shallow and Deep Foundations," John Wiley & Sons, ISBN 0-471-43159-1, pp. 441-536

Reese, L.C. and Wang, S.T., Isenhower, W.M., and Arrellaga, J.A. (2000), "Computer program LPILE plus version 4.0 technical manual," Ensoft, Inc., Austin, Texas

Reese, L.C., Cox, W. R., and Koch, F.D. (1974), "Analysis of Laterally Loaded Piles in Sand," Proceedings, Offshore Technology Conference, Houston, TX, Vol. II, Paper No. 2080, pp. 473-484

Rollins Kyle M., M.ASCE and Andrew Sparks, M.ASCE(2002), "Lateral Resistance of Full-Scale Pile Cap with Gravel Backfill," Journal of Geotechnical and Geoenvironmental Engineering, September 2002 / 723; DOI: 10.1061/(ASCE)1090-0241(2002)128:9(711)

Rollins, K.M., Johnson, S.R., Petersen, K.T., and Weaver T.J. (2003a), "Static and dynamic lateral load behavior of pile groups based on full-scale testing," 13th International Conference on Offshore and Polar Drilling, International Society for Offshore and Polar Engineering, paper 2003-SAK-02, pp. 8

Rollins, K.M., Olsen, R.J., Egbert, J.J., Olsen, K.G., Jensen, D.H., and Garrett, B.H. (2003b), "Response, analysis and design of pile groups subjected to static and dynamic lateral loads," Utah Department of Transportation Research and Development Division, Report No. UT-03.03.

Rollins, K.M., Peterson, and Weaver, T.J. (1998), "Lateral load behavior of full-scale pile group in clay," Journal of Geotechnical Engineering, ASCE, Vol. 124, No. 6, pp. 468-478

Ruesta, P.F., and Townsend, F.C. (1997), "Evaluation of laterally loaded pile group at Roosevelt bridge," Journal of Geotechnical and Geoenvironmental Engineering, ASCE, Vol. 123, No. 12, pp. 1153-1161

Salokangas L.S. (2007), “Suurpaalut, laskenta ja mitoitus,” http://www.tkk.fi/Yksikot/Silta/opinnot/rak-11/107/luennot/15.pdf, 25.09.2007, pp. 3-5

Schmidt, H.G. (1981), “Group Action of Laterally Loaded Bored Piles,” Proceedings, Tenth International Conference, Soil Mechanics and Foundation Engineering, Stockholm, pp. 833-837

Schmidt, H.G. (1985), “Horizontal Load Tests on Piles of Large Diameter Bored Piles,” Proceedings, Eleventh International Conference, Soil Mechanics and Foundation Engineering, San Francisco, pp. 1569-1573

Snyder J. L.,(2004), “Full-scale lateral-load tests of a 3 x 5 pile group in soft clays and silts"; Thesis, Master of Science in Civil Engineering, Brighan Young University

Taciroglu Ertugrul, Assoc. Member, ASCE, Chang Soon Rha, Jonathan P. Stewart, Member, ASCE, John W. Wallace, Member, ASCE (2003), ” Robust numerical models for cyclic response of columns embedded in soil,” 16th ASCE Engineering Mechanics Conference July 16-18, 2003, University of Washington, Seattle

Terzaghi. K., (1955), “Evaluation of coefficients of subgrade reaction,” Geotechnique, Vol. 5, pp. 297-326, London

Walsh, J. M., (2005), “Full-scale lateral load test of a 3 x 5 pile group in sand,” Thesis, Master of Science in Civil Engineering, Brigham Young University

Wang, S-T. (1986), “Analysis of Drilled Shafts Employed in –earth-Retaining Structures,” Ph.D. Dissertation, Department of Civil Engineering, University of Texas at Austin

Welsh, R.C., and Reese, L.C. (1972), “Laterally Loaded Behavior of Drilled Shafts,” Research Report No. 3-5-65-89, Center for Highway Research, University of Texas at Austin, May

http://www.ce.washington.edu/~geotech/opensees/NEES-SSI/Chapter1.pdf, 22.11.2007

http://www.dot.ca.gov/hq/esc/construction/manuals/Falsework/C-9.pdf, 1.10.2007

http://www.dot.state.fl.us/statematerialsoffice/geotechnical/conference/grip/2004/mcvay-shaft_py.pdf, 21.11.2007

Appendices

Appendix 1

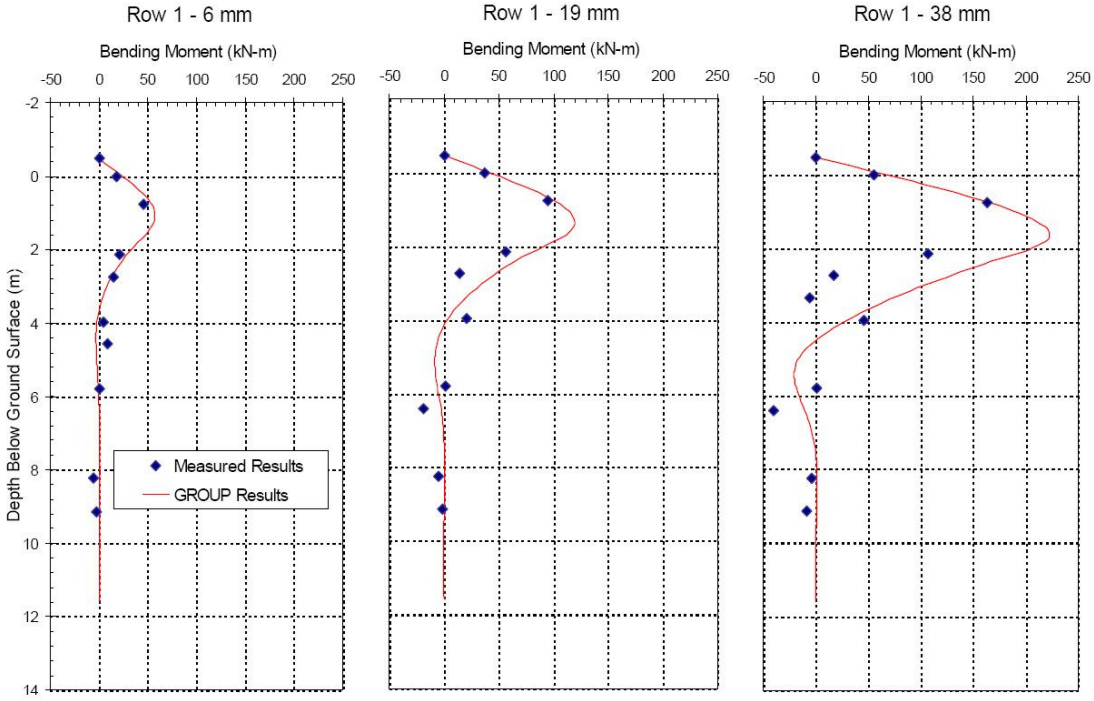

Appendix 2

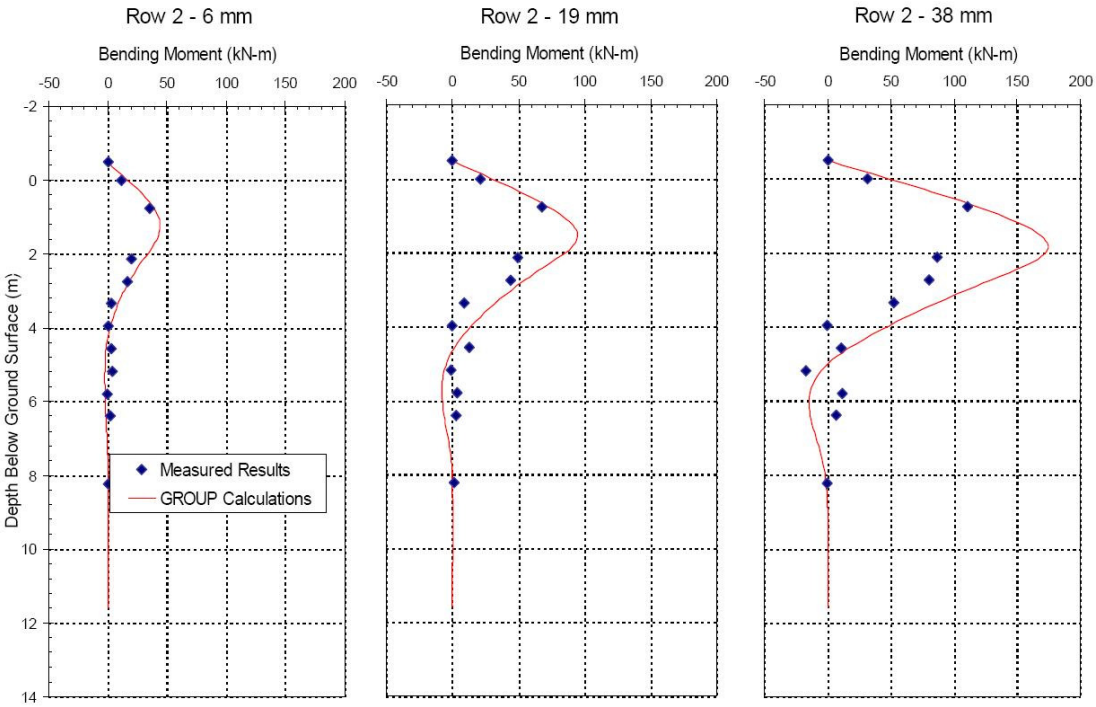

Appendix 3

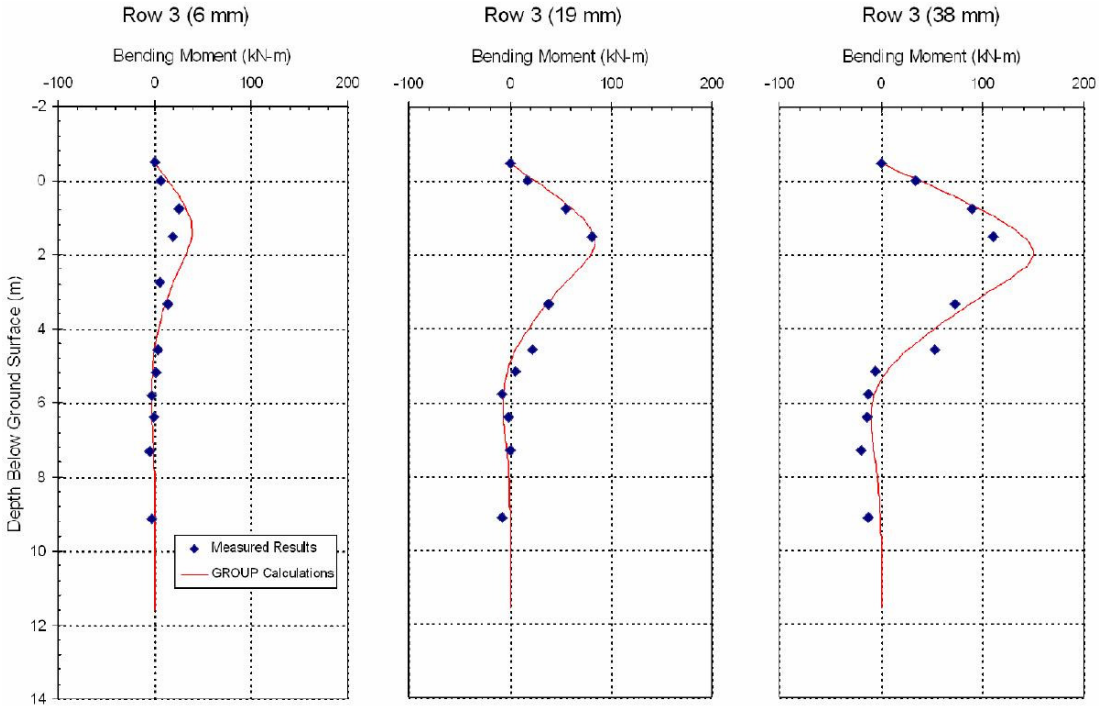

Appendix 4

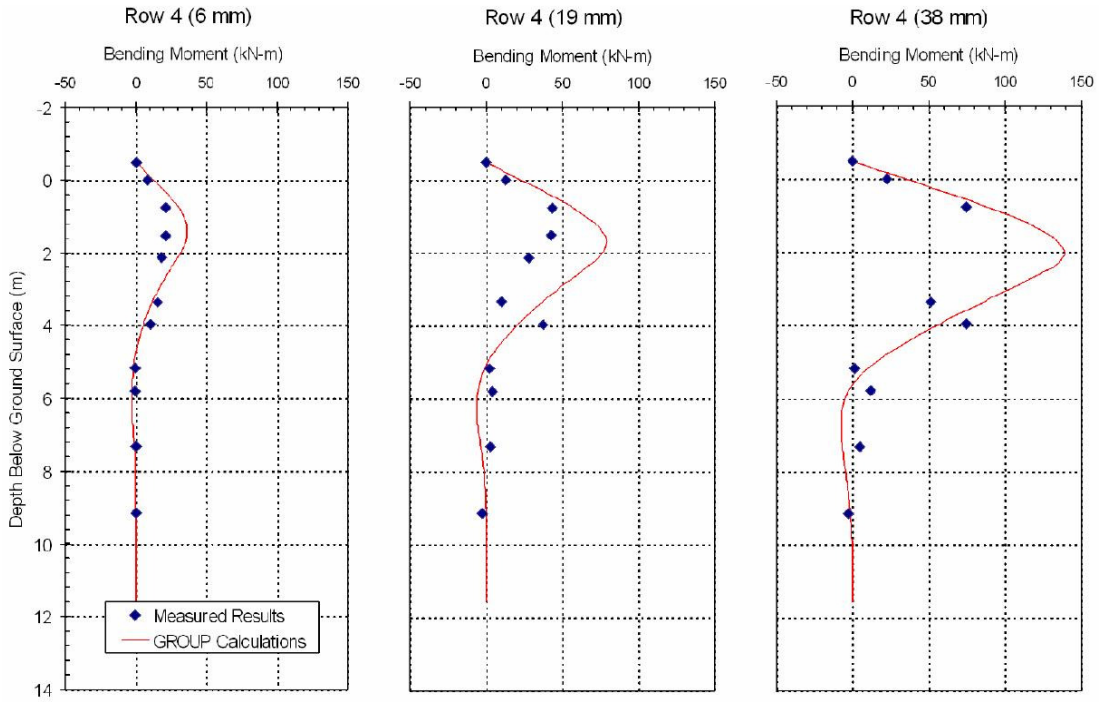

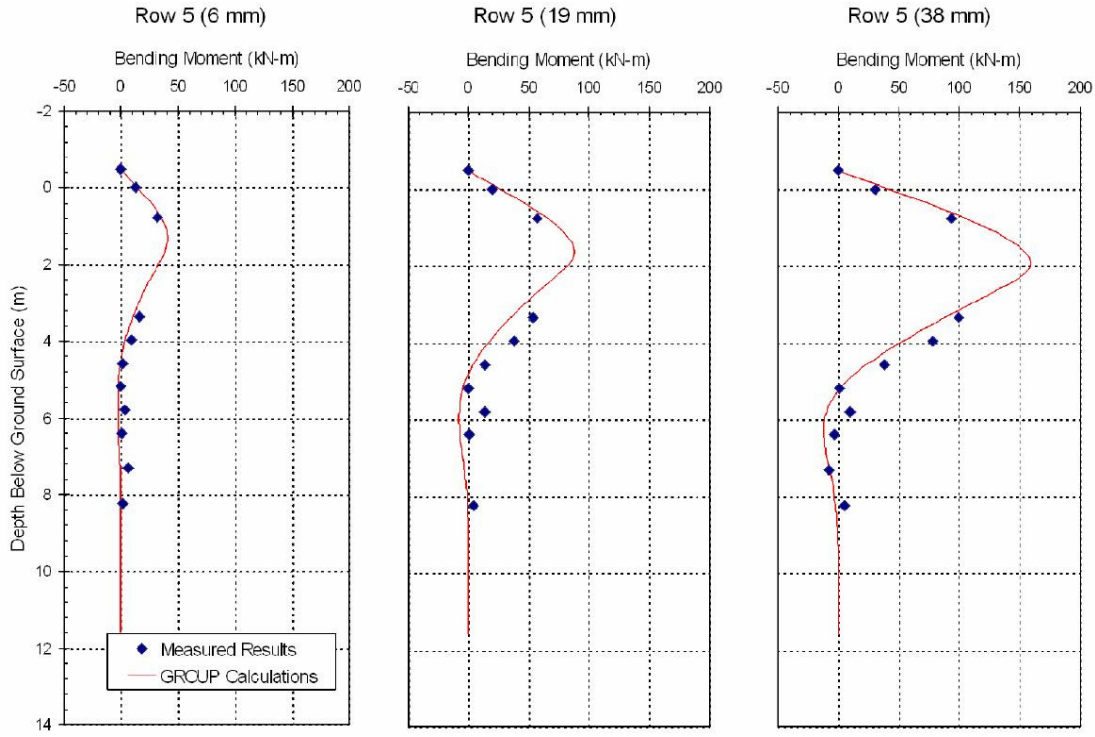
Row 5 (6 mm)
Row 5 (19 mm)
Row 5 (38 mm)
Bending Moment (kN-m)
-50
0
50
100
150
200
-2
0
2
4
6
8
10
12
14
Depth Below Ground Surface (m)
Measured Results
GROUP Calculations